ARL -

INVESTIGATIONS OF THE EFFECT OF ACOUSTIC VIBRATIONS ON CONVECTIVE HEAT TRANSFER

by

Thomas W. Jackson
Kenneth R. Purdy
Henry G. Keith
Robert S. Rudland

January 1965

1965

Engineering Experiment Station

GEORGIA INSTITUTE OF TECHNOLOGY

Atlanta, Georgia

ARL -

INVESTIGATIONS OF THE EFFECT OF ACOUSTIC VIBRATIONS ON CONVECTIVE HEAT TRANSFER

Thomas W. Jackson
Kenneth R. Purdy
Henry G. Keith
Robert S. Rudland

January 1965

FOREWARD

This final report was prepared by the staff of the Georgia Institute of Technology, Atlanta, Georgia, on Contract AF 33(616)-8396 for the Aerospace Research Laboratories, Office of Aerospace Research, United States Air Force. The report presents the results of experimental and analytical studies, which were performed on Task 706301 of the above contract, to determine the influence of acoustic vibrations on convective heat transfer. The research was administered under the technical cognizance of Dr. Max G. Scherberg of the Thermo-Mechanics Research Laboratory, Aerospace Research Laboratories. Dr. Scherberg's interest in the work and his many helpful suggestions are deeply appreciated.

ABSTRACT

This report presents the experimental and analytical results obtained for the heat transfer coefficients in an isothermal tube which had an unheated starting length. The experimental apparatus used in the investigations was a 10 foot long heated section of 3.86 inch I.D. copper tubing with an inlet supply duct length of 28.22 feet. The heated section was designed to give local values of the heat transfer coefficient as well as overall values. Data on heat transfer coefficients for Reynolds numbers from approximately 10,000 to 65,000 are presented for conditions of no-sound (without resonant acoustic vibrations) and for conditions of a resonant frequency in the tube of approximately 90 cps. For turbulent flow the effect of the resonant sound field is to reduce the heat transfer coefficients. A half-wave length periodic effect on the local heat transfer coefficient was noted. The local values of the turbulent heat transfer coefficients are correlated in relation to the no-sound values as a function of U_o^2/Uc_o, where U_o is the maximum sound particle velocity, U is the mean through flow velocity and c_o is the speed of sound.

The parameter U_o^2/Uc_o was determined to have a theoretical basis from the solution of the energy equation for the laminar flow situation with sound. The analytical solution for the local heat transfer coefficient for laminar flow in a channel is given and compared to the results obtained in the heat transfer tube.

A preliminary determination of velocity profiles by means of a hot wire anemometer for both no-sound and sound conditions, indicated that the sound tends to alter the profile.

An insert was placed in the tube to determine the effect of pressure gradients on the heat transfer coefficients. The effect appears to be similar to that obtained with the tube flow if the local velocity of the flow is considered.

NOMENCLATURE

c_o	isentropic speed of sound, ft/sec
c_p	specific heat, Btu/lbm° F
C	coefficient
D	tube diameter, feet
h	heat transfer coefficient, Btu/hr ft^2° F
k	thermal conductivity, Btu/hr ft° F
ℓ	length, measured from the thermal entrance, over which the heat transfer coefficient is averaged, ft
$\dot{m}$	mass flow rate of air lbm/hr
M	Mach Number
P	pressure, lbf/in^2
T, t	temperature, °F or time, seconds
U	velocity, ft/sec
U_o	maximum sound particle velocity, ft/sec
w, ω	circular frequency of sound wave, radians per second
x, z	axial distances from thermal entrance, ft
λ	wave length of acoustic field, ft
μ	viscosity
ν	kinematic viscosity ft^2/sec
ρ	density, lbm/ft^3
Nu	Nusselt number, $\dfrac{hD}{k}$
Pr	Prandtl number, $\dfrac{c_p \mu}{k}$
Re	tube Reynolds number based on diameter, $\dfrac{UD}{\nu}$
SPL	sound pressure level (see page 14)

Superscripts

$-$	average value
$'$	dimensionless number

Subscripts

x	local value at distance from thermal entrance, ft
f	based on film temperature
ℓ	average value over length ℓ
∞	asymptotic value
max	maximum value
no-sound	without acoustic vibrations
am	based on arithmetic mean temperature difference
o	at thermal entrance section

TABLE OF CONTENTS

EXPERIMENTAL HEAT TRANSFER SYSTEM

The purpose of the experimental system described herein was to determine the local convective heat transfer characteristics for turbulent flow in a horizontal, isothermal circular tube. The velocity field was to be fully developed before the fluid (atmospheric air) entered the thermal entrance. The characteristics were to be determined with and without a resonant acoustic field superimposed upon the flow field.

The experimental heat transfer system which was designed to measure these characteristics consisted of four subsystems: the air circulation system, the heat transfer system, the thermometer system, and the sound system.

Air Circulation System

The air circulation system which is shown schematically in Figures 1 and 2 consisted of the following components:

Secondary Blower. Atmospheric air from an eight by twenty-eight foot air conditioned room was drawn through a Fiberglas filter and discharged into the return duct by a one-horsepower centrifugal blower. This blower was used only when system Reynolds numbers greater than 50,000 were desired.

Primary Blower. The return duct discharged the air into a 22 by 22 by 18-inch plenum chamber which housed the primary blower (see Figure 2). The flow rate through the blower (Lockwood Model PB-10 pressure blower) was regulated by a manually operated six-inch gate valve on the blower inlet. The discharge from the blower entered a 22 by 22 by 25-inch plenum chamber which housed the air filter for the laminar flow meter.

Laminar Flow Meter. A Meriam Instrument Company Model 50MC2-4PF laminar flow meter was used to determine the mass flow rate of air. For this flow meter the mass flow rate was given by
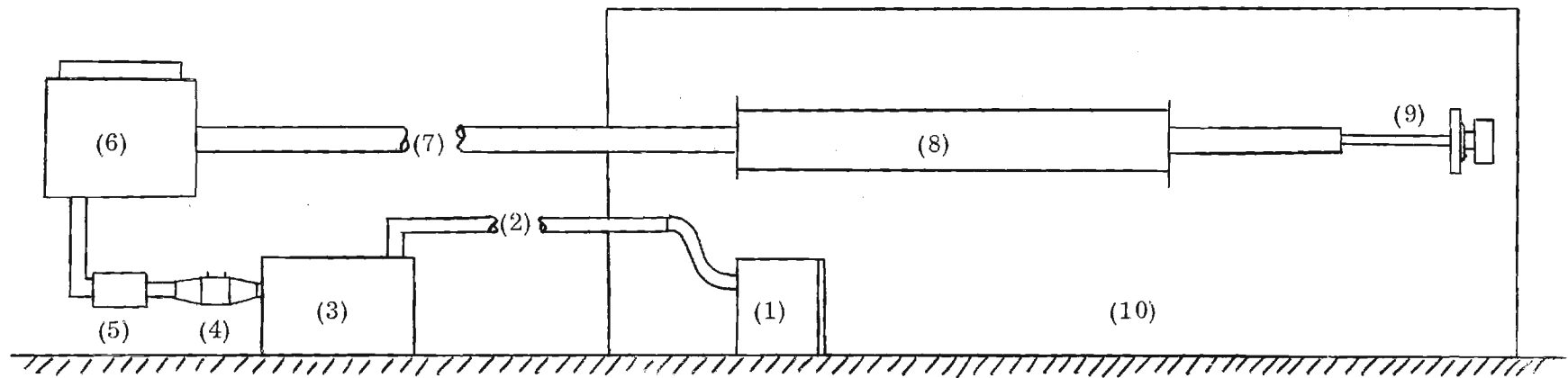
$$\overset{\circ}{m} \ = \ 53.75 \ C_\mu \ \rho \ \Delta P \tag{1}$$

where $\overset{\circ}{m}$ = mass flow rate in lbm/min,

C_μ = $\mu_{70^\circ F}/\mu$,

μ = dynamic viscosity of air at the flow meter static temperature in lbf-sec/ft.^{2},

ρ = density of air at the flow meter inlet static temperature and pressure in lbm/ft.^{3},

Figure 1. Schematic Drawing of Experimental Apparatus

1. Secondary Blower
2. Return Duct
3. Primary Blower
4. Laminar Flow Meter
5. Air Preheater

6. Plenum Chamber
7. Unheated Inlet Section (Supply Duct)
8. Heat Transfer Section
9. Vibrator and Horn
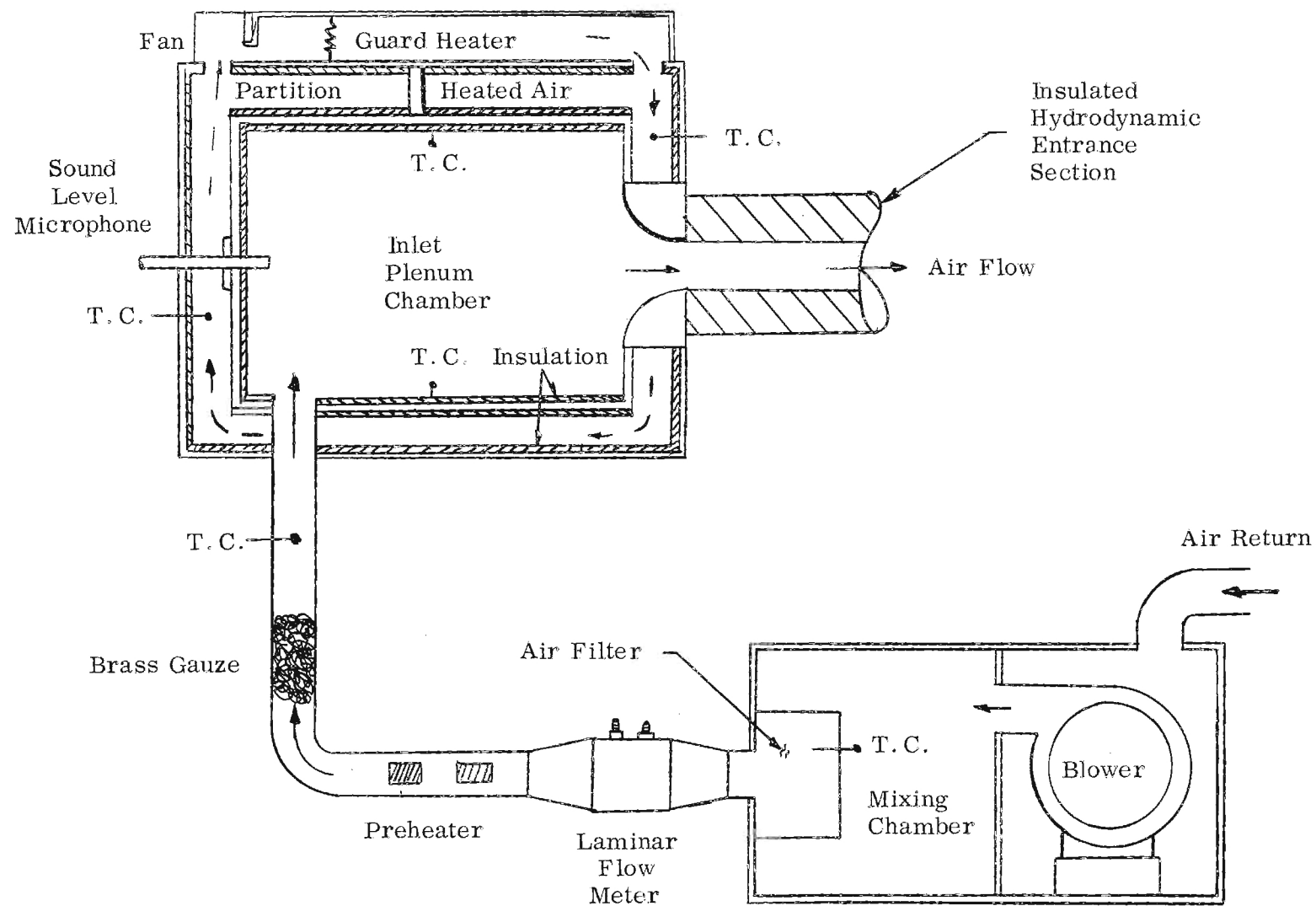10. Air Conditioned Room

Figure 2. Air Circulation System

and ΔP = pressure drop across the flow meter in inches of water.

The static pressure and the pressure drop were both measured with a Meriam Instrument Company Model 34FB2 micromanometer to within ± 0.001 inches of water.

Air Preheater. After leaving the laminar flow meter the air entered the preheater, which consisted of two spirally wound 600-watt electrical resistance heaters. One heater was manually controlled by a 0-140 volt Powerstat while the other heater was automatically controlled by a Leeds and Northrup Series 60 three action control unit in conjunction with a Speedomax Type G recorder. With this system it was possible to maintain the inlet plenum chamber air temperature constant to within ± 0.25° F. Before the air entered the plenum chamber it passed through a maze of brass gauze. This eliminated temperature gradients in the air thereby helping to assure isothermal conditions in the plenum chamber.

Plenum Chamber. The plenum chamber consisted of two plywood boxes, one within the other (see Figure 2). The inner chamber was 23 by 23 by 30-inches and was constructed from three-quarter inch plywood. The sides of this chamber were covered with one-inch thick Johns-Manville Fiberglas to reduce the heat transfer to the surroundings. The air entered this chamber from a rectangular diffuser and left the chamber through an artifically roughened bell-mouth entrance section. No provisions were made to reduce the turbulence level in the plenum chamber since fully developed turbulent flow was to be obtained.

The outer chamber was 33 by 33 by 40-inches and was constructed from one-half inch plywood whose inside surfaces were also covered with one-inch thick Fiberglas. The air in the gap between the two chambers was circulated by a small blower and was heated by a manually controlled electrical resistance heater to the inlet plenum temperature. This temperature was maintained to within ± 1° F of the inlet plenum temperature and thereby essentially eliminated heat transfer to or from the inlet plenum chamber.

A compression seal was provided in the rear surface of the inlet plenum to permit the insertion of the sound level microphone.

Supply Duct. The supply duct which served as a hydrodynamic development section was constructed from 28.22 feet of 3.86 inch I.D. (4.125 inch O.D. Type K) copper tube in three sections. The initial section was 18.39 feet long; the second section was 3.00 feet long; and the third section was 6.83 feet long. All of the joints were fitted with 6 1/2-inch brass plate flanges. The flanges were soldered to the pipe and then machined. This insured alignment within the manufacturing tolerance limits of the copper tube.

The three foot section of pipe served as a dummy section during the heat transfer tests. It was replaced later by a three foot section containing a hot-wire anemometer, which was used to measure velocity profiles and turbulence levels. (See Chapter IV.).

When assembled, the entire supply duct was covered with two inches of Johns Manville "Micro-Lox" insulation.

4

O-ring seals were used at both ends of the supply duct. In order to reduce axial heat conduction from the thermal entrance to the supply duct a one-inch thick Johns Manville "Colorlith" spacer was placed between the supply duct and the thermal entrance.

After leaving the supply duct the air passed through the heat transfer section and was then exhausted into the air-conditioned room where it was cooled to its initial conditions. The air then started the cycle again. The air circulation system, therefore, operated on a closed loop cycle which permitted accurate control of the mass flow rate and the inlet air temperature.

Heat Transfer Section

The heat transfer section which is shown schematically in Figure 3 consisted of the following three basic components:

Steam Heated Tube. Convective heat transfer was achieved by blowing air which had a fully developed turbulent profile through a ten foot section of 4.125-inch O.D. (3.86-inch I.D.) steam heated copper tubing. The tube was mounted inside a ten foot section of 16-inch black iron pipe and saturated steam was admitted to the annular region formed. A pressure of six inches of water gage was arbitrarily chosen for the saturated steam.

Condensate Collection System. Quasi-local heat transfer rates were obtained by soldering 21 collection chambers along the ten foot tube. (See Figure 3.) The first two chambers at the thermal entrance were each 3-inches long and the other 19 chambers were each 6-inches long. A hole at the bottom of each chamber allowed the condensate to drain into a 5/16-inch O.D. copper stand pipe. Each stand pipe was connected to a separate drain line which ran horizontally through the annular steam chest, through the head plate, and to the condensate measuring system. Since the condensate drain lines ran through the steam chest and since they contained liquid water there was no possibility of picking up extraneous condensate. In addition, a drip shield covered the collection chambers to prevent extraneous condensate from entering the collection chambers.

Condensate Measuring System. The drain line from each of the 21 condensate collection chambers was connected to a transfer cup with neoprene tubing. The 21 transfer cups were clipped to a rack which could be raised or lowered. The drain line between the stand pipe for the condensate collection chamber and the transfer cup was actually the leg of a U-tube manometer since the difference in elevation between the water level in the stand pipe and the drain outlet in the transfer cup must be equal to the static pressure of the steam. Thus the water level in the stand pipe could be varied by raising or lowering the transfer cup. The water level was maintained 1/2-inch below the bottom of the condensation collection chamber by this method. A pointer which was attached to the rack and a manometer which indicated the steam pressure were used to properly position the transfer cups. The surface tension effect on the draining of the water from the drain line into the transfer cups was eliminated by the use of wicks. The condensate from each cup drained into a calibrated burette where it was measured as a function of time.

Thermometer System

The following temperatures were measured with 24-gauge copper-constantan thermocouples in conjunction with a Leeds and Northrup Model 8686 portable precision potentiometer:
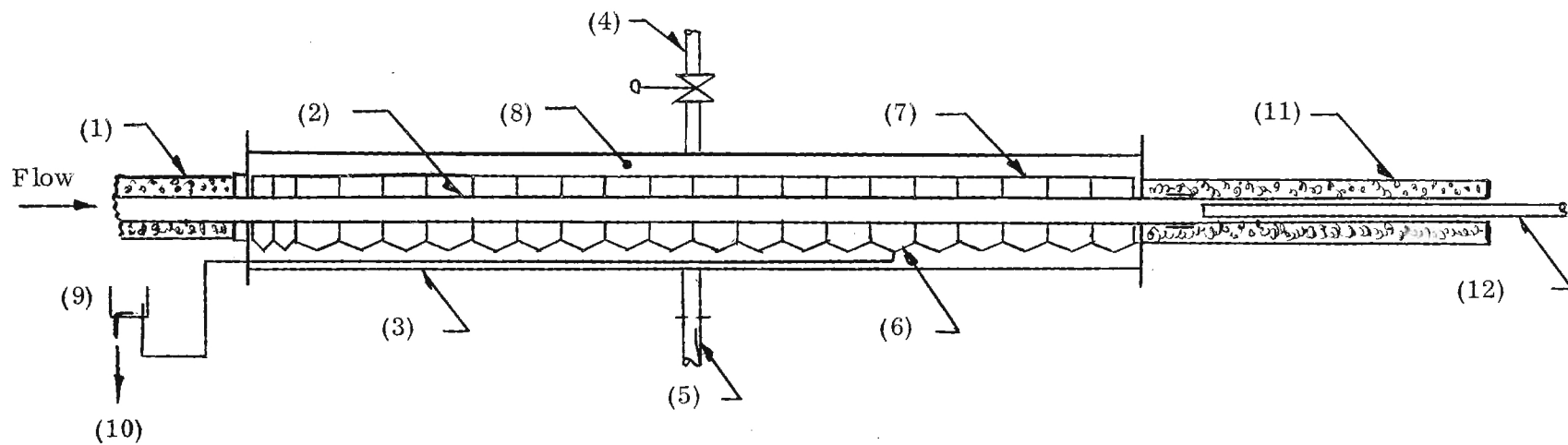
1. Supply Duct
2. Steam Heated Tube
3. Insulated 16-inch Pipe
4. Steam Inlet
5. Steam Outlet
6. Condensate Collecter

7. Drip Shield
8. Saturated Steam
9. Condensate Transfer Cup
10. To Burette
11. Insulated Duct
12. Horn

Figure 3. Drawing of Heat Transfer Tube

t_1. The wet bulb temperature of the air at the inlet to the secondary blower was measured to determine the moisture content of the air.

t_2. The dry bulb temperature of the air at the blower entrance was also measured for this purpose.

t_3. The static temperature at the inlet to the laminar flow meter was measured to determine the mass flow rate of the air.

t_4. The static temperature of the air in the inlet plenum chamber was fixed at either $105°$ F or $110°$ F and was maintained constant at these values to within $\pm 0.25°$ F. Since this temperature was quite critical in the determination of the local heat transfer characteristics it was measured by four thermocouples connected in parallel. Each of the four protruded approximately 2-inches from the surface of one of the side walls of the inlet plenum. A second series of thermocouples in the inlet plenum was used as the sensing element for the automatic controller.

t_5. The static temperature of the condensing steam was measured for a cross check on the saturation pressure of the steam. Since the heat transfer coefficient for condensing steam is so much larger than the coefficients for forced convection, this temperature was also assumed to be equal to the tube wall temperature.

t_6. The tube wall temperature at the thermal entrance was measured as a check on the previous assumption that the tube wall was essentially at the steam saturation temperature.

t_7. Since the supply duct carried air at approximately $100°$ F there was heat transfer from the air to the surroundings. In order to determine the actual air temperature at the thermal entrance it was necessary to measure the temperature of the outer surface of the supply duct insulation which was exposed to the laboratory atmosphere. An average value of this temperature was obtained by connecting three thermocouples equally spaced along the length of the duct in parallel.

t_8. The temperature of the outer surface of the supply duct which was exposed to the atmosphere in the air conditioned room was also measured to correct the air temperature at the thermal entrance. Two thermocouples wired in parallel were used to determine this temperature.

In addition to these eight temperatures the temperature in the region between the inlet plenum chamber and its outer shell was measured by two 24-gauge iron-constantan thermocouples in conjunction with a Leeds and Northrup Type H direct reading temperature indicator.

The temperatures of the micromanometer water column and the barometer mercury column were measured with mercury in glass thermometers.

Sound System

Sound Generation Equipment. The resonant acoustic field was generated by a MB Electronics Model T-112531 Control Cabinet in conjunction with a

Model C11-D vibration exciter. The exciter was mechanically coupled to a 12 1/2-inch diaphragm, which was fastened to a 13 1/2-inch cylinder with a neoprene impregnated cloth seal. The cylinder "discharged" into a seven foot long 2 1/2-inch Type L copper tube which served as a cylindrical horn. The horn outlet was placed very close to the last pressure antinode in the resonant tube. Low distortion resonant sound fields were produced by this system with sound pressure levels up to 166 decibels.

The sound generation components are shown schematically in Figure 4 and photographically in Figures 5 and 6.

Sound Measurement Equipment. The sound measurement equipment consisted of the following General Radio items:

Item	Type
Sound level meter	1551-A
Power supply	1262-A
High level microphone assembly	1551-P1H
Attenuator pad (20 db)	1551-P11
Sound level calibrator	1552-B
Transistor oscillator	1307-A

In addition to the General Radio items a Hewlett-Packard Model 302A wave analyzer was used to analyze the sound pressure in the supply and heat transfer ducts.

In order to measure the axial distribution of the sound pressure in the supply and heat transfer ducts a pressure probe was made by mounting the high level microphone (Altec 21-BR-180 condenser microphone) on the end of a 40-foot long, 0.915-inch O.D. tube. The microphone was checked periodically with the calibrator which produced a sound-pressure level of 121 ± 1 decibels at 400 cps. Thus the absolute accuracy of the sound pressure level measurements was estimated to be within ± 1.1 decibels of the true value. The relative sound levels were estimated to be accurate to within ± 0.1 decibel.

A Sorensen Model 2501 A.C. line voltage regulator supplied 117-volt 60-cycle A.C. power to all of the electrical equipment.

Acoustic Characteristics

Resonance Conditions. The resonant tube consisted of the supply duct and the heat transfer section as shown in Figure 7. The effective length of the resonant air column according to Morse (1) is given by the actual duct length plus approximately 0.724 times the tube diameter. Thus the effective length was approximately 43.33 feet. For a resonant tube open at both ends this corresponded to the wave lengths for the first eight harmonics given in Table I.

Table I. Harmonic Wave Lengths

n	1	2	3	4	5	6	7	8
λ_n	86.66	43.33	28.89	21.67	17.33	14.44	12.38	10.83

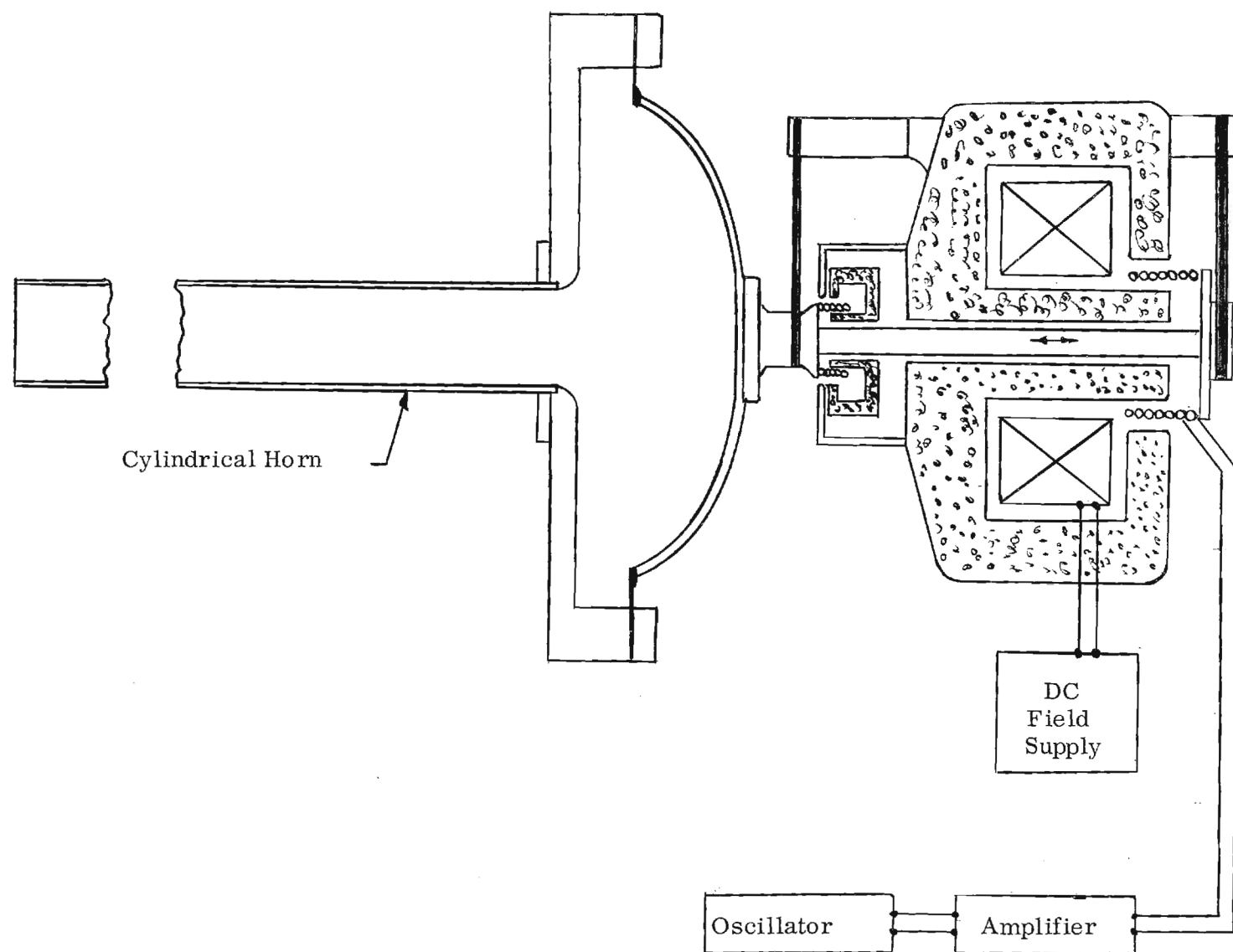Cylindrical Horn

DC
Field
Supply

Oscillator   Amplifier

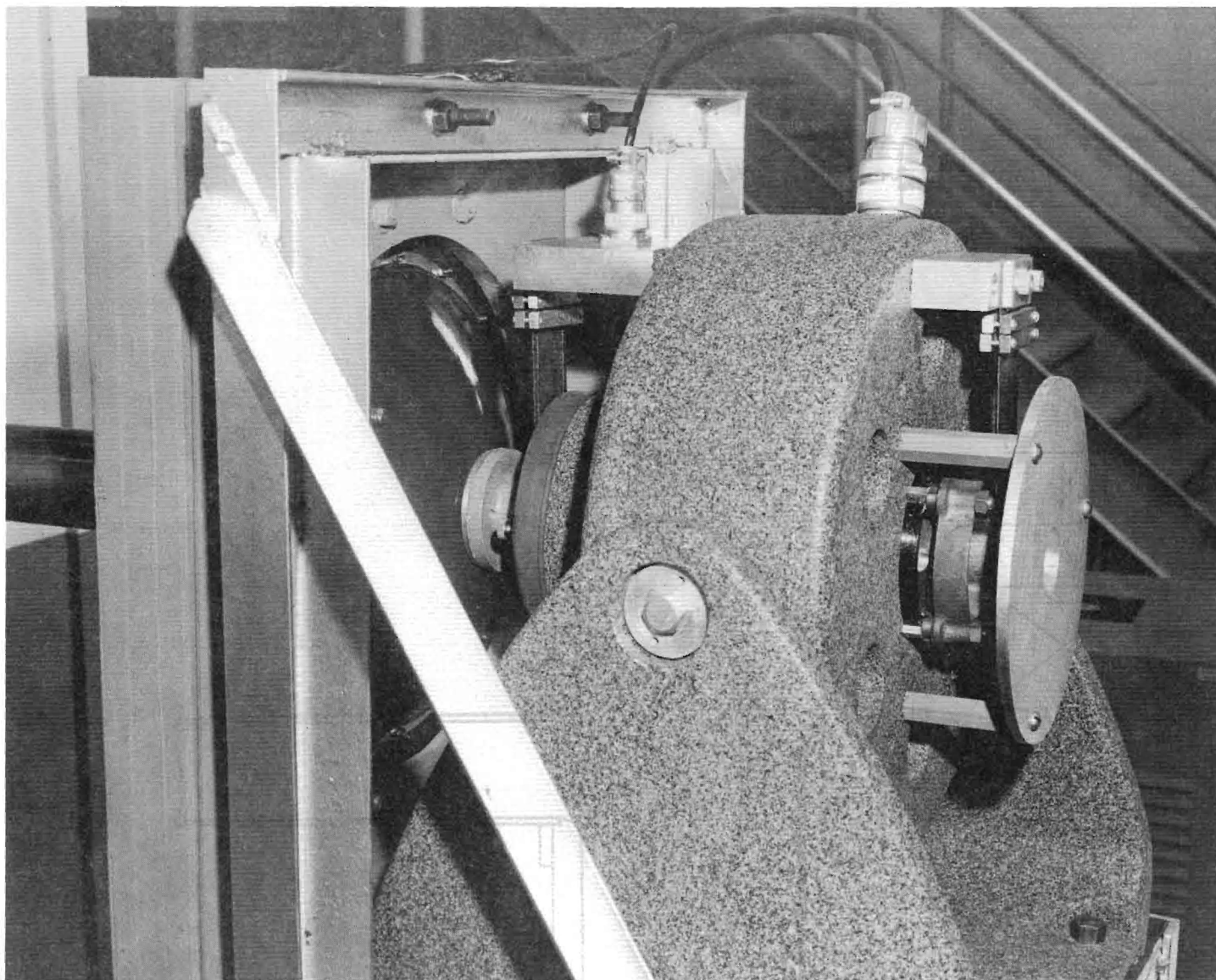Figure 4. Drawing of Sound Generating Equipment

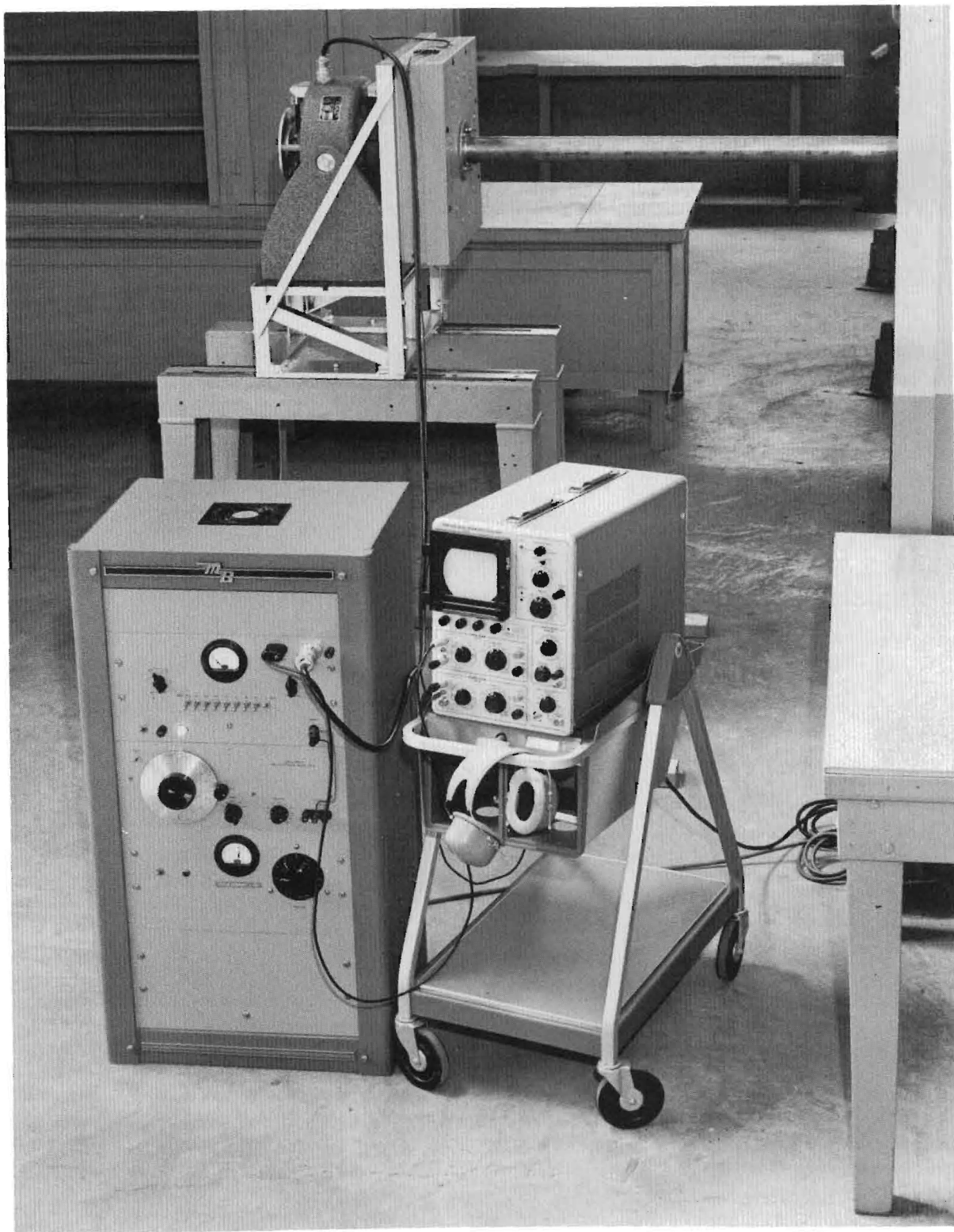Figure 5. Transducer and Sound Generating Diaphragm.

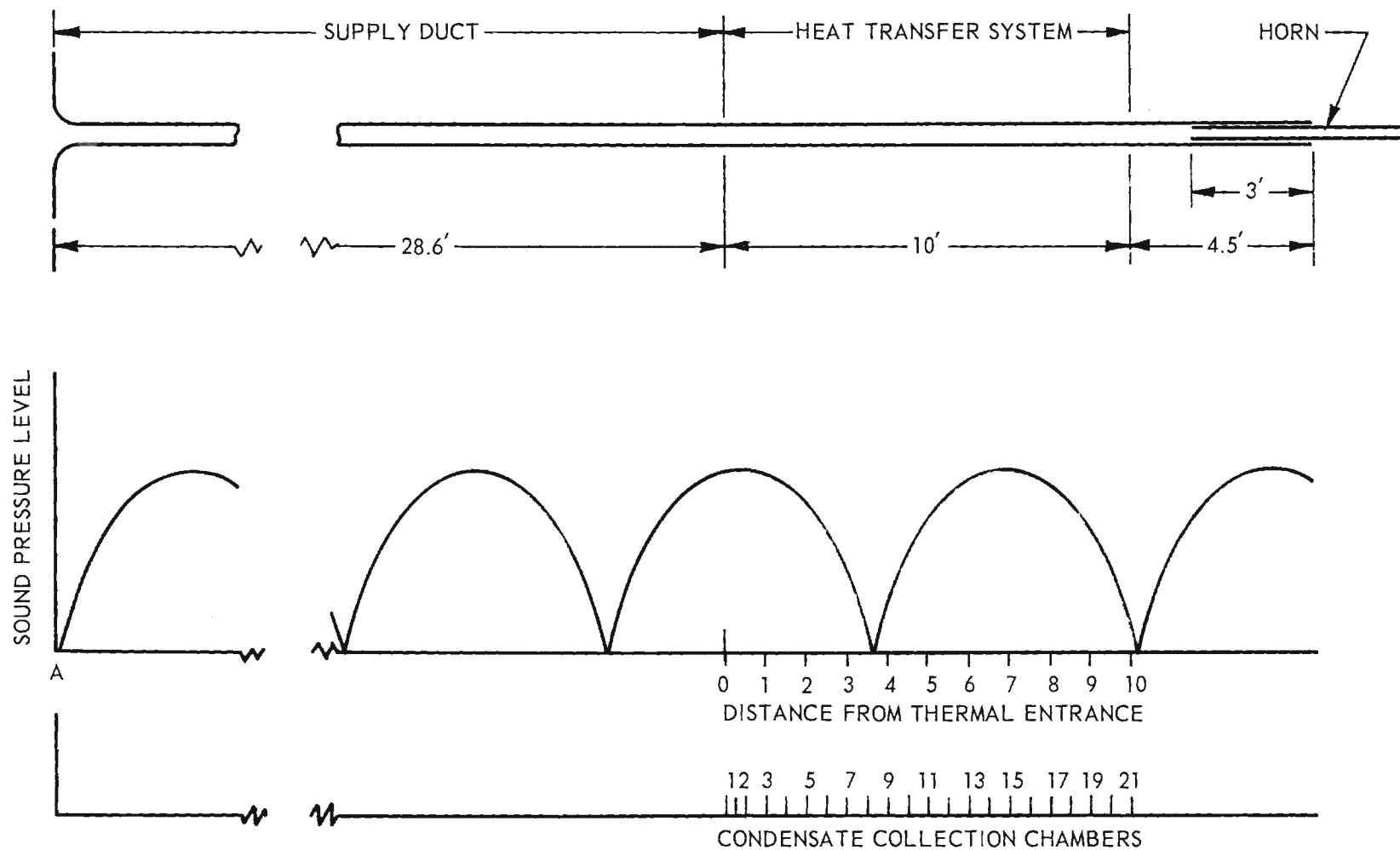Figure 6. Transducer Installation into Heat Transfer Tube.

Figure 7. Sound Pressure Level Versus Distance in Tube.

12

The horn and transducer were mounted on a rigid track so that the axial position of the outlet could be varied to obtain the maximum sound pressure level under resonant conditions.

The seventh harmonic was chosen for the tests reported herein since it gave the best combination of high sound level (166 db) and detailed "local" heat transfer characteristics. The best horn outlet position was found to be approximately one-quarter wave length from the duct outlet. A coupling occurred between the horn and the resonant tube which resulted in a slight variation in the standing wave pattern. Instead of $\lambda_7 = 12.38$ ft. it was actually $\lambda_7 = 12.92$ ft.

The actual standing wave distribution as determined by a sound pressure probe of the tube is shown in Figure 7. Within the accuracy of the measurements no change in the position of the wave could be determined as a function of the through flow.

Sound Pressure Distribution. From first order acoustics for a single frequency sine wave, the pressure deviation from the time mean static pressure caused by a resonant acoustic field is given by (2)

$$p_1(z,t) = \frac{\rho_o c_o U_o}{g_c} \sin(2\pi z/\lambda_n) \sin(w t) \tag{2}$$

where z = axial distance from the first pressure node
            (point A Figure 7) in feet

    t = time in seconds

    w = circular frequency of the sound wave in radians
            per second

    ρ_o = time-mean density of air in lbm/ft.^3

    c_o = isentropic speed of sound in ft/sec.

    U_o = maximum sound particle velocity in ft/sec.

    g_c = 32.174 ft-lbm/lbf-sec.^2

The product $\rho_o c_o U_o/g_c$ is also equal to the amplitude of the pressure deviation P_o, i.e.,

$$P_o \equiv \rho_o c_o U_o/g_c \tag{3}$$

and, therefore,

$$p_1(z,t) = P_o \sin(2\pi z/\lambda_n) \sin(w t) \tag{4}$$

The sound pressure level by definition is

$$SPL \equiv 20 \log_{10} \left[\frac{p_{1_{rms}}}{p_{ref}} \right] \ db \qquad (5)$$

where $\qquad p_{ref} \equiv 0.0002 \ \mu bar$ and

$$p_{1_{rms}} = \frac{1}{\sqrt{2}} \ P_0 |\sin(2\pi z/\lambda_n)| .$$

Thus the sound-pressure level distribution may be written as

$$SPL(z) - SPL(\lambda/4) = 10 \ \log_{10} \left[\sin^2(2\pi z/\lambda_n) \right] . \qquad (6)$$

The actual sound-pressure level (SPL) distribution in the tube was found to be given very accurately by equation (6) except in the immediate vicinity of the pressure nodes. This is shown graphically in Figure 8 for a selected through-flow Reynolds number and maximum SPL.

From equations (3), (4), and (5) it can be shown that the maximum sound particle velocity is given by

$$U_0 = 0.2 \ c_0 \ 10^{\left[(SPL(\lambda/4) - 180)/20 \right]} C_p \ ft/sec. \qquad (7)$$

where $\qquad C_p \equiv 29.92/\bar{p}$ and

$\bar{p} \equiv$ time-mean static pressure of the air in inches of mercury

Equation (7) is shown graphically in Figure 9 for selected values of $\bar{p}$ and c_0.

Experimental Procedure

In order to determine the relative effects of a resonant acoustic field on the local convective heat transfer characteristics, data were taken both with and without the resonant sound field. The experimental procedure which was used to obtain these data may be divided into the following two phases:

Heat Transfer Tests Without Sound. Heat transfer tests without a resonant acoustic field were run to determine the absolute accuracy of the heat transfer system. Since the velocity profile was fully developed at the thermal entrance, there existed in the literature numerous data and correlations which
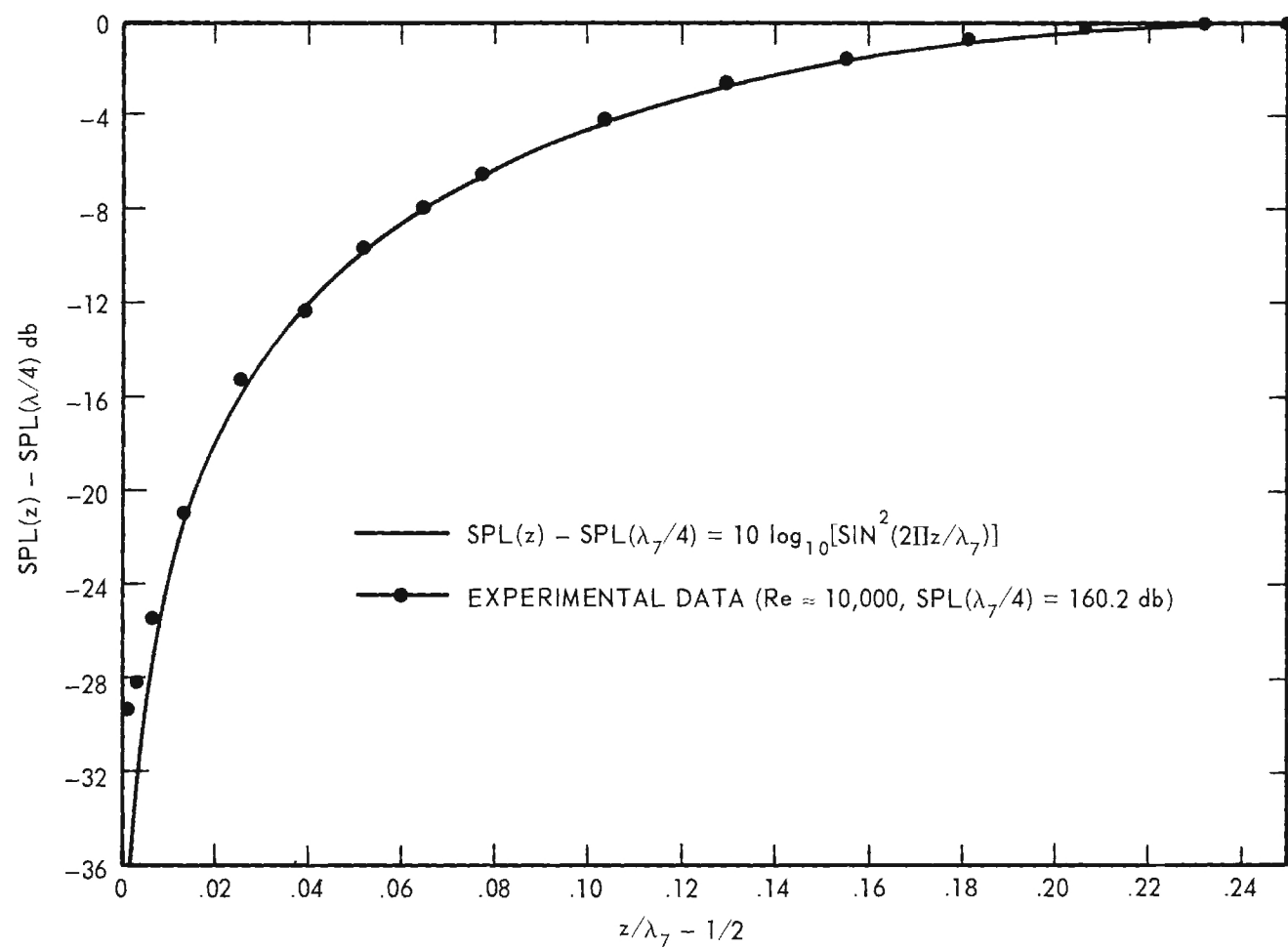
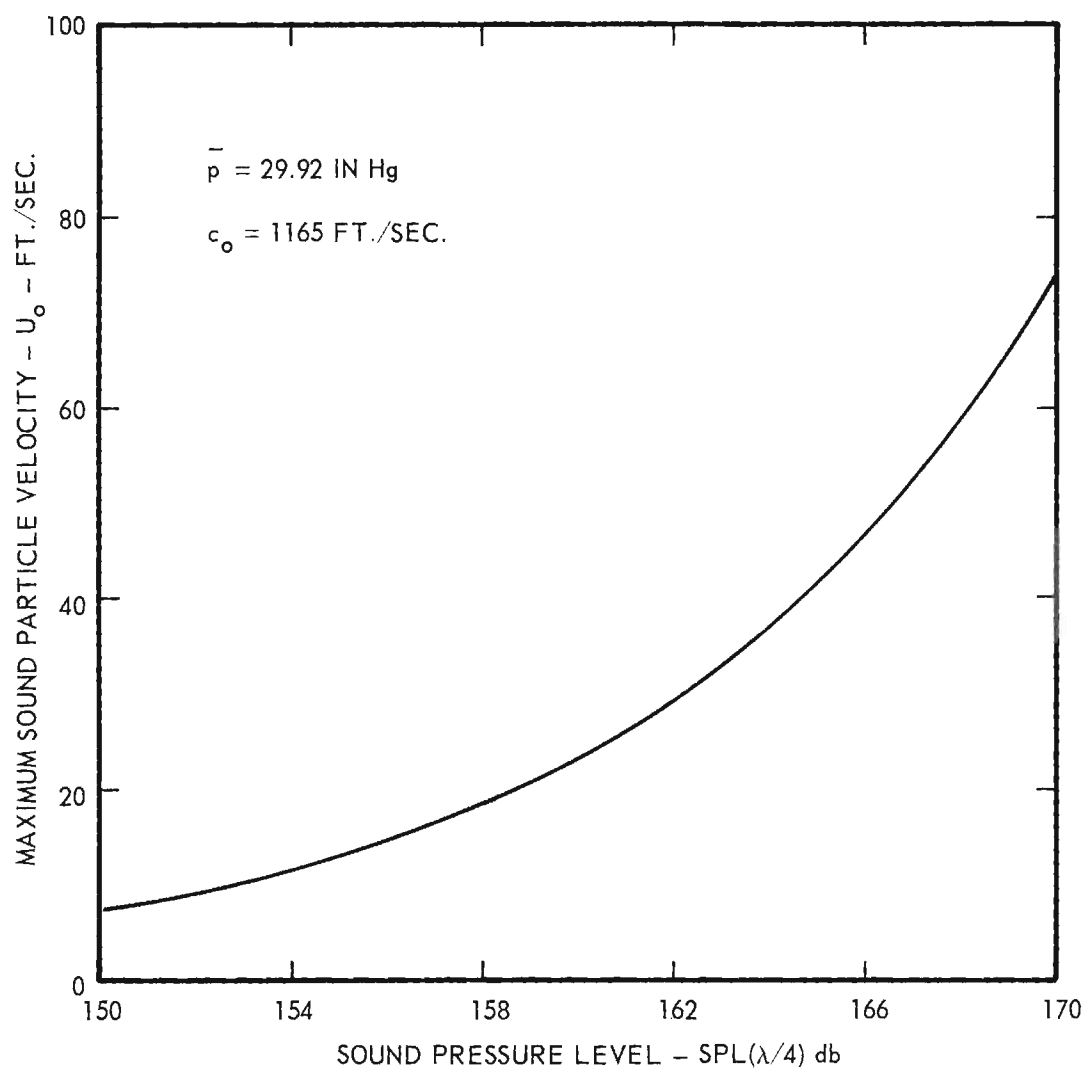Figure 8. Sound Pressure Level as a Function of Distance.

- Y-axis: $\text{SPL}(z) - \text{SPL}(\lambda/4)$ db
- X-axis: $z/\lambda_7 - 1/2$

Legend:
- $\text{SPL}(z) - \text{SPL}(\lambda_7/4) = 10 \log_{10}[\text{SIN}^2(2\Pi z/\lambda_7)]$
- EXPERIMENTAL DATA (Re $\approx$ 10,000, $\text{SPL}(\lambda_7/4) = 160.2$ db)

Figure 9.   Sound Particle Velocity Versus Sound Pressure Level.

could be used for this purpose. The no-sound tests were run for Reynolds numbers from approximately 11,000 to 65,000 and for initial air to wall temperature differences of either 102°F or 107°F. The following procedure was used to conduct the no-sound tests:

1.   The desired inlet plenum air temperature (105°F or 110°F) was converted to an appropriate emf equivalent and this was set as the control point for the 3-Action controller.

2.   The primary blower (also the secondary blower for Re > 45,000), the plenum blower, the preheater, and the plenum guard heater were all energized.

3.   The plenum guard heater Powerstat was set to maintain a temperature of either 105°F or 110°F.

4.   The gate valve on the primary blower inlet was set to provide the desired flow rate.

5.   The steam flow into the annular steam chest was regulated to produce a static chest gage pressure of six-inches of water. The steam flow was not shut off unless the heat transfer test section was to be removed for repairs or cleaning.

6.   The system was allowed to run for from three to 24 hours depending on the Reynolds number and the time available. During this period fine adjustments in the air gate valve, the steam valve and the guard heater Powerstat were made to obtain the desired conditions.

7.   A run was initiated by taking the following data:

> wet bulb temperature
> dry bulb temperature
> laminar flow meter temperature
> inlet plenum air temperature
> steam temperature
> tube wall temperature
> insulation surface temperature
> laminar flow meter static pressure
> laminar flow meter differential pressure
> barometric pressure
> steam gage pressure
> barometer temperature

These data were also taken at the middle and the end of a run and the three values of each parameter were arithmetically averaged.

8.   The steam condensate rate was determined by first starting the clock (Precision Scientific Co., "Time-It") and then by starting each of the 21 burettes. This was accomplished by closing the stopcock at the bottom of each burette and recording the time that the condensate levels reached each of the zero graduations. The time that each burette became full was finally recorded. The difference in the "full" time and the "zero" time was the time necessary to collect 50 ml of condensate. From two to four fill times were obtained for each burette. The fill times were compared and if any one of the first 20 collectors behaved irrationally then the run was repeated. Deviations in the fill time were usually less than two percent with an even smaller mean deviation.

Heat Transfer Tests With Sound. Heat transfer tests with a resonant acoustic field were run for Reynolds numbers from approximately 19,800 to 65,000, initial air to wall temperature differences of either 102°F or 107°F and sound-pressure levels up to 166 decibels. The following procedure was used to conduct the sound tests:

1. Steps 1 through 6 of the no-sound procedure were executed with one addition. After the preliminary adjustment in the air flow rate was made, the vibration exciter was energized. A frequency of approximately 90 cps was set on the audio oscillator and the amplifier gain was increased. The frequency was then varied slightly to obtain a minimum in the amplifier output current. A minimum in the output current for a constant amplifier gain corresponded to resonance in the tube. A change in frequency of less than 0.05 cps from the resonant frequency could be detected by this method. After minimizing the output current the sound-pressure microphone was inserted into the tube to a position which corresponded to the first SPL maximum. The amplifier gain was then varied until the desired SPL was obtained. The microphone probe was then removed from the tube and an additional time of from one to three hours was allowed to assure an equilibrium condition.

2. Steps 7 and 8 of the no-sound procedure were executed. The only additional data that were recorded were:

> maximum sound pressure level
> minimum sound pressure level
> oscillator frequency
> D.C. field current
> amplifier output current

At the end of the run the sound-pressure probe was inserted to the position of the first SPL maximum and the SPL was read and recorded. If this value differed by more than 0.2 db from the initial value then the run was repeated.

Data Reduction Procedure

The method which was used to calculate the local and average Nusselt and Reynolds numbers for the open system shown in Figure 10 was as follows:

Mass Flow Rate of Air - $\dot{m}$. The mass flow rate of air was determined from equation (1), i.e.,

$$\dot{m} = 3225 \ c_\mu \ \rho \ \Delta P \ \text{lbm/hr.} \tag{1}$$

In this equation the dynamic viscosities were assumed to be the same as those for dry air as given in reference (3). For computational purposes an interpolating polynomial was fitted to these data by the method of least squares. The density was obtained by assuming atmospheric air to be a mixture of dry air and water vapor each of which was assumed to be an ideal gas. Thus

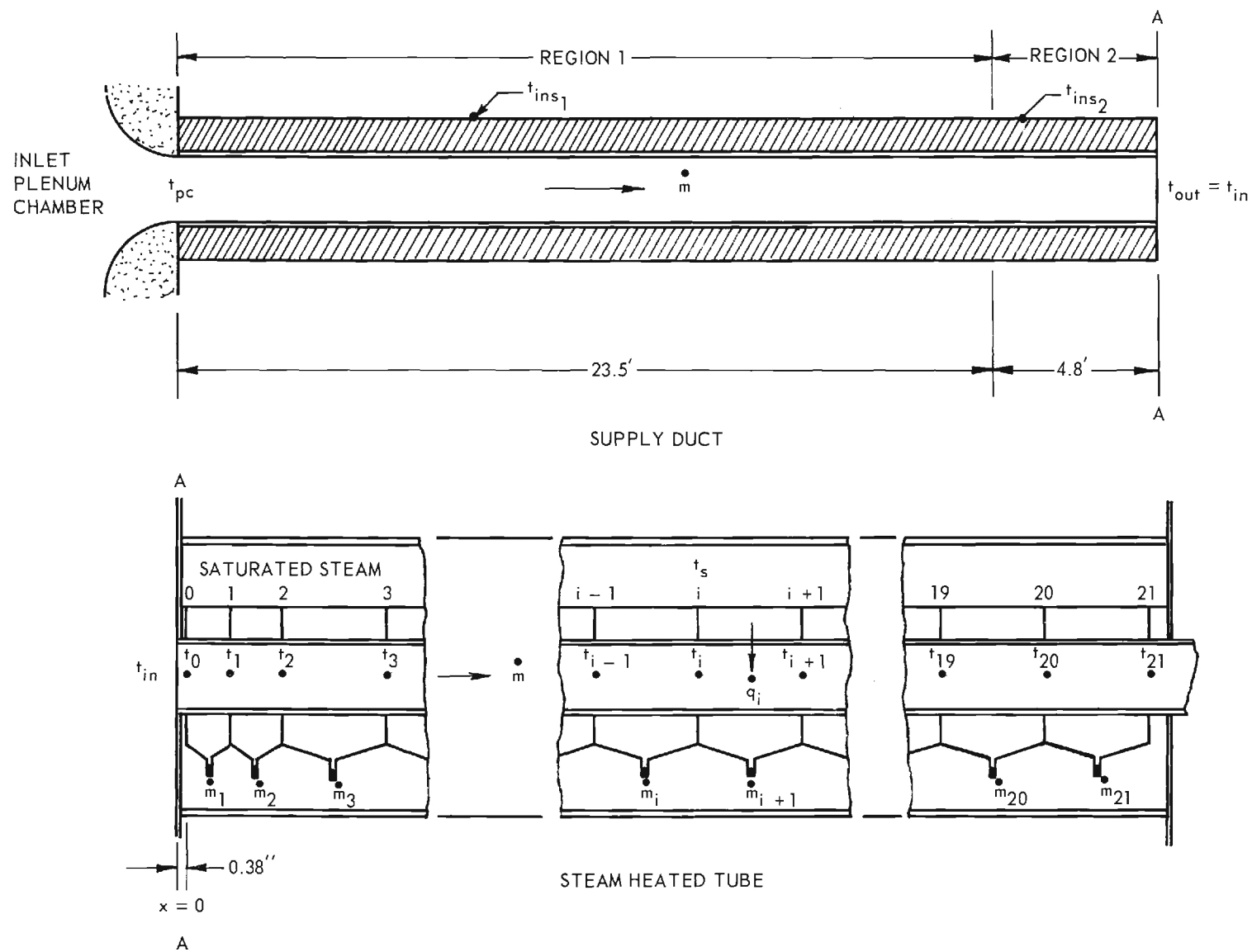$$\rho = \frac{(1 + \alpha) (70.73 \ P_{fm})}{(53.35 + 85.58 \ \alpha) (t_{fm} + 459.7)} \ \text{lbm/ft.}^3 \tag{8}$$

18

REGION 1

REGION 2

t_{ins_1}

t_{ins_2}

INLET
PLENUM
CHAMBER

t_{pc}

$\dot{m}$

$t_{out} = t_{in}$

23.5′

4.8′

SUPPLY DUCT

SATURATED STEAM

t_s

0 1 2 3

i − 1   i   i + 1

19   20   21

t_{in}

t_0 t_1 t_2 t_3

t_{i-1} t_i t_{i+1}

t_{19} t_{20} t_{21}

$\dot{m}$

q_i

$\dot{m}_1$ $\dot{m}_2$ $\dot{m}_3$

$\dot{m}_i$ $\dot{m}_{i+1}$

$\dot{m}_{20}$ $\dot{m}_{21}$

0.38″

STEAM HEATED TUBE

$x = 0$

Figure 10. Nomenclature for Heat Transfer Calculations.

where $\quad\alpha\quad$ = humidity ratio in lbm H_2O/lbm dry air

$\quad\quad\quad t_{fm}$ = laminar flow meter temperature in $°F$

$\quad\quad\quad P_{fm}$ = laminar flow meter static pressure in inches of mercury

The humidity ratio, α, was determined from the wet and dry bulb temperatures which were taken at the secondary blower inlet.

Inlet Temperature – t_o. In order to find the inlet temperature to the steam heated tube it was necessary to make the following computations:

Supply Duct Temperature Change – The air temperature in the supply duct was higher than the duct's surroundings and, therefore, "heat" was transferred from the duct to its surroundings. The temperature change associated with this energy transfer was estimated by considering the duct to be exposed to two regions; region 1 was the laboratory atmosphere and region 2 was the controlled atmosphere of the air conditioned room which enclosed the heat transfer system. The convection from the outer surface of the insulation was eliminated from the analysis by measuring the average insulation surface temperature in each region. The analysis which included the thermal resistances due to internal convection and heat conduction through the copper tube and the Fiberglas insulation gave the following expression for the temperature at the outlet of the supply duct.

$$t_{out} = t_{ins_2} + (t_{ins_1} - t_{ins_2}) \exp (-10.11\,\bar{U}/\dot{m}\,c_p) +$$

$$(t_{pc} - t_{ins_1}) \exp (-60.2\,\bar{U}/\dot{m}\,c_p) \qquad (9)$$

where $\quad t_{pc}$ = temperature in inlet plenum chamber in $°F$

$\quad\quad t_{ins_1}$ = temperature insulation in region 1 in $°F$

$\quad\quad t_{ins_2}$ = temperature insulation in region 2 in $°F$

$\quad\quad \bar{U}$ = $1/(12.52 + 29.4/\left[Re^{4/5} Pr^{1/3} k \right])$ in Btu/hr. ft.$^2 °R$

$\quad\quad Re$ = tube Reynolds number based on plenum chamber properties

$\quad\quad Pr$ = Prandtl number based on plenum chamber temperatures(t_{pc})

$\quad\quad \dot{m}$ = mass flow rate of air in lbm/hr.

$\quad\quad c_p$ = constant pressure specific heat of moist air in Btu/lbm.

$\quad\quad k$ = thermal conductivity of dry air in Btu/hr. ft.$°R$

For Reynolds numbers greater than 20,000 the temperature change was usually less than one degree Fahrenheit.

Thermal Entrance Temperature Change – In order to eliminate extraneous condensate from the first condensate collector, it was started 0.38-inches downstream of the thermal entrance. Thus to accurately determine the

heat transfer characteristics downstream of section "O" ($x = 0.38$ inches) the rate of heat transfer, $\dot{q}_o$, for this region must be established.

Writing the steady-flow energy equation for the heated tube between $x = 0$ and $x = 0.38$ inches yields

$$\dot{q}_o = \dot{m} c_p (t_o - t_{in}) \cong \bar{h} \pi D \Delta x (t_s - t_{in}) \tag{10}$$

where
t_o = bulk temperature at section "O" (see Figure 10) in $^\circ F$

$t_{in} = t_{out} = t_{x=0}$ in $^\circ F$

t_s = saturated steam temperatures in $^\circ F$

D = inside diameter of the tube in ft.

Δx = 0.38/12 ft.

$\bar{h}$ = mean heat transfer coefficient in Btu/hr. ft.$^2 \, ^\circ F$

Equation (10) can be solved for $\dot{q}_o$ or t_o if $\bar{h}$ is known. The best estimate for $\bar{h}$ which was found was Latzko's (see reference 4) prediction for the starting region in a circular tube with a bellmouthed entry. After reduction this gave

$$\dot{q}_o = 3.77 \times 10^{-3} \, Re_f^{0.855} \, k_f (t_s - t_{in}) \text{ Btu/hr.} \tag{11}$$

where the Reynolds number and thermal conductivity of the air were based on the film temperature. Thus the actual inlet temperature, t_o, was

$$t_o = t_{in} + \dot{q}_o / \dot{m} c_p \, ^\circ F \tag{12}$$

Bulk Temperature Distribution - t_i. The bulk temperature distribution was found by writing the steady flow energy equation for each of the 21 condensate collection chambers. The rate of heat transfer to the air for chamber i is given by

$$\dot{q}_i = \dot{m}_i h_{fg} = \dot{m} c_p (t_i - t_{i-1}) \text{ Btu/hr.} \tag{13}$$

where
$\dot{m}_i$ = steam condensate rate for chamber i lbm/hr.

h_{fg} = latent heat of vaporization of water in Btu/lbm.

t_{i-1} = bulk temperature of the air at section "i-1" in $^\circ F$

t_i = bulk temperature of the air at section "i" in $^\circ F$

Thus since t_o, $\dot{m}_i$ ($i = 1, 2, \cdots, 21$) and $\dot{m} c_p$ were known, equation (13) was solved

21

for $t_i (i = 1, 2, 3, \cdots, 21)$. A typical bulk temperature distribution is shown in Figure 11.

Local Heat Transfer Coefficient – h_{x_i} . A quasi-local heat transfer coefficient was calculated from the definition of the local heat transfer coefficient, i.e.,

$$h_x \equiv (q_x/A)/\Delta t \text{ Btu/hr. ft.}^{2\circ} F \qquad (14)$$

The quasi-local heat transfer coefficient was defined as

$$h_{x_i} \equiv \left[q_i / \quad \pi D(x_i - x_{i-1}) \quad \right] / \Delta t_{x_i} \text{ Btu/hr. ft.}^{2\circ} F \qquad (15)$$

where $\quad \Delta t_{x_i} \equiv \left[2 t_s - t_{i-1} - t_i \right] / 2 \,^{\circ} F \quad$ and

$i \quad = 1, 2, 3, \cdots, 21.$

$x_i \quad$ = distance from the thermal entrance to the end of the i th chamber in feet (see Table II)

Table II. Distance From Thermal Entrance to End of i th Chamber

Chamber	x_i (ft.)
1	0.277
2	0.527
3	1.023
4	1.526
5	2.022
6	2.518
7	3.017
8	3.520
9	4.010
10	4.521
11	5.016
12	5.515
13	6.015
14	6.516
15	7.017
16	7.514
17	8.013
18	8.515
19	9.017
20	9.518
21	10.018
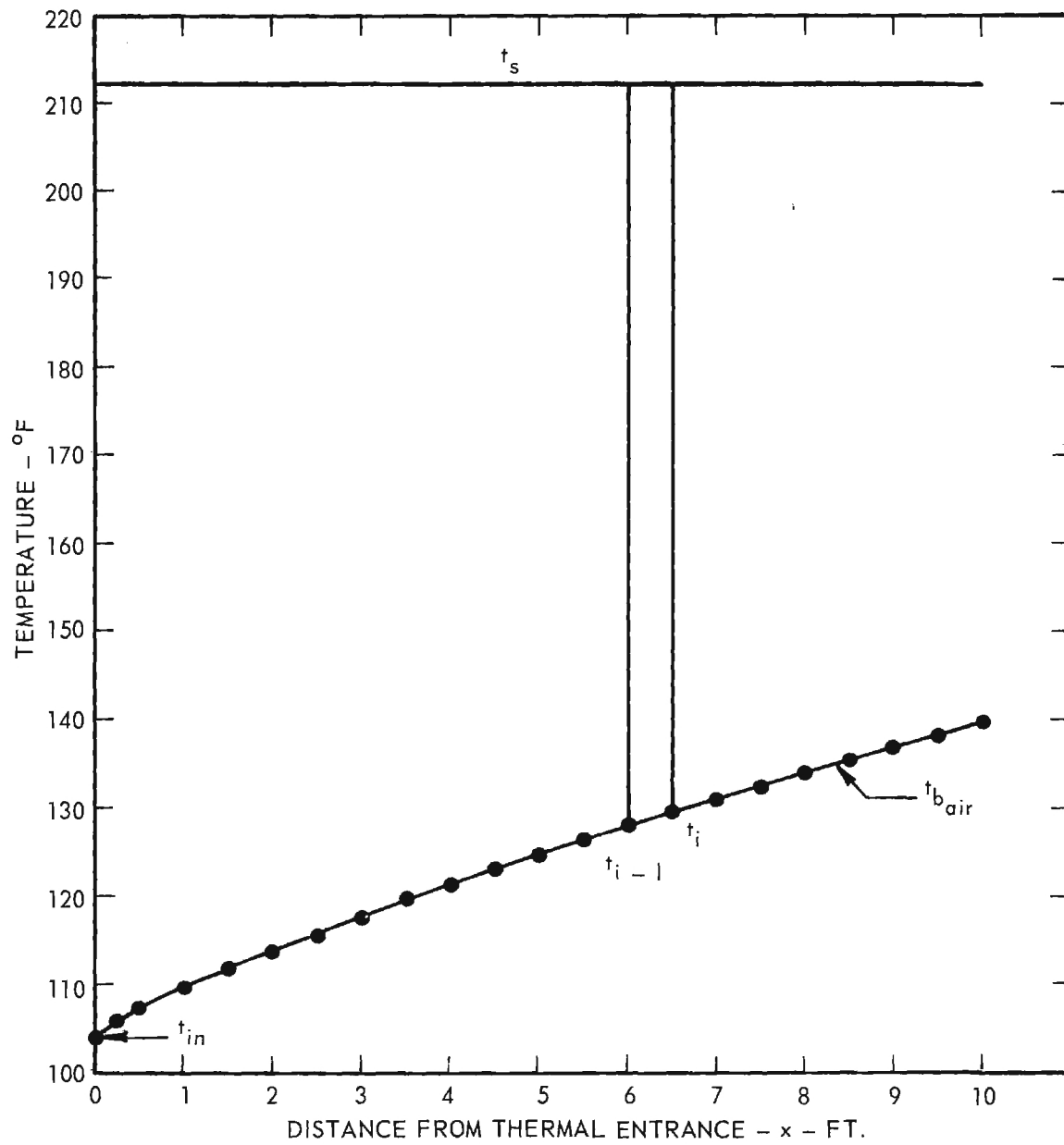
Figure 11. Bulk Temperature of Fluid Versus Distance from Thermal Entrance.

It should be noted that the arithmetic mean temperature difference is based on the saturated steam temperature rather than the inside tube wall temperature. Calculations have shown that the maximum error in h_{x_i} which this could have caused was less than 0.8 percent and in most cases it was less than 0.4 percent. Had the heat transfer coefficient for the condensing steam been known accurately, the tube wall temperature would have been used to calculate Δt_{x_i}.

This "error" in computation produced values of h_{x_i} which were slightly low.

Local Nusselt Number - Nu_{x_i}. The local Nusselt number was calculated from its definition, i.e.,

$$Nu_{x_i} \equiv h_{x_i} D/k_{f_{x_i}} \tag{16}$$

where $k_{f_{x_i}}$ = thermal conductivity of air based on $t_{f_{x_i}}$ in Btu/hr. ft. °R

$$t_{f_{x_i}} \equiv \left[2t_s + t_{i-1} + t_i \right]/4\ °F$$

Log-Mean Heat Transfer Coefficient - $\bar{h}_i$. The log-mean heat transfer coefficient was calculated from the following equation

$$\bar{h}_i = \left[\sum_{j=1}^{i} \dot{q}_j \ / \ \pi D x_i \right]/\overline{\Delta t_i} \ \text{Btu/hr. ft.}^2\ °F \tag{17}$$

where $\overline{\Delta t_i}$ = log-mean temperature difference in °F, i.e.,

$$\overline{\Delta t_i} \equiv \frac{t_i - t_{in}}{\log_e \dfrac{t_s - t_{in}}{t_s - t_i}}\ °F$$

Log-Mean Nusselt Number - $\overline{Nu_i}$. By definition

$$Nu_i \equiv \bar{h}_i D/k_{f_i} \tag{18}$$

where k_{f_i} = thermal conductivity of air based on t_{f_i} in Btu/hr. ft. °R

24

$$t_{f_i} \equiv \left[2\, t_s + t_{in} + t_i \right] / 4 \; °F$$

An ALGOL program was written for the Burroughs 220 electronic digital computer to perform all of the calculations for each set of data.

CHAPTER II

TURBULENT FORCED CONVECTIVE HEAT TRANSFER

The experimental study to be discussed herein was concerned with the effect of a resonant acoustic field on turbulent forced convective heat transfer. The experimental system which was described in detail in Chapter I was used to perform the study. Heat transfer data were obtained for through flow Reynolds numbers from 19,800 to 64,600 and sound-pressure levels from no sound (no input to the vibration exciter) to 166.5 decibels.

Turbulent Forced Convection Without Sound

In order to accredit the experimental system the study was first concerned with turbulent forced convection without sound. The physical system under consideration was turbulent flow entering a heated section with a fully developed velocity profile and an isothermal temperature profile. The wall temperature was constant and it was some $107°$ F higher than the entering fluid temperature.

Latzko (5) in an analytical treatment of this problem obtained the following expressions (see also reference (6)) for the local and average heat transfer co-efficients:

$$h_x = B h_\infty \qquad (19)$$

$$\bar{h}_\ell = \left[1 + 0.067 \, Re^{0.25 \, D/\ell} \right] h_\infty, \quad \ell/D > 5 \qquad (20)$$

where $\quad B \equiv \left[1 + 0.1 \, \exp(-2.7 \, Re^{-0.25} \, x/D) \right. +$

$\qquad 0.9 \, \exp(-29.27 \, Re^{-0.25} \, x/D \quad -$

$\qquad 0.023 \, \exp(-31.96 \, Re^{-0.25} \, x/D) \left. \right],$

$h_\infty =$ heat transfer coefficient when both the thermal and the velocity profiles are fully developed

$x \; =$ distance from the thermal entrance to the position of interest

$\ell \; =$ length, measured from the thermal entrance, over which the heat transfer coefficient is averaged.

Boelter has proposed an alternate form for equation (20), namely

$$\bar{h}_\ell = \left[1 + K\, D/\ell \right] h_\infty , \quad \ell/D > 5 \tag{21}$$

He found from his experimental study (6) that $K \approx 1.4$.

In order to obtain a numerical value for either h_x or h_ℓ, an expression for h_∞ must be obtained. Of the many data correlations for h_∞, Colburn's (4) appeared to be the most reliable. Colburn's equation is

$$Nu_{\infty f} \equiv \frac{h_\infty D}{k_f} = 0.023\, Re_f^{0.8}\, Pr_f^{1/3} \tag{22}$$

where the subscript "f" indicates that the fluid properties are based on the film temperature. More recent correlations by Drexel (4) and Desmon (4) indicate that the constant 0.023 may be slightly large for air.

The local Nusselt numbers which were obtained in the present study are shown in Figure 12 as a function of distance from the thermal entrance. It was found from these data that the local Nusselt number was approximately equal to its asymptotic value when $x/D > \sim 20$ and Re was between 30,000 and 65,000. This is shown graphically in Figure 13. In Figure 13 the ratio of the local Nusselt number to its asymptotic value (i.e., Nu_{x_f}/Nu_{∞_f}) is shown as a function of x/D. There was no apparent effect of through flow Reynolds number on this ratio for Reynolds number between 30,000 and 65,000. If by definition $F \equiv Nu_x/Nu_\infty$ then

$$Nu_{x_f} = F \cdot Nu_{\infty f} \tag{23}$$

when $x/D > 1.5$ and

$$30,000 \leq Re < 65,000.$$

The data for $Nu_{\infty f}$ were correlated by assuming the form of Colburn's equation, i.e.,

$$Nu_{\infty f} = C\, Re_f^{0.8}\, Pr_f^{1/3} \tag{24}$$

27
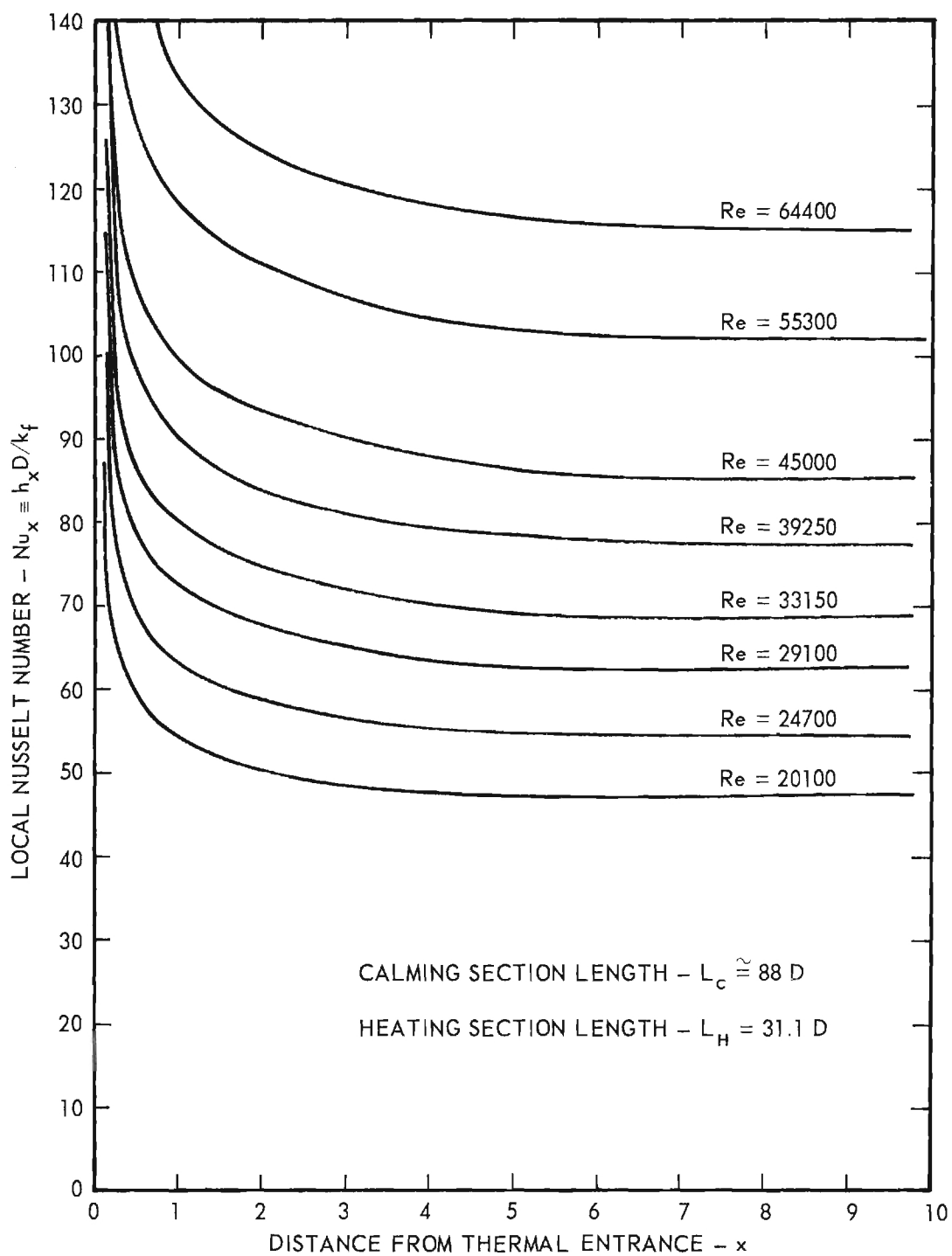
Figure 12. Local Nusselt Number Versus x.

28
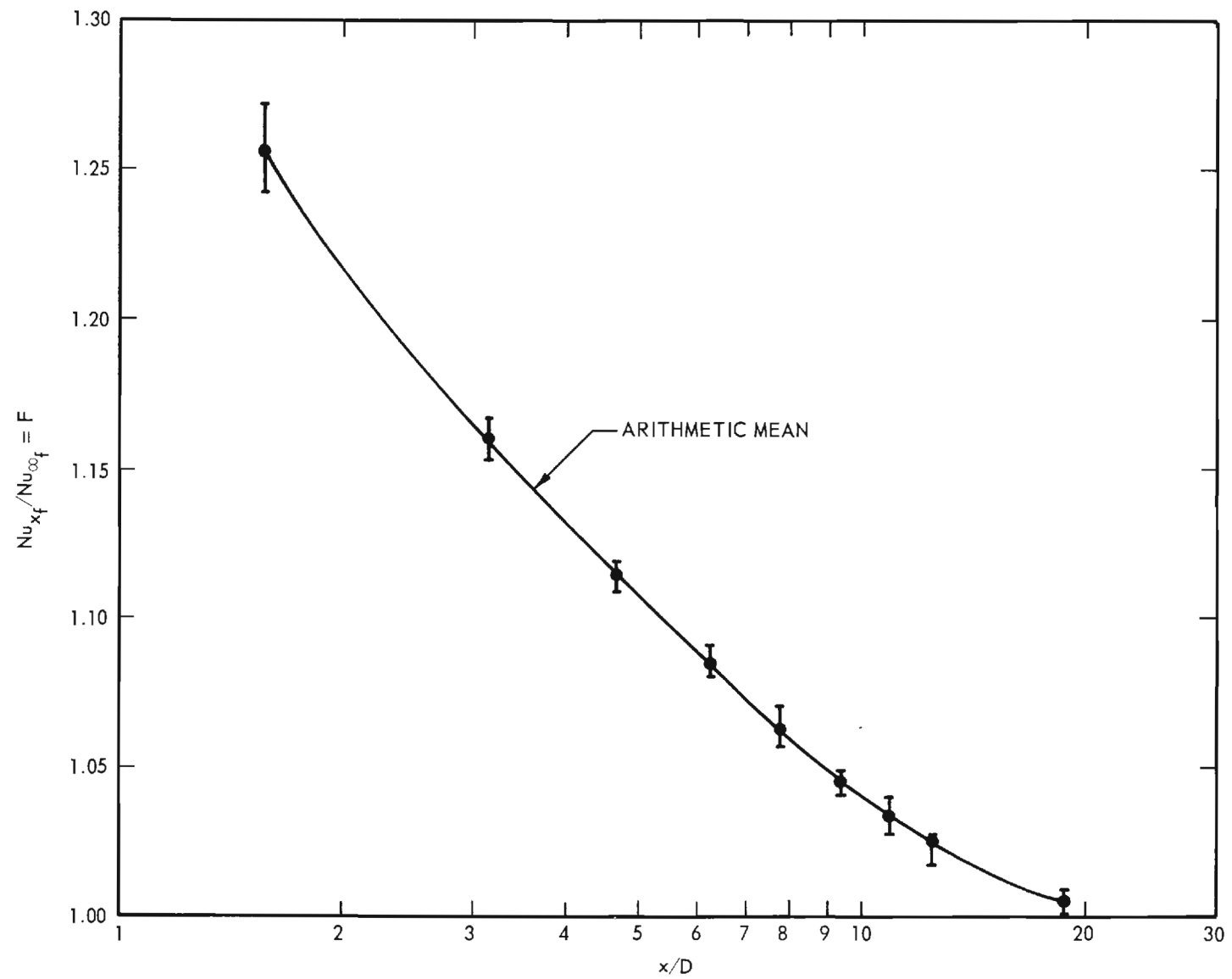
Figure 13. Ratio of Local Nusselt Number to Asymptotic Value Versus x/D.

and then solving for the constant "C". The values of the Colburn Coefficient "C" which were obtained are shown in Table III. It is clear from this table that the Colburn coefficient depends upon the Reynolds number when $Re < \sim$ 39,000, but is a constant when $Re > \sim$ 39,000. Thus for large Reynolds numbers

$$\text{Nu}_{\infty_f} = 0.0197 \ \text{Re}_f^{0.8} \ \text{Pr}_f^{1/3} \tag{25}$$

and, therefore,

$$\text{Nu}_{x_f} = 0.0197 \ F \ \text{Re}_f^{0.8} \ \text{Pr}_f^{1/3} \tag{26}$$

Table III. Colburn Type Coefficients

Re	20,1000	24,700	33,150	39,250	45,000	55,300	64,400
C	0.0208	0.0202	0.0200	0.0197	0.0196	0.0197	0.0197

Latzko's analytical prediction of the local heat transfer coefficient (Nusselt number) was found to be unsatisfactory since his equation (equation (19)) predicted local values which were more than ten percent low for small values of x/D.

The average Nusselt number data were not satisfactorily correlated by equation (20) since it also predicted low values of Nu_ℓ. Boelter's equation (equation (21)), however, correlated the data to within plus 1/2 percent and minus two percent with $K = 1.4$. That is,

$$\text{Nu}_\ell \equiv h_\ell \ D/k_f = \left[1 + 1.4 \ D/\ell \right] \text{Nu}_{\infty_f}, \quad \ell/D > 5 \tag{27}$$

where

$$\text{Nu}_{\infty_f} = 0.0197 \ \text{Re}_f^{0.8} \ \text{Pr}_f^{1/3} \ \text{and} \tag{25}$$

$$39,200 < \text{Re} \leq 64,400$$

The actual experimental data are compared with values calculated from equation (27) in Figure 14. It should be noted that there is a definite trend to the deviation of the data from the correlation equation as a function of ℓ/D. Even though a more complex function of ℓ/D than the assumed linear one is indicated, it seems, from an engineering point of view, to be hardly worth the added complication.

Turbulent Forced Convection With Sound

Experimental forced convection data were taken for turbulent flow ($19,800 \leq \text{Re} \leq 64,400$) under the influence of a resonant acoustic field. A resonant
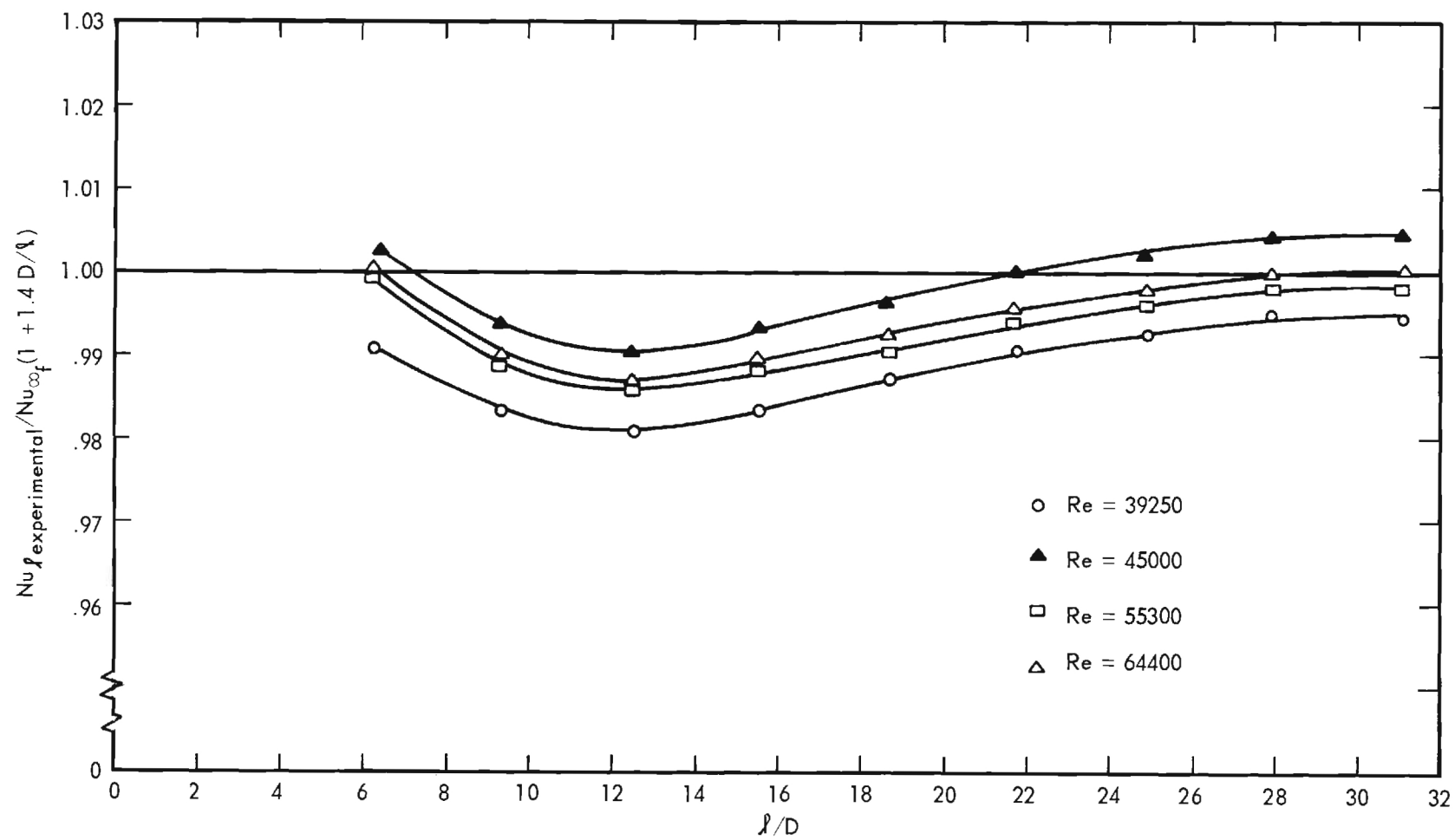
Figure 14.   Comparison of Experimental and Calculated Nusselt Numbers.

frequency of approximately 90 cps was used since this frequency (harmonic) produced the best combination of maximum sound-pressure level (166.5 db) and detailed local heat transfer data. Typical data are shown graphically in Figures 15 through 22. The positions of the velocity nodes and antinodes are indicated on each figure.

It is interesting to note that the sound field serves only as a local depressant on the heat transfer coefficient. The position of maximum depression moved toward the thermal entrance for increasing Reynolds number, but it became stationary at $x \approx 4.5$ ft. for $Re > \sim 30,000$.

A plot of the nondimensional deviation of the Nusselt number from its no-sound value versus distance from the thermal entrance is given in Figure 23 for typical combinations of sound-pressure level and through flow Reynolds number. The data are not sufficiently accurate to determine the exact form of this deviation but it appears to deviate as the absolute value of the cosine of position to a power between one and two.

The percent of maximum deviation of the local Nusselt number from its local value is shown in Figure 24 as a function of the dimensionless parameter $U_o^2/U c_o$, where U_o is the maximum sound particle velocity, U is the mean through flow velocity and c_o is the speed of sound. These data which are given in Table IV are correlated for Reynolds numbers above 30,000 by

$$\frac{\Delta Nu_{x_{max}}}{Nu_{x_{no-sound}}} = 2.45 \, (U_o^2/U c_o). \tag{28}$$

Table IV. Maximum Deviation in Local Nusselt Number

Re	U_o	U	$U_o^2/U c_o \cdot 1000$	$\Delta Nu_x/Nu_{x_{no-sound}} \cdot 100$
45000	35.54	26.21	41.40	11.06
45300	29.22	26.28	27.94	6.98
47900	34.72	27.99	37.04	10.04
43600	18.44	25.74	11.32	2.82
44200	23.22	26.26	17.65	4.80
39500	23.22	23.29	19.93	4.92
39800	28.90	23.36	30.72	7.24
38400	36.41	22.51	50.70	12.00
38300	41.79	22.67	66.40	14.62
42700	41.78	25.23	58.76	14.03
64600	49.32	38.86	53.50	12.96
55000	48.20	32.93	60.30	14.96
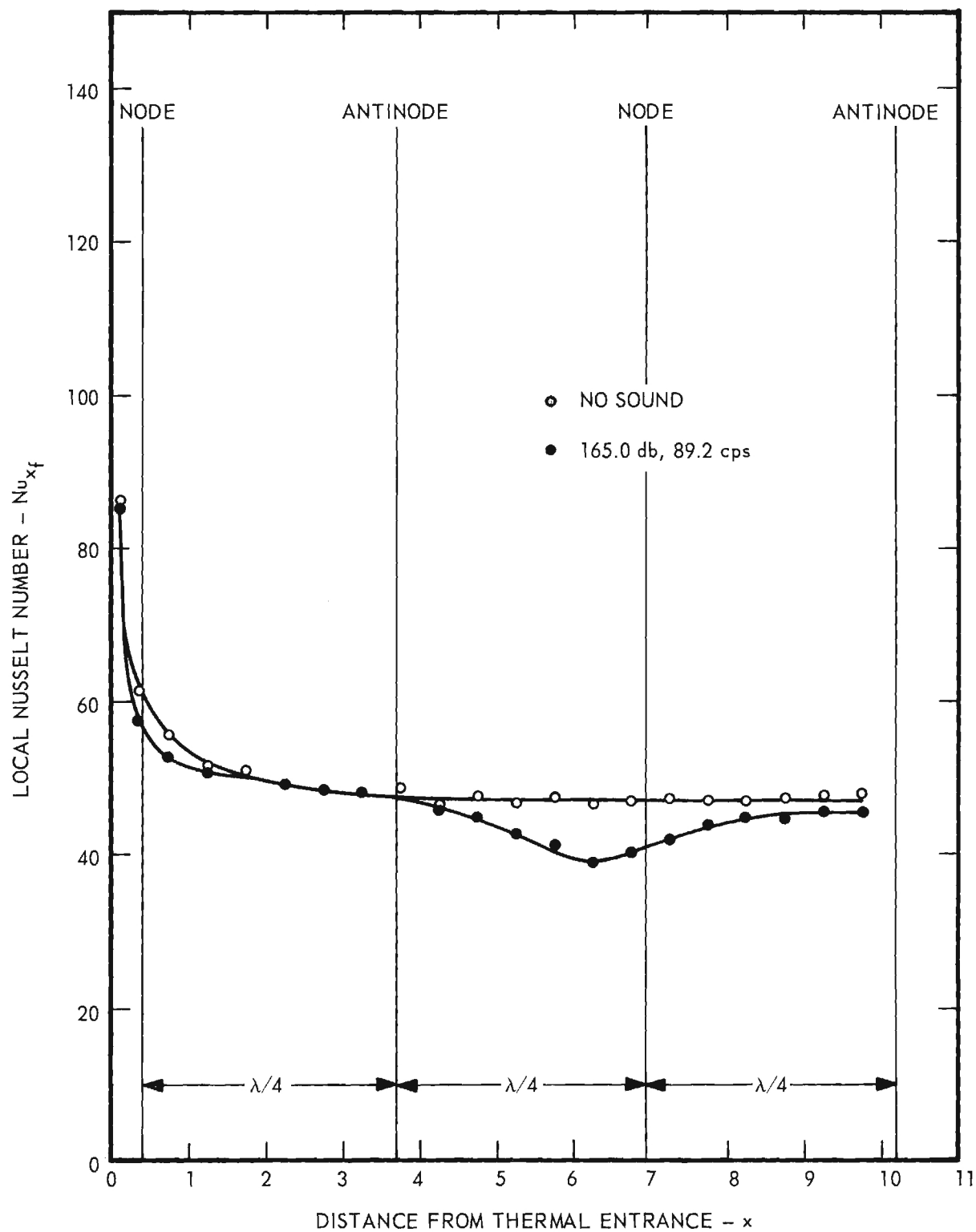
Figure 15. Nu_{x_f} Versus x for Re ≈ 19,800.
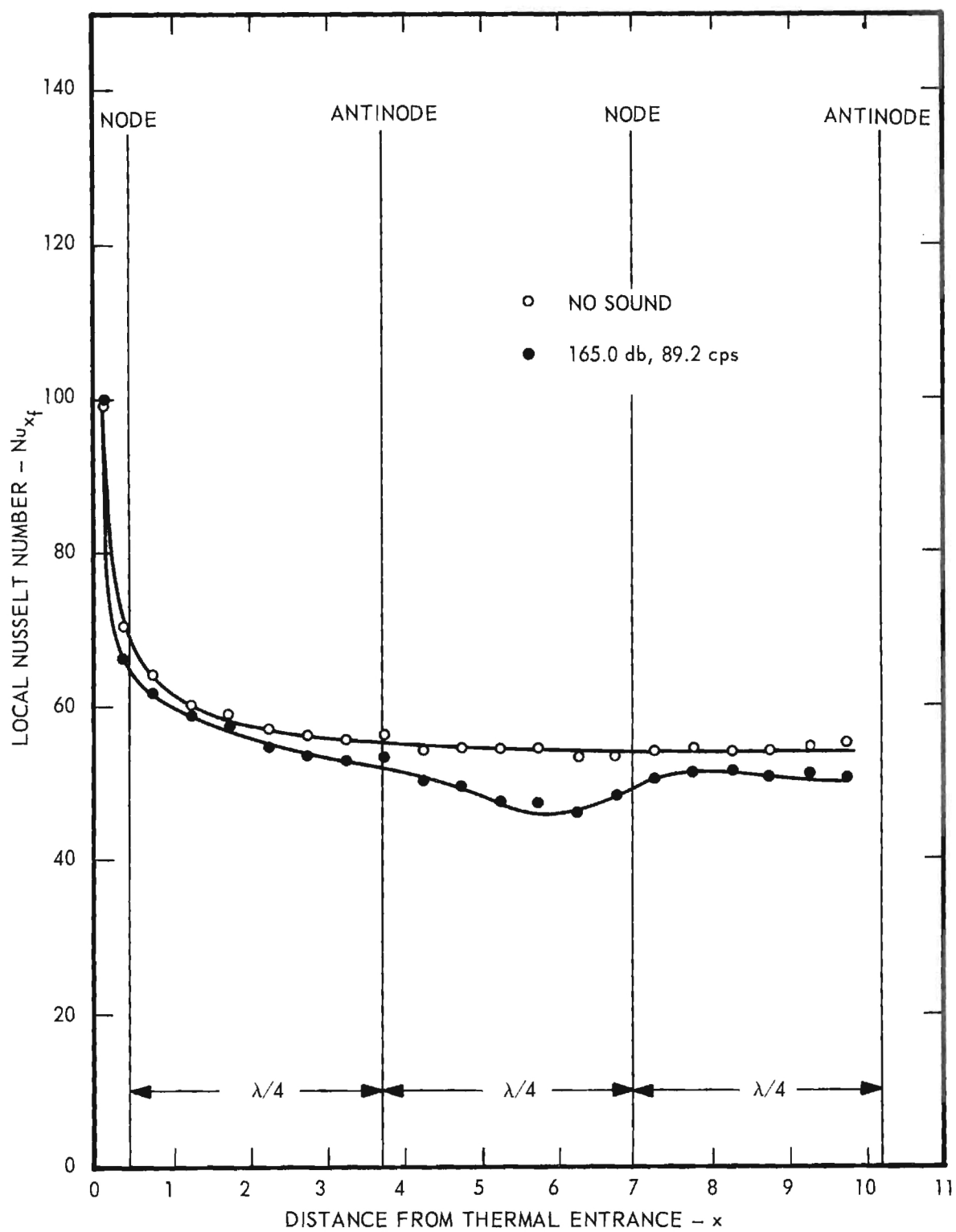
Figure 16. Nu_{x_f} Versus x for Re $\approx$ 24,300.
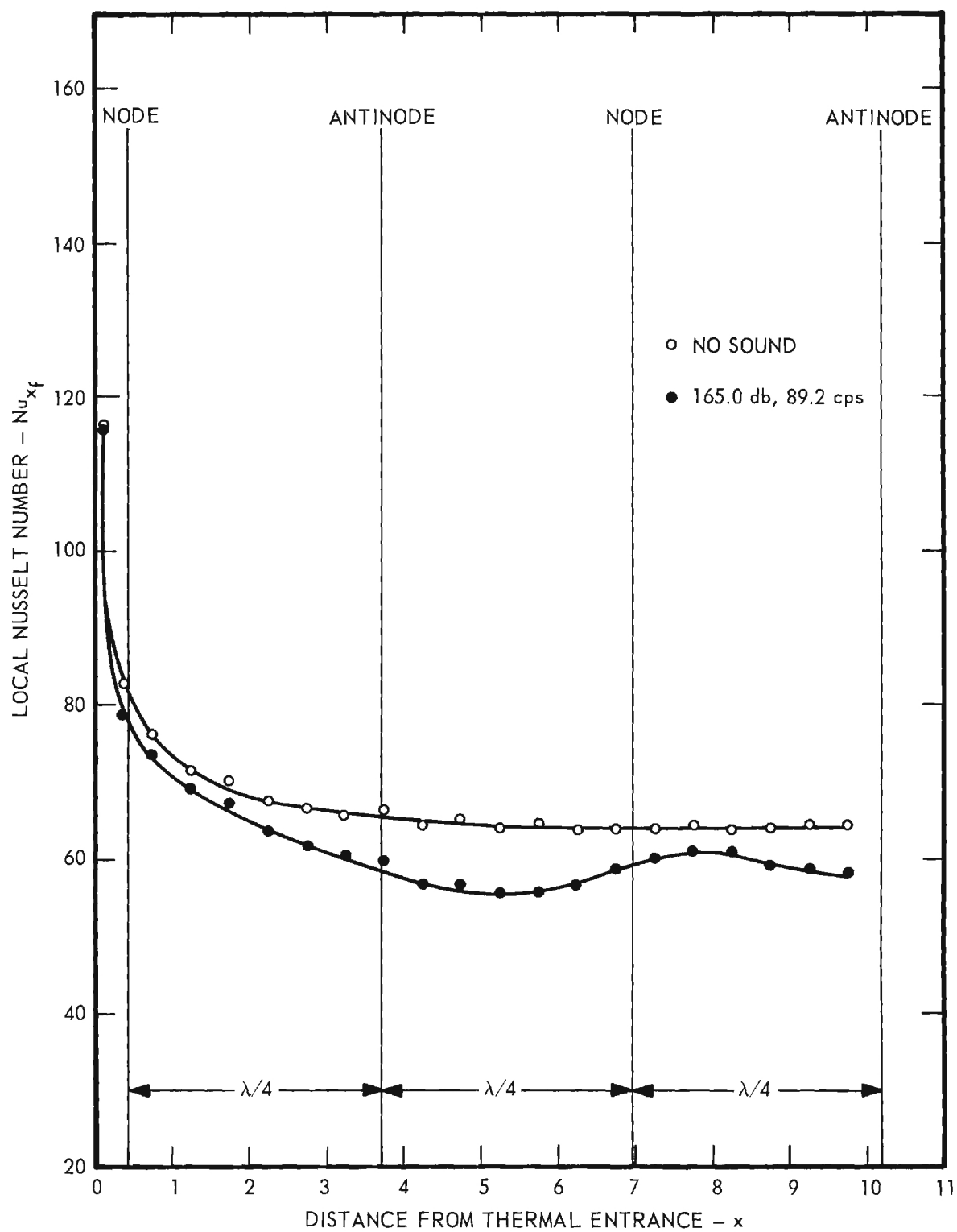
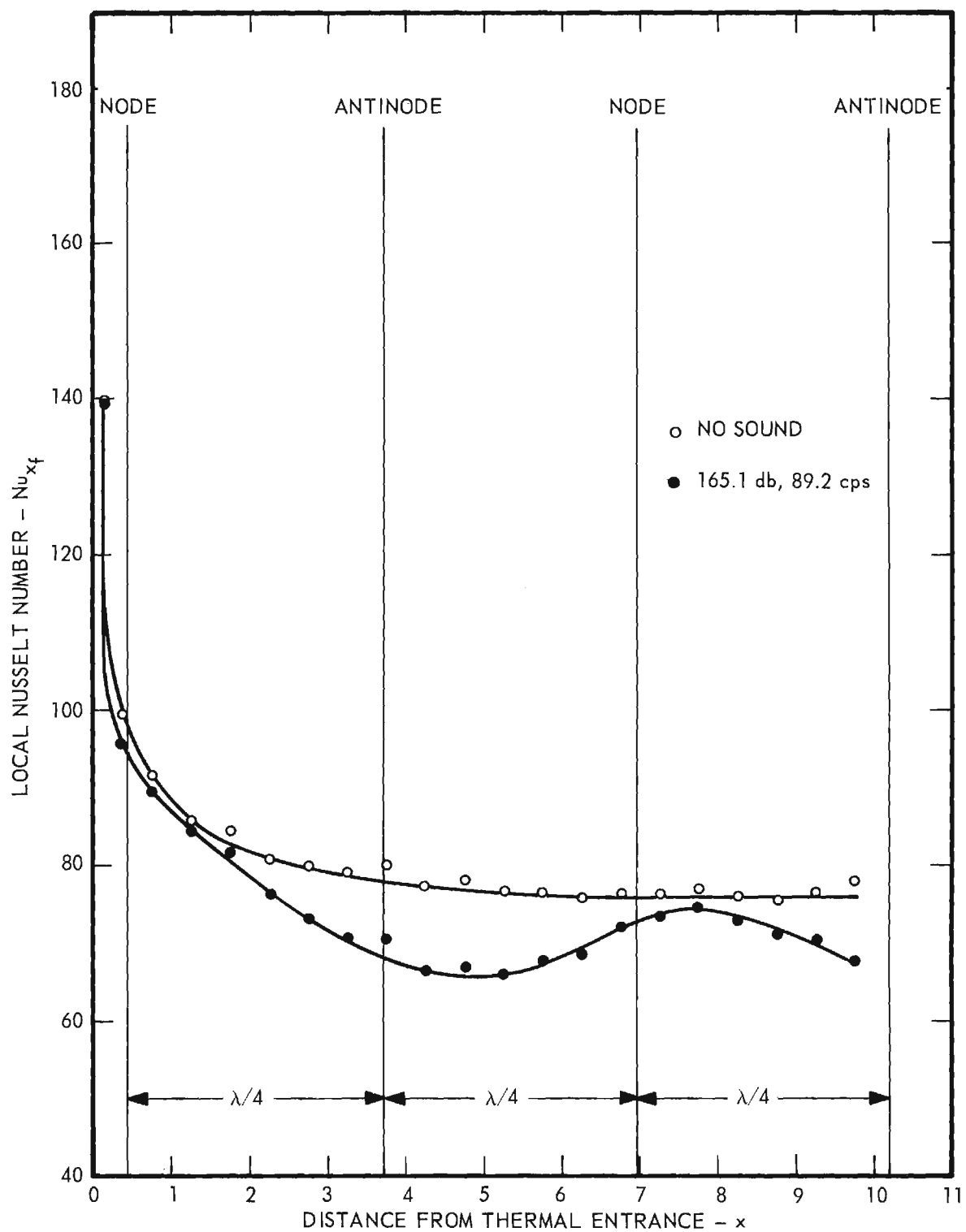Figure 17. Nu_{x_f} Versus x for Re $\approx$ 29,700.

Figure 18. Nu_{x_f} Versus x for Re $\approx$ 33,000.
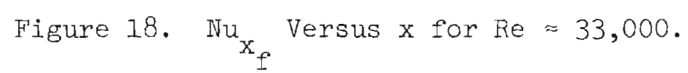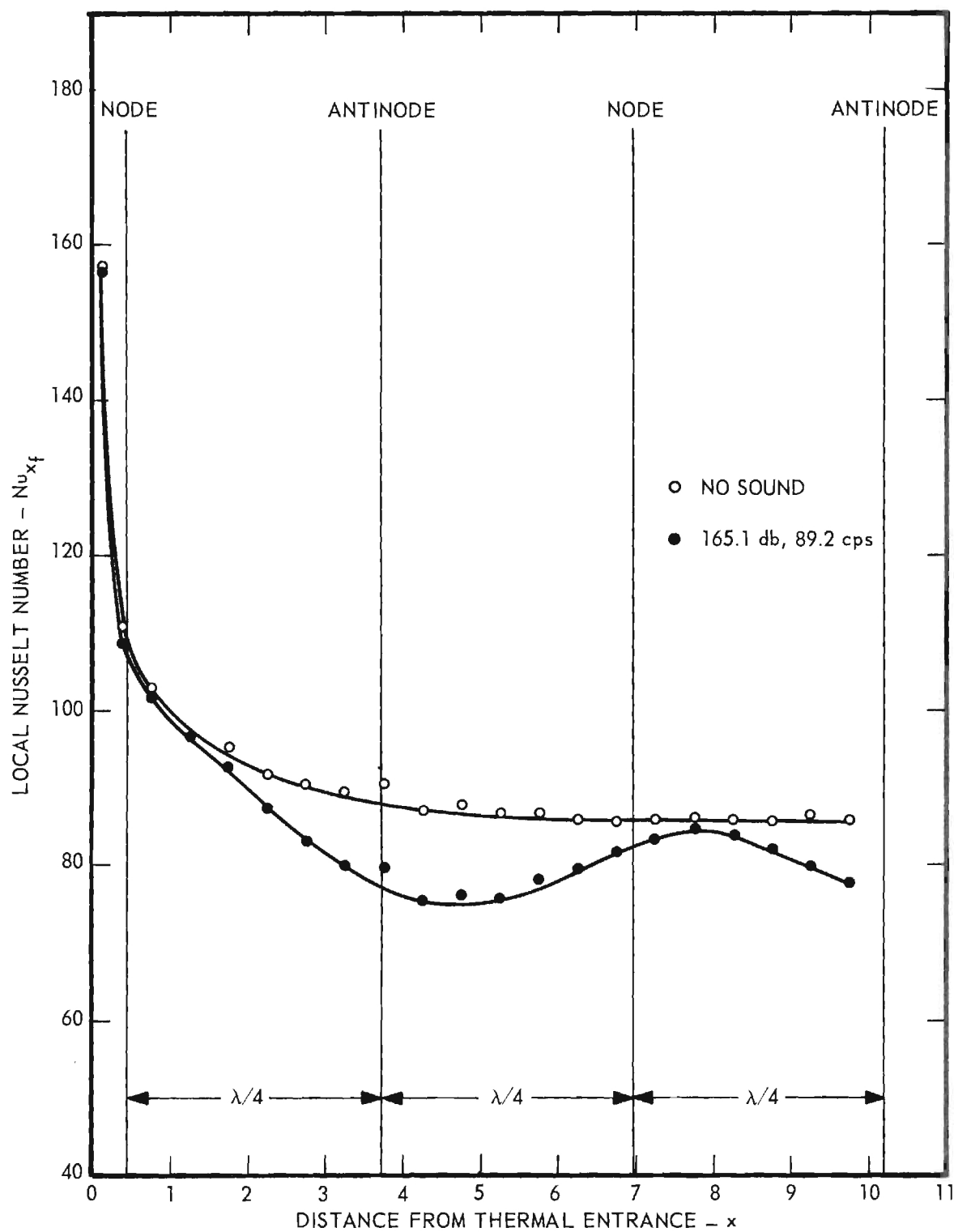
Figure 19. Nu_{x_f} Versus x for Re ≈ 38,300.
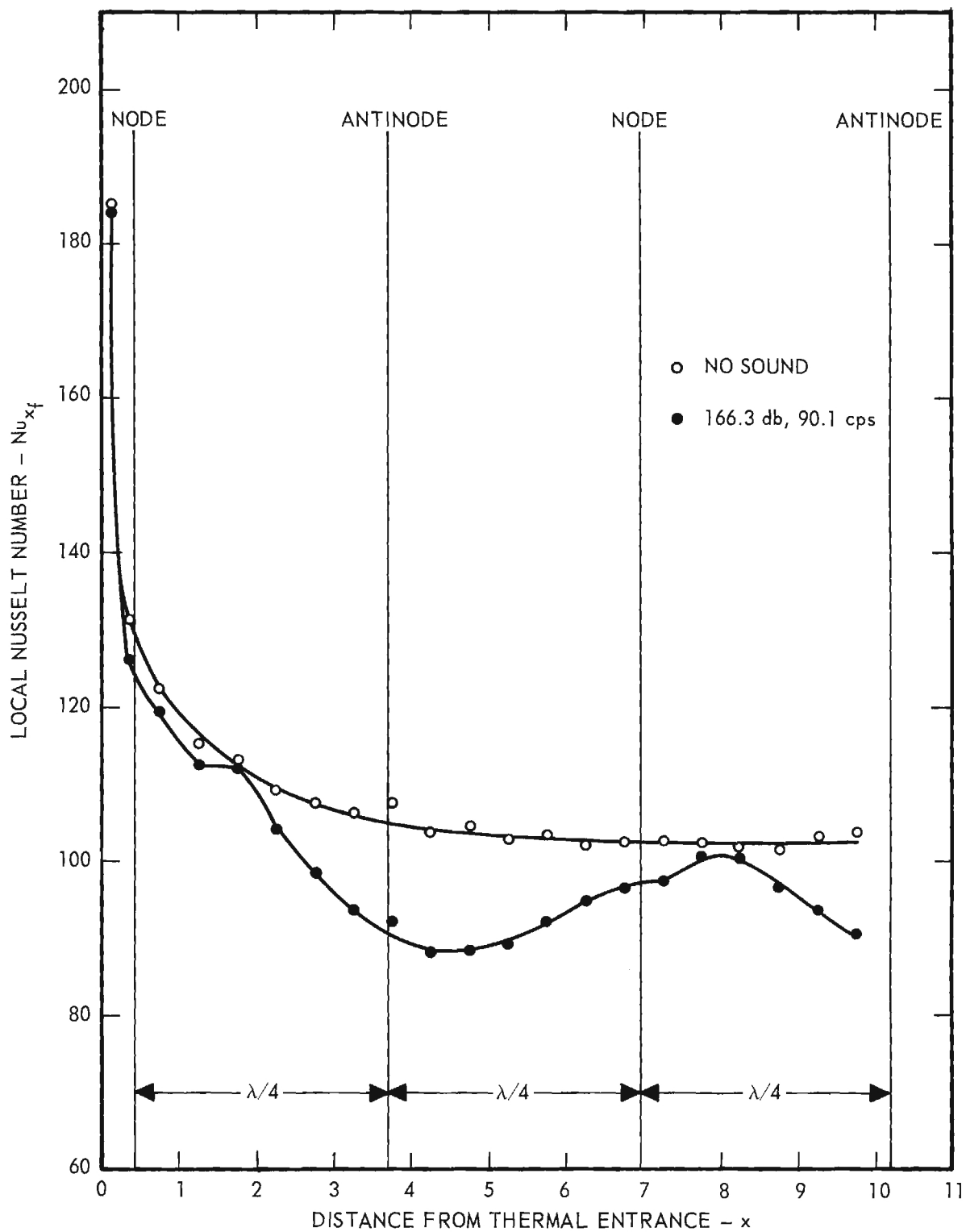
Figure 20. Nu_{x_f} Versus x for Re ≈ 45,000.

Figure 21. Nu_{x_f} Versus x for Re $\approx$ 55,000.

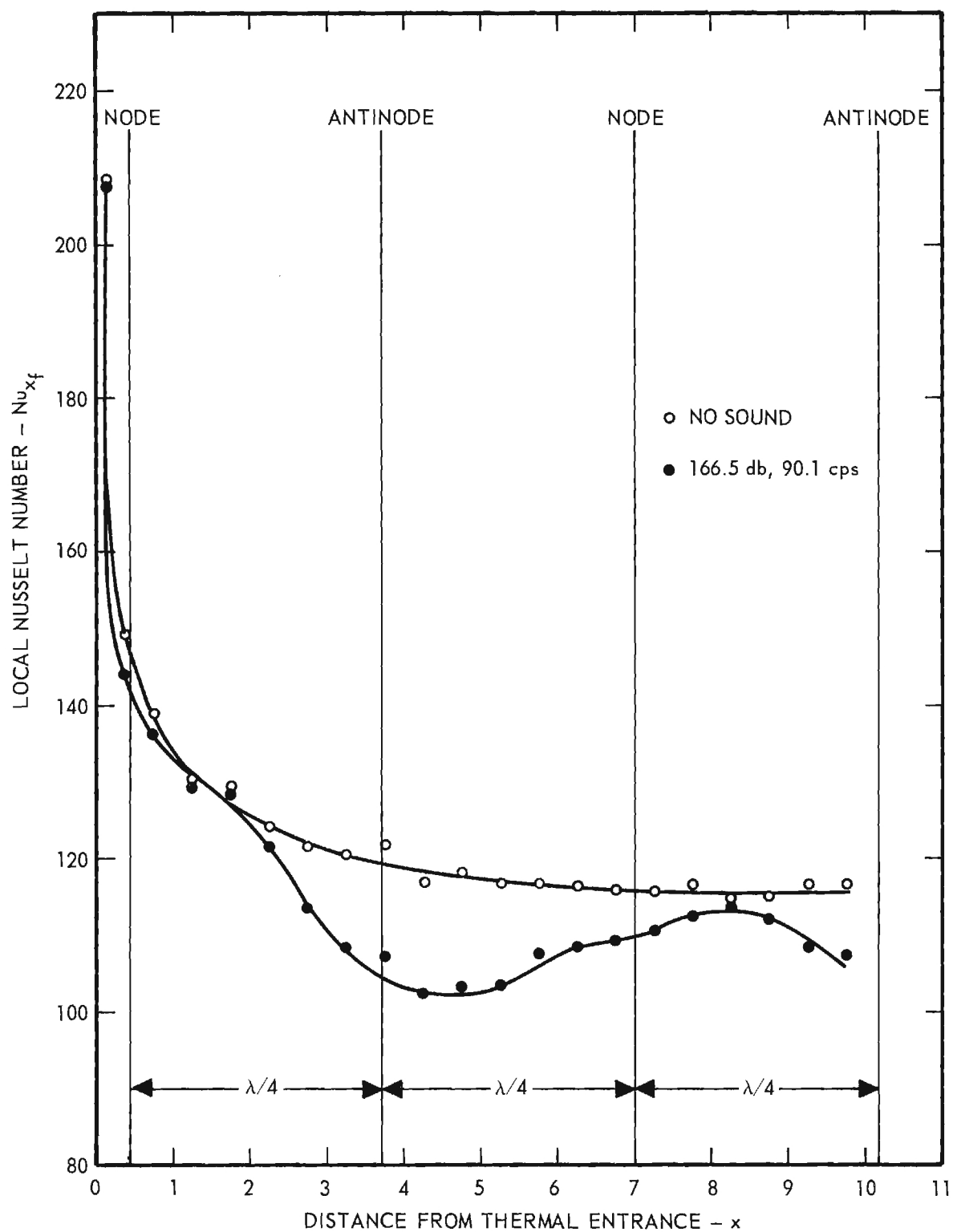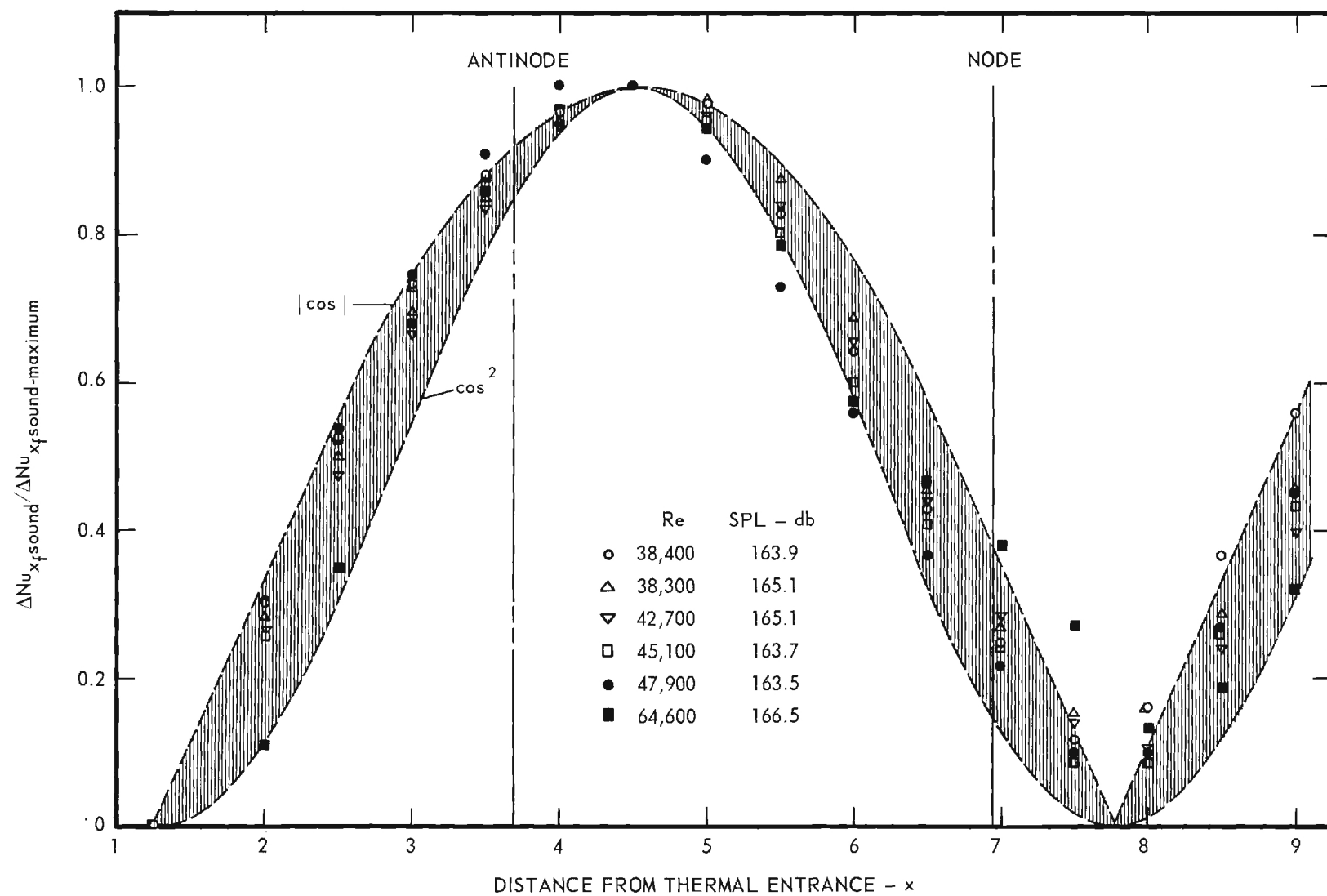Figure 22. Nu_{x_f} Versus x for Re $\approx$ 64,600.

Figure 23.   Nondimensional Deviation of Nusselt Number from No Sound Value Versus Distance
              from Thermal Entrance.
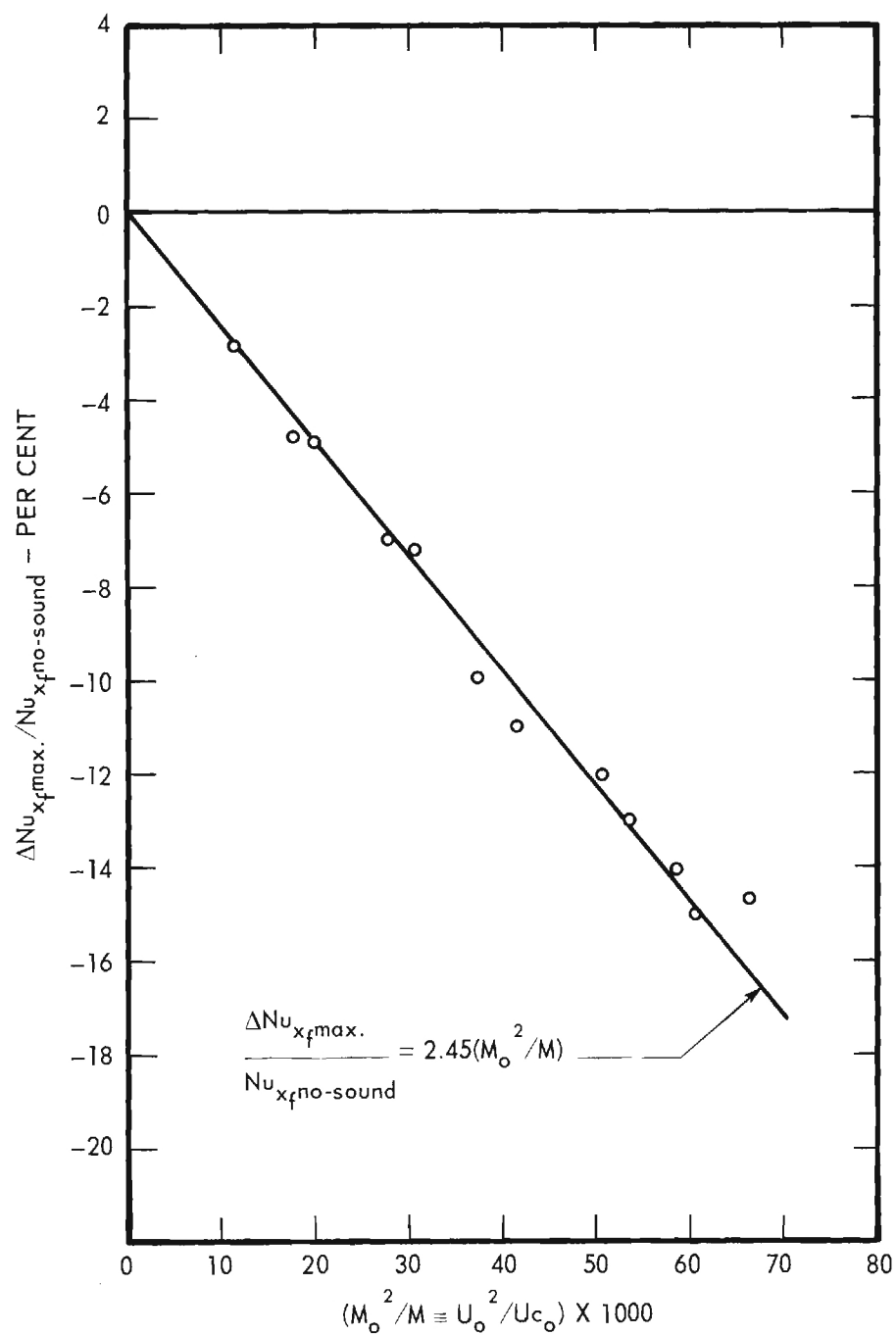
Figure 24. Ratio of Maximum Deviation of Nusselt Number to No Sound Nusselt Number Versus M_o^2/M. (Re > 30,000).

42

Since the maximum percent deviation in the local Nusselt number is a linear function of U_o^2/Uc_o it is plausible to assume that $\Delta Nu_x/\Delta Nu_{x_{max}}$ varies as the square of the cosine of axial position with a suitable phase shift. In other words the percent deviation in the local Nusselt number is a linear function of the square of the local sound particle velocity. Based on this premise, the correlation equation becomes

$$Nu_{x_{sound}} = \left[1 - 2.45 \, (U_o^2/Uc_o) \cos^2 \left(\frac{2\pi z}{\lambda} - \frac{\pi}{8} \right) \right] Nu_{x_{no-sound}} \qquad (29)$$

where z is axial position measured from a velocity antinode. Thus the position of the maximum deviation in Nu_x lags the position of the velocity antinode by a distance of $\lambda/16$.

It should be noted that there does not seem to be a sound threshold level below which there is no effect due to sound. An artificial level, however, can be defined by neglecting maximum deviations of less than one percent or, correspondingly, values of U_o^2/Uc_o less than 4.08×10^{-3}.

Equation (29) was based on data for a single frequency (wave length) and, therefore, no contribution of frequency was determined.

43

CHAPTER III

LAMINAR FORCED CONVECTIVE HEAT TRANSFER

The analytical and experimental study to be discussed in this chapter was concerned with the effect of a resonant acoustic field on laminar forced convective heat transfer. More details of the work can be determined from reference 7. Because of the complexity of the round tube solution of the energy equation, the work herein concerns itself with laminar forced convection due to the unsteady flow of a viscous, compressible fluid between horizontal parallel plates as illustrated in Figure 25. An isothermal entrance region is assumed to be of sufficient length that at the start of the heat transfer region (thermal entrance) the velocity profile is fully developed and the temperature profile is isothermal at T_o. In the present context, the term "fully developed" is used in the sense that the flow, i.e., the velocity profile, is repeated in half wave length sections. Heat generation and conduction within the duct walls are neglected so that a known boundary condition may be specified at the inside of the duct wall. The condition selected is a constant wall temperature; thus heat transfer results from the step increase in wall temperature from T_o to T_w at $x = 0$.

The present investigation assumes the flow to be viscous, compressible, unsteady, and two-dimensional. These assumptions are the major differences between this work and previous investigations (8, 9, 10, 11, and 12).

Development of Mathematical Model

The mathematical model of the problem, as shown in Figure 25, consists of "fully-developed" laminar flow between infinite parallel plates which are separated by a distance 2a. In order to develop the mathematics to describe the selected model the following assumptions were made:

1. The fluid and the parallel plates are assumed to be at a constant temperature throughout the hydrodynamic entrance length; i.e., for $x < 0$. The walls of the channel in the entrance length are assumed to be maintained at a fixed temperature, T_o. The channel walls in the heated section are also assumed to be at a constant temperature, T_w, where T_w is greater than T_o.

2. The fluid is assumed to be flowing laminarly in the positive x-direction. The flow is assumed to be independent of the z-direction, but due to the secondary flow caused by the impressed acoustic field there is a y-component of velocity; hence, the flow is two-dimensional.

3. The fluid properties - viscosity, specific heat, and thermal conductivity - are constant.

4. The temperature variations in the gas are assumed to be small enough so that free convection effects may be neglected.
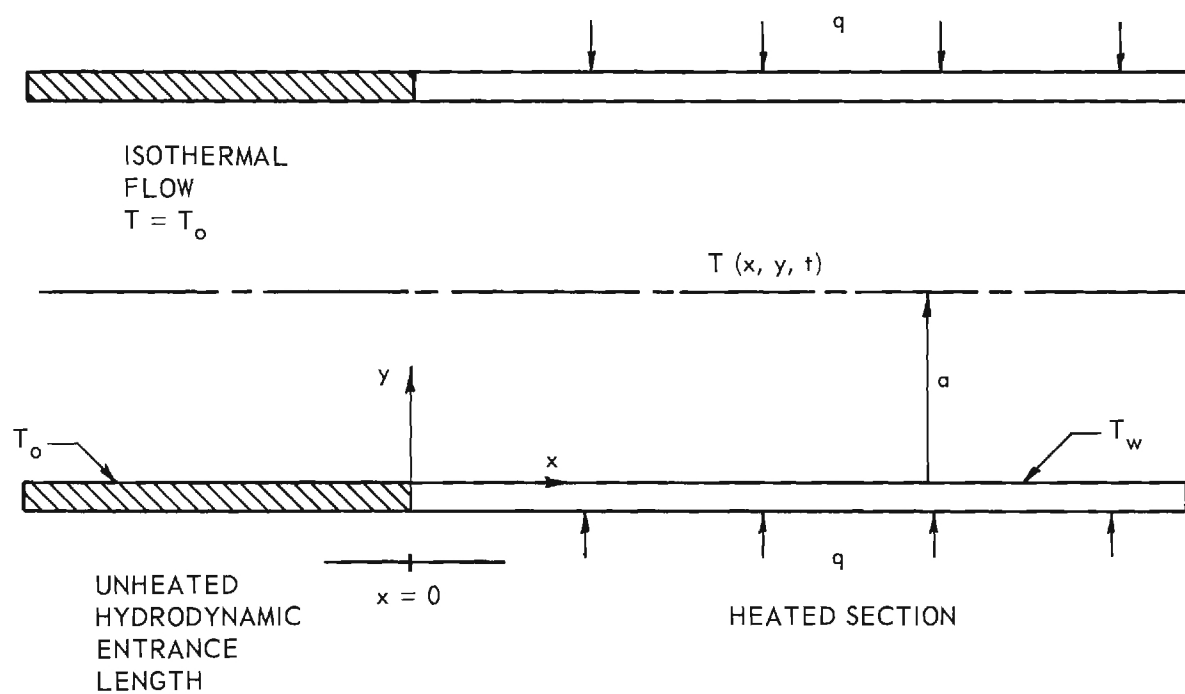
Figure 25.   Flow Between Parallel Plates With an Isothermal Entrance Region
and a Heat Transfer Region With Constant Wall Temperature.

Governing Equations and Boundary Conditions

The problem is described mathematically by the following basic equations together with their associated boundary conditions:

Continuity

$$\frac{\partial \rho}{\partial t} + \frac{\partial}{\partial x} (\rho u) + \frac{\partial}{\partial y} (\rho v) = 0$$

$$\int_{0}^{a} \overline{\rho u} \; dy = \text{Constant}$$

Momentum

$$\frac{\partial u}{\partial t} + u \frac{\partial u}{\partial x} + v \frac{\partial u}{\partial y} = -\frac{1}{\rho} \frac{\partial p}{\partial x} +$$

$$\frac{1}{\rho} \frac{\partial}{\partial x} \left\{ \mu \left[2 \frac{\partial u}{\partial x} - \frac{2}{3} \left(\frac{\partial u}{\partial x} + \frac{\partial v}{\partial y} \right) \right] \right\} +$$

$$\frac{1}{\rho} \frac{\partial}{\partial y} \left\{ \mu \left[\frac{\partial u}{\partial y} + \frac{\partial v}{\partial x} \right] \right\}$$

$$\frac{\partial v}{\partial t} + u \frac{\partial v}{\partial x} + v \frac{\partial v}{\partial y} = -\frac{1}{\rho} \frac{\partial p}{\partial y} +$$

$$\frac{1}{\rho} \frac{\partial}{\partial y} \left\{ \mu \left[2 \frac{\partial v}{\partial y} - \frac{2}{3} \left(\frac{\partial u}{\partial x} + \frac{\partial v}{\partial y} \right) \right] \right\} +$$

$$\frac{1}{\rho} \frac{\partial}{\partial x} \left[\mu \left(\frac{\partial u}{\partial y} + \frac{\partial v}{\partial x} \right) \right]$$

The boundary conditions for the momentum equations are

$$u(x, 0, t) = v(x, 0, t) \equiv 0$$

$$\frac{\partial u}{\partial y} = 0; \quad y = a, \text{ all } x \text{ and } t$$

$$v(x, a, t) = 0$$

46

Energy

$$\rho \, c_p \, \frac{DT}{Dt} = \frac{Dp}{Dt} + k \, \nabla^2 T + \mu \, \Phi$$

where

$$\Phi = 2 \left[\left(\frac{\partial u}{\partial x}\right)^2 + \left(\frac{\partial v}{\partial y}\right)^2 \right] + \left(\frac{\partial v}{\partial x}\right) + \frac{\partial u}{\partial y}\right)^2 - \frac{2}{3} \left(\frac{\partial u}{\partial x} + \frac{\partial u}{\partial y}\right)^2$$

The boundary conditions for the energy equation are

$$T(x,0,t) = T_w = \text{Constant}, \ x \geq 0$$

$$\frac{\partial T}{\partial y} = 0; \ y = a, \ \text{all } x \text{ and } t$$

$$T(0,y,t) = T_o, \ 0 < y < 2a$$

Reduction of the Governing Equations

Since Purdy (13) has solved the continuity and momentum equations corresponding to this problem, his solution for the velocity and pressure fields will be used to determine the coefficients in the energy equation. The validity of this approach is based upon one of the previous assumptions, i.e., that free convection effects are negligible.

In addition to the assumptions previously made the following assumptions are necessary:

5. The temperature is represented by the sum of a time-dependent component and a time-mean component. Purdy (13) in his analysis of the velocity field formed by resonant acoustic vibrations in a parallel plate channel, assumed that the density, pressure, and velocity components could be represented in this manner.

6. The energy equation can be reduced by an order of magnitude analysis and made dimensionless as indicated in reference 7.

Using the above assumptions and performing the indicated operations, the following equation for the dimensionless time-mean temperature is obtained:

$$\frac{\partial^2 \overline{T}'}{\partial \overline{y}'^2} - \frac{2}{\pi} \Pr_o (M_o a')^2 \, \overline{u}' \, \frac{\partial \overline{T}'}{\partial x'} - \frac{1}{\pi} \Pr_o (M_o a')^2 \, \overline{v}' \, \frac{\partial \overline{T}'}{\partial \overline{y}'} = 0 \tag{30}$$

where the time-dependent temperature is assumed to be of the form,

$$T_1(x,y,t) = \mathrm{Re} \left[\sum_{n=1}^{\infty} T_{1n}(x,y) \exp(-inwt) \right] \tag{31}$$

By performing the above operations the present analysis is reduced to the problem of finding a solution to equation (30).

Solution of the Temperature Field

The foregoing assumptions and reductions give a linear partial differential equation for the dimensionless time-mean temperature and a system of defining equations for the components $T_{1n}(x,y)$ which represent the time-dependent temperature (equation (31)). Purdy's (13) solution for the velocity components, $\bar{u}'(x',\bar{y}')$ and $\bar{v}'(x',\bar{y}')$, indicates the complexity of equation (30).

An attempt was made to solve equation (30) by a closed form solution without success. Separation of variables, power series, and Fourier-type series were considered. Finally a numerical solution was obtained by approximating the derivatives with finite differences. The total number of gridpoints used was 200,000.

Figures 26 and 27 show typical temperature distributions, one case is with sound and the other is without sound. As can be seen from the figures the effect of sound upon the dimensionless temperature is much less pronounced than in the case of the velocity profile. In fact, without comparing actual values, it is difficult to discern any effects at all on the temperature. However, if the two figures are compared quantitatively, it will be found that the profiles with sound do deviate from the profiles without sound.

Analytical Heat Transfer Results. After the temperature distribution had been determined it was used to calculate the rate of heat transfer through the channel wall into the fluid. The heat transfer calculations are based on the time-mean temperature since any heat transfer which is due to the fluctuations of the time-dependent temperature will average out to zero over a complete cycle.

The local convective heat transfer coefficient as defined by the energy equation, neglecting changes in kinetic energy, is

$$h A \Delta T_{am} = \dot{m}\, c_p \Delta T_B$$

where

A	=	heat transfer area
ΔT_{am}	=	arithmetic mean temperature difference
$\dot{m}$	=	mass flow rate
c_p	=	constant pressure specific heat
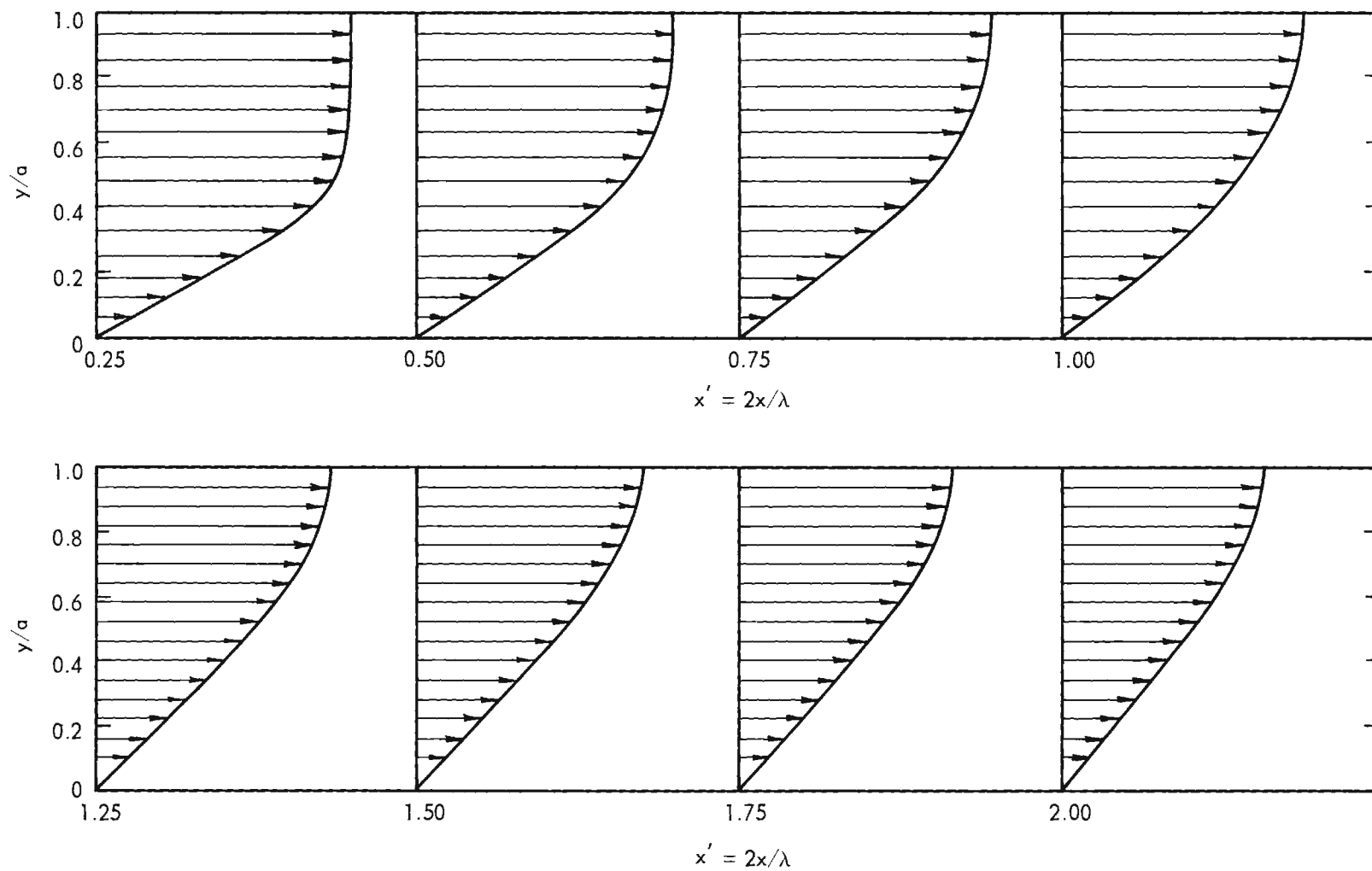
Figure 26. Typical Dimensionless Temperature Profiles, $\dfrac{T_w - \bar{T}}{T_w - T_o}$, for the Case of No Sound.
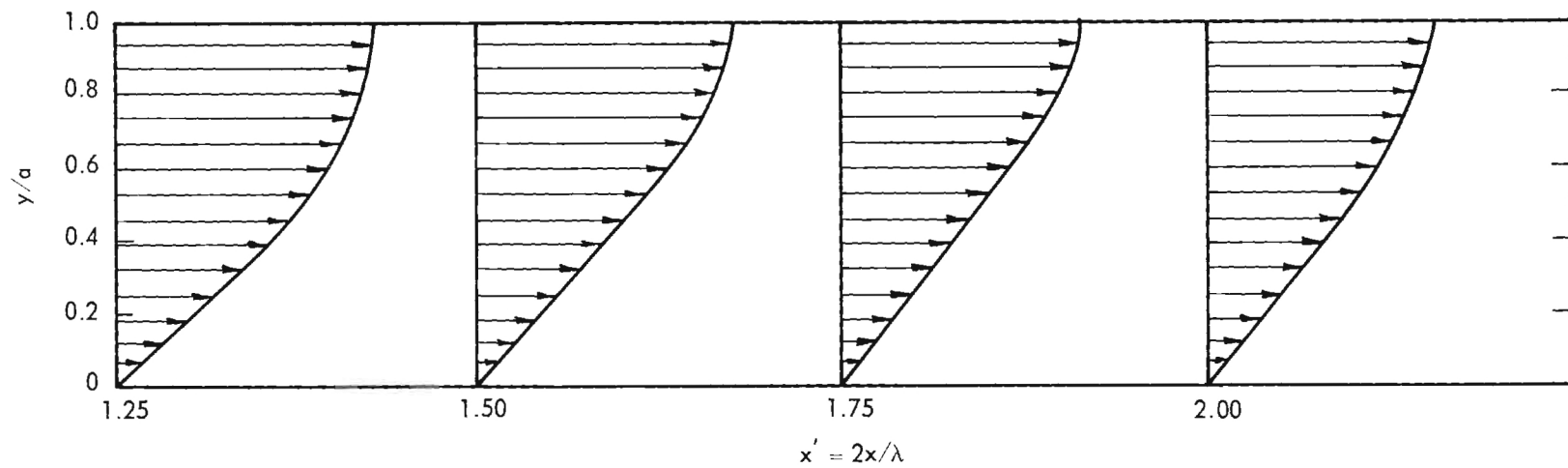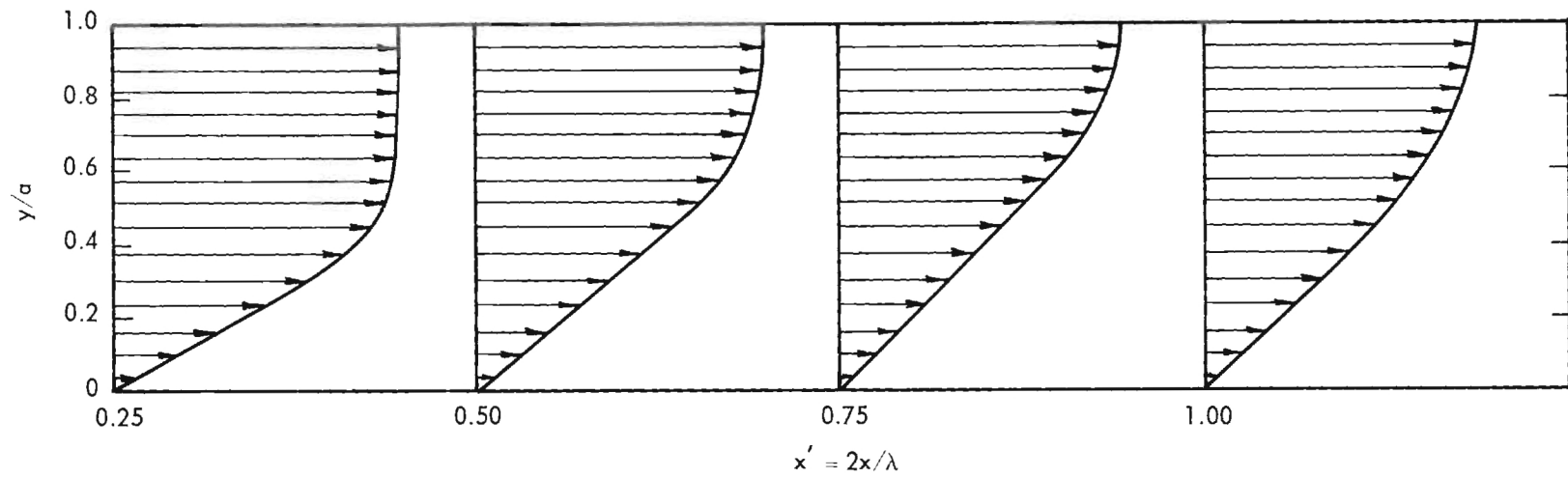
Figure 27. Typical Dimensionless Temperature Profiles, $\dfrac{T_w - \bar{T}}{T_w - T_o}$, with Resonant Accoustic Field Impressed upon the Flow.

ΔT_B =   change in bulk temperature

h   =   local heat transfer coefficient.

In order to test the validity of the numerical technique used to solve the equation, several solutions were obtained for various through-flow rates without the presence of an acoustic field. The values of the average Nusselt number obtained are compared to the results of Norris and Streid (14) in Figure 28 and to Sellar, Tribus, and Klein (15) who have also solved the problem in Figure 29. The results appear to be in excellent agreement. In addition to the average Nusselt number, Sellars, Tribus, and Klein's results can be used to derive an equation for the local Nusselt numbers as a function of the parameter Φ. A comparison of the local Nusselt numbers of reference 15 with those of this investigation are given in Figure 30. The agreement is excellent.

A conclusion which can be drawn from the foregoing discussion is that the numerical solutions of this investigation for the average and local Nusselt numbers without an acoustic field agree well with published results in the literature.

In order to obtain a solution of equation (30) for the case of heat transfer with sound a slight modification in the technique proved to be necessary. It was found that the solution was extremely divergent when the methods used for the no-sound results were used without any modification. The problem of divergence was caused by the velocity $\bar{u}'(x',\bar{y}')$. Whenever this function was negative the system of equations became extremely difficult to handle and the results were rapidly divergent. This problem was avoided by forcing the velocity $\bar{u}'(x',\bar{y}')$ to be essentially zero in regions where it was actually negative (i.e., in a region containing a vortex.) (See Figure 31.) By making this simple modification to the numerical technique the problem of divergence ceased to be critical and a solution was obtained.

A logical question which should be asked at this point is how is the solution affected by the above modification of the velocity profile? This can be answered by referring to Figure 31 which shows a plot of the local Nusselt number as a function of x'. In the unshaded intervals of the figure the velocity profile was unaltered. As can be seen the values of heat transfer coefficient which were obtained form a smooth curve with no discernable discontinuities, and since the curve was plotted with only a small number of the actual points calculated, it seems reasonable to say that the alteration of the velocity profile does not alter the validity, or usefulness, of the results.

However, in order to obtain an additional check on the numerical procedure, a relaxation technique was employed. After integrating through the region of the vortex the temperatures thus obtained were used to calculate the residual at each grid point. Due to the limited storage space of the computer the mesh size used in the relaxation method was approximately ten times as large as the mesh size used for integration purposes. The residual at each grid point was then relaxed to zero by altering the temperature at the central grid point. After several iterations of the relaxation process the temperatures had
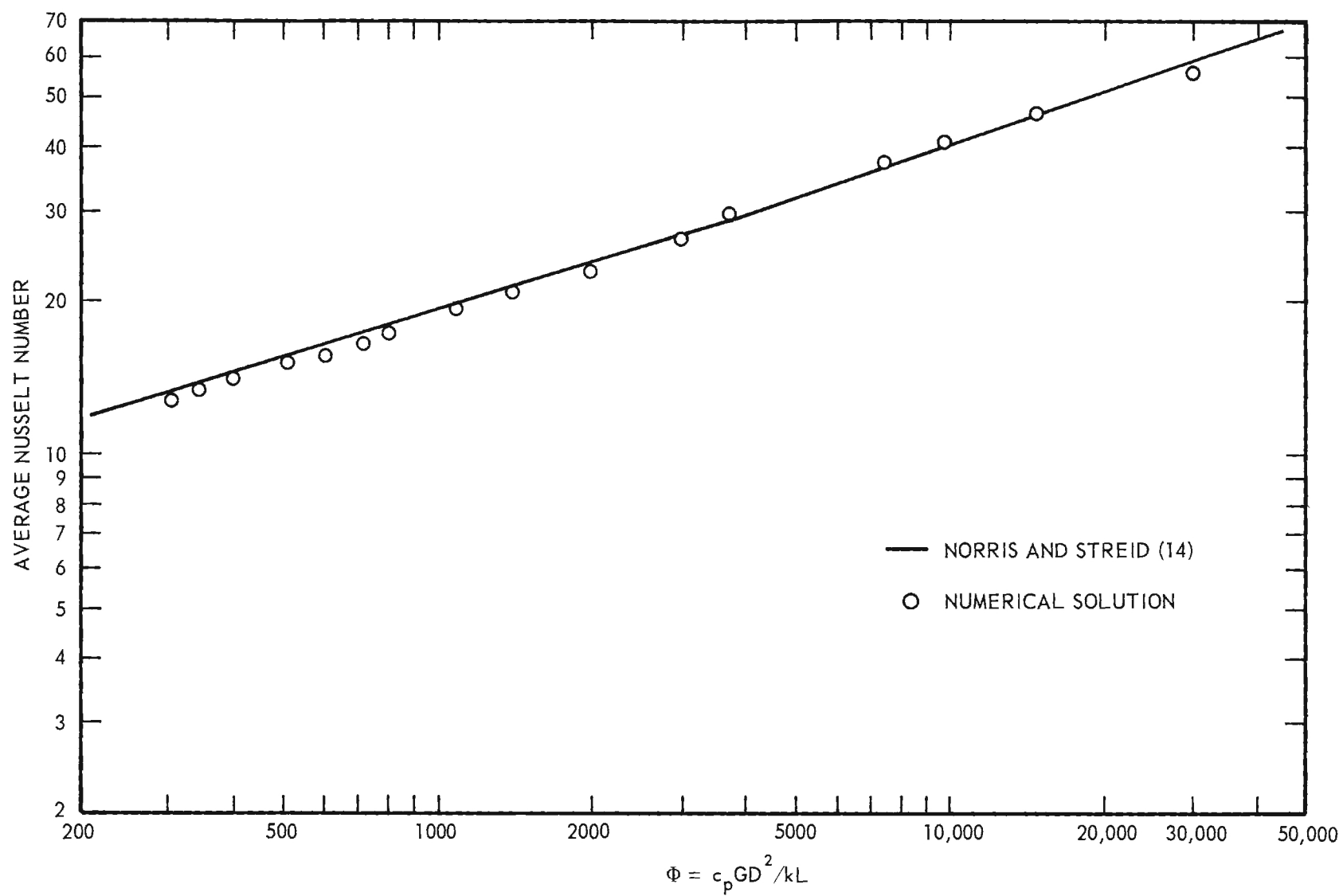
51

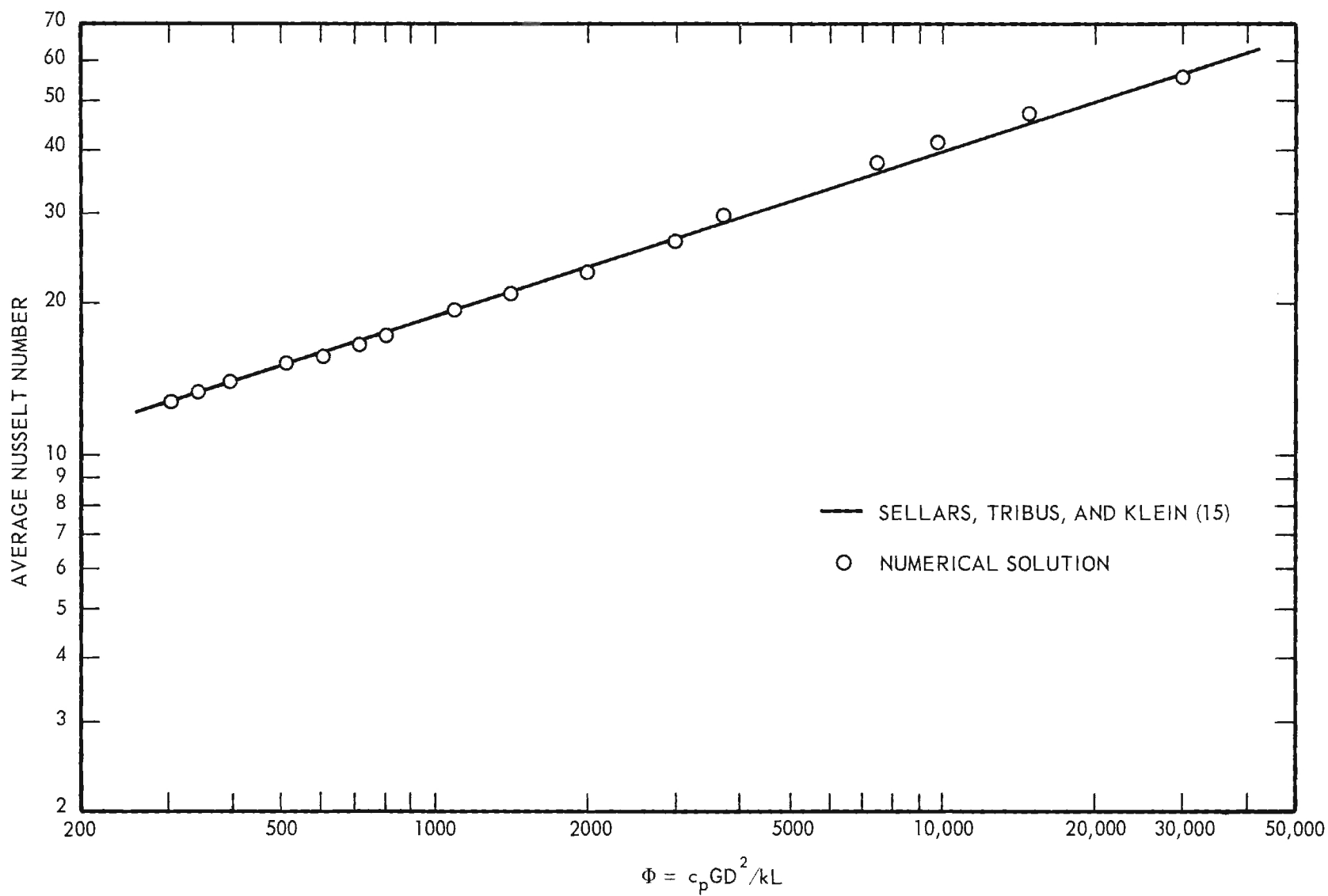Figure 28. Average Nusselt Number Versus Φ. Correlation of No Sound Data.

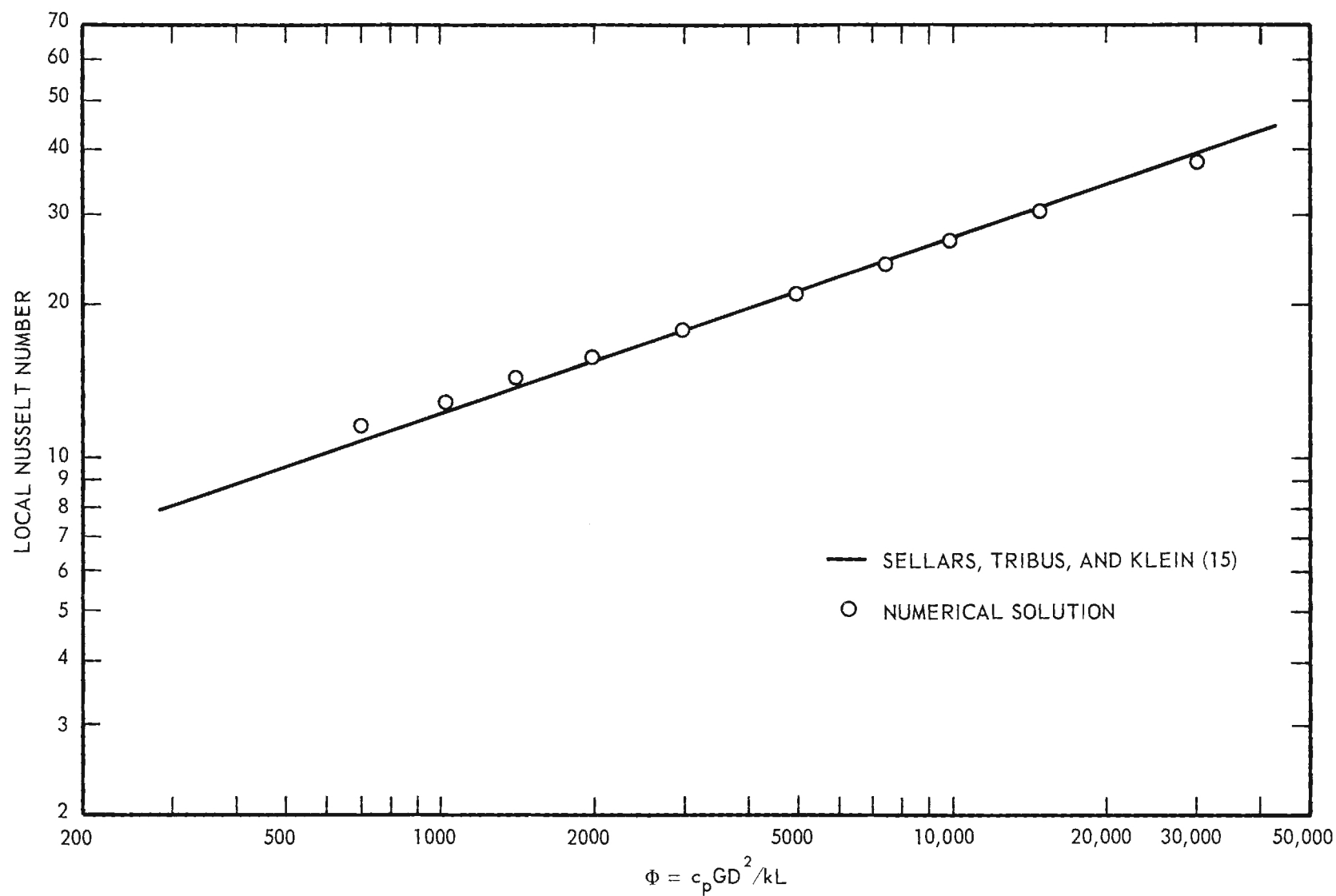Figure 29.   Average Nusselt Number Versus Φ.   Correlation of No Sound Data.

Figure 30. Local Nusselt Number Versus Φ. Comparison of Present Work With that of Sellars, Tribus, and Klein.
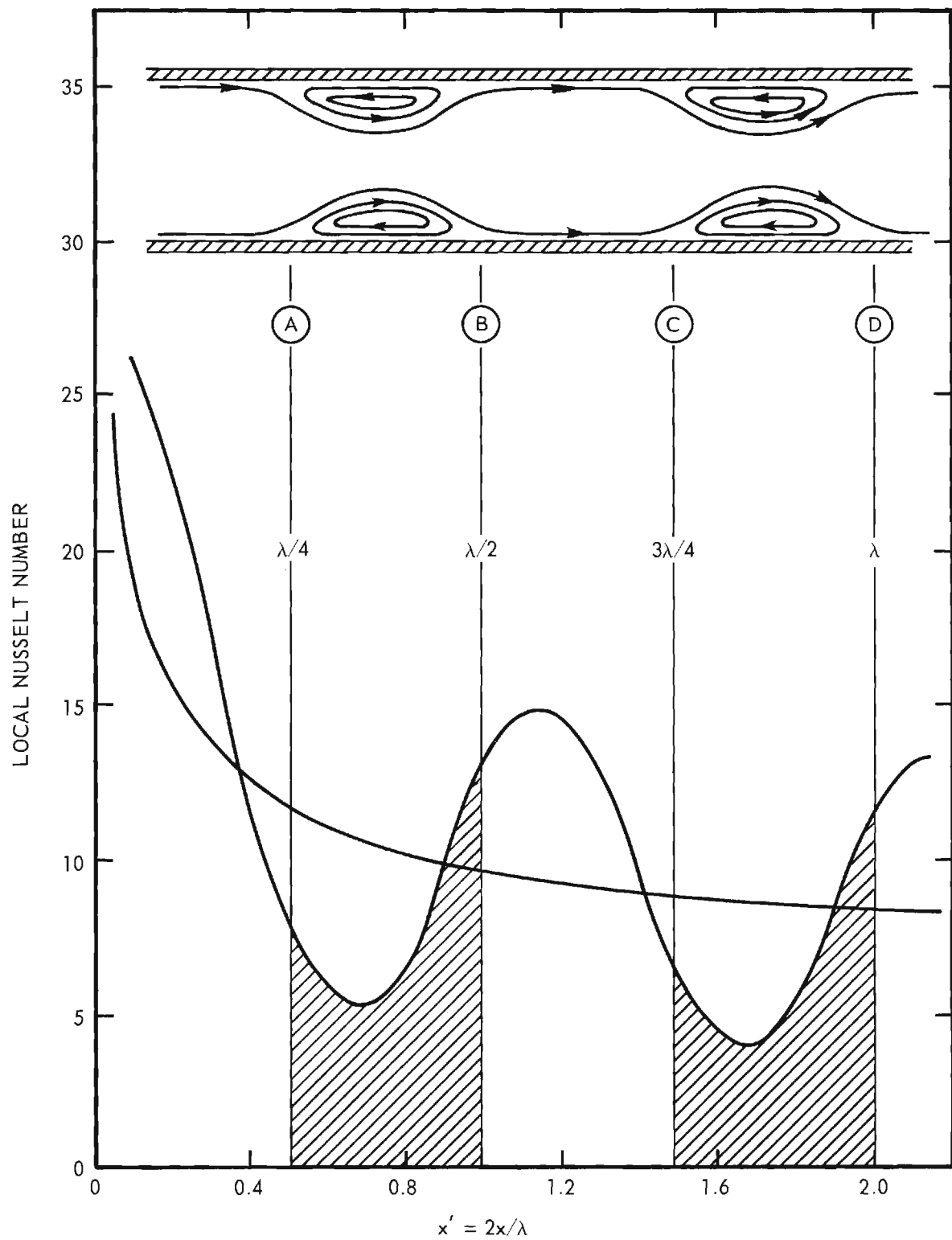
Figure 31. Local Nusselt Number Versus x' Showing Relation of Heat Transfer
and Velocity Field and Regions of Approximation.

55

changed by only a negligible amount and the Nusselt numbers were changed also by a negligible amount. Therefore, the relaxation technique was not used except as a check on the results of the numerical integration.

An energy balance was also calculated by noting that the energy which crosses the wall of the channel must show up as a change in the mixed-mean, or bulk, temperature of the fluid. These two quantities were calculated separately and the results agreed within ± 5 percent.

Using the methods heretofore described several solutions of the equation were obtained using various values of the parameters $M_o^2 Pr_o$, $M_o^2 Pr_o a'$, and M/M_o^2. A typical result is shown in Figure 32. It is to be noted from Figure 32 that the resonant acoustic field produced a very pronounced effect upon the local Nusselt number. It is also evident that the local Nusselt number varies as a slightly damped periodic function. In other words, an envelope may be drawn such that it is tangent to the maxima (or minima) of the curves representing the effect of sound and the resulting envelope has the shape of an exponentially-decaying function. This envelope, however, will not be parallel to the no-sound curve because it may be noted (by actual measurement) from the curves that the magnitude of the deviation from the no-sound curve is slowly diminishing as x' increases. The period of the function is one-half the wave length of the acoustic vibration and the amplitude is a function of the intensity or amplitude of the vibration. It is interesting to note that another important correlation of the data shown in Figure 32 exists. For a given sound pressure level, the maximum deviation of the local Nusselt number from the corresponding no-sound Nusselt number can be used to form the ratio $\Delta Nu_{max}/Nu_{no-sound}$; then if this ratio is divided by the cube root of the Reynolds number and plotted as a function of the parameter M_o^2/M the result is a straight line as shown in Figure 33.

Another interesting effect is shown in Figure 31. Purdy (13) predicted the existence of standing vortices which were one-quarter wave length long. He then theorized that the minimum heat transfer coefficient should occur at the points labeled A and C in the figure and that the maximum heat transfer coefficient should occur at the points labeled B and D. However, the results of the numerical solution of the energy equation indicate that there will be a phase lag and that the maxima and minima of the heat transfer coefficient actually occur downstream of the positions at which they would be expected to occur from Purdy's explanation. This phase lag has been observed experimentally for the round duct.

The effect of frequency and channel width variations is shown in Figures 34 through 41. It may be seen that modest changes in frequency have negligible effect in the regions of maximum deviation from the corresponding no-sound value of the Nusselt number, whereas changes in channel width have a marked effect upon the local values of the Nusselt number. These results are somewhat misleading since a frequency change shifts x' for no change in the no-sound Nusselt number. Also, for constant sound intensity (M_o) and constant Reynolds number, the parameter M_o^2/M is directly proportional to the duct width; hence, increasing the duct width will increase the effect of the sound field.
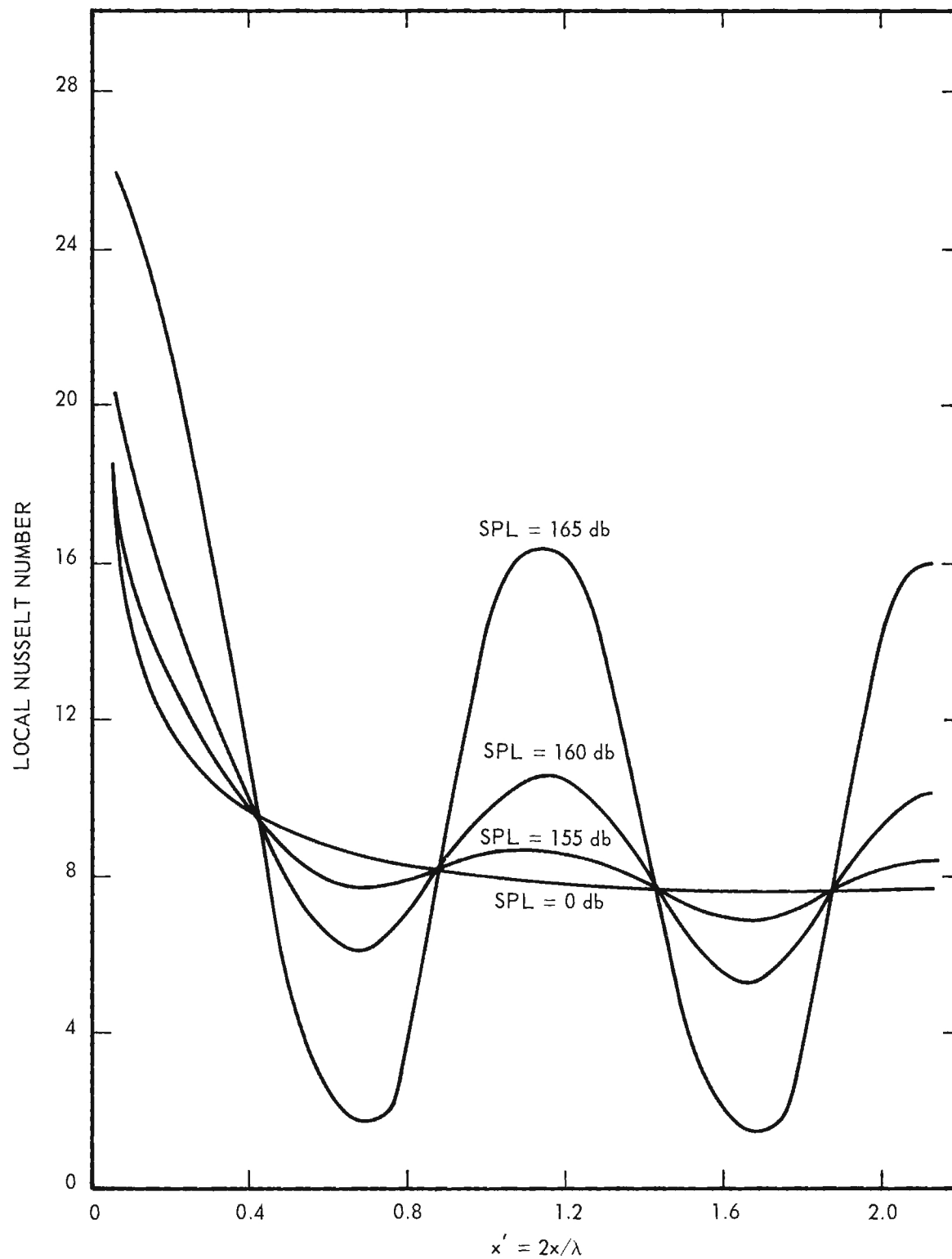
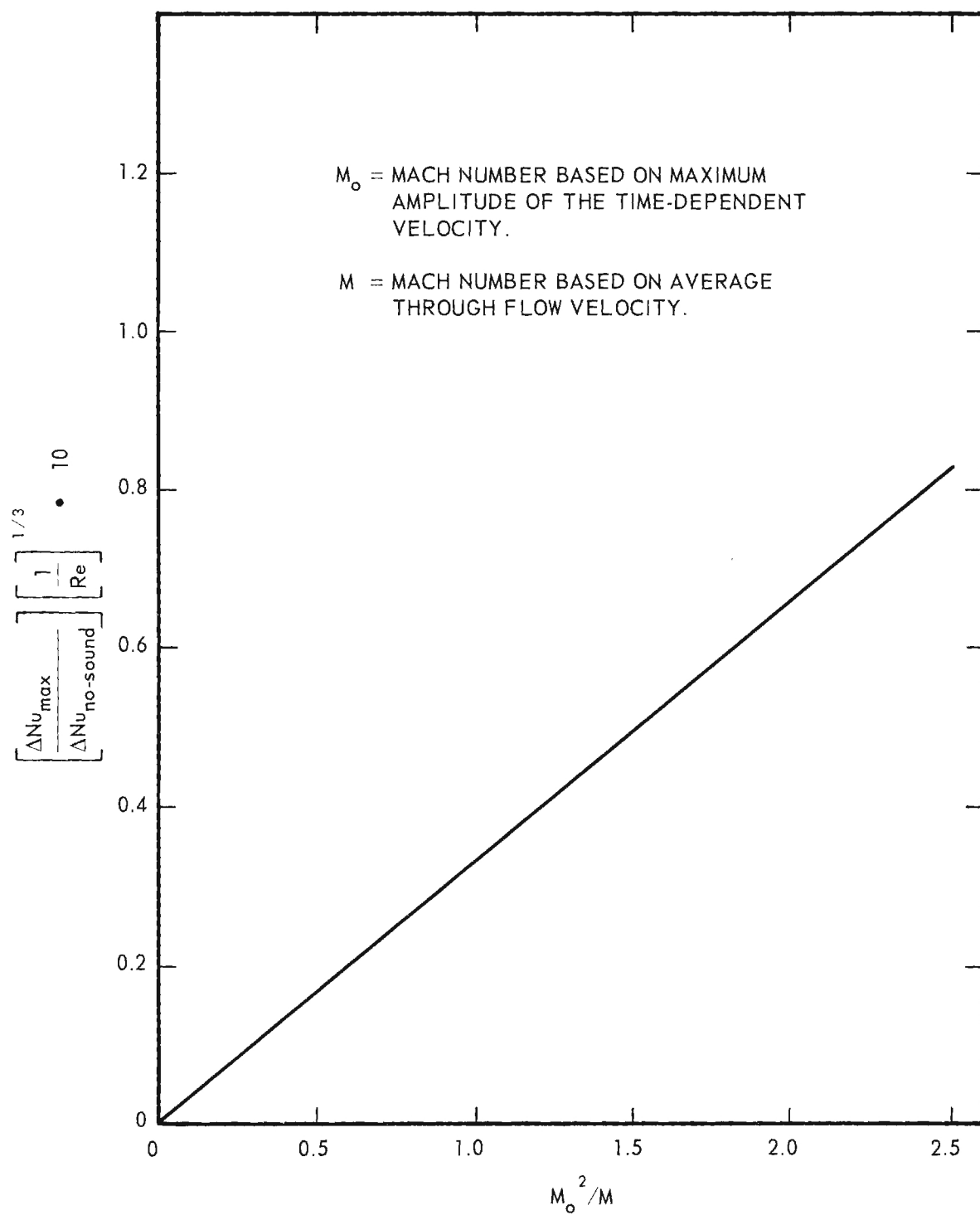Figure 32. Local Nusselt Number Versus x'. Channel Reynolds
Number ≈ 2000.

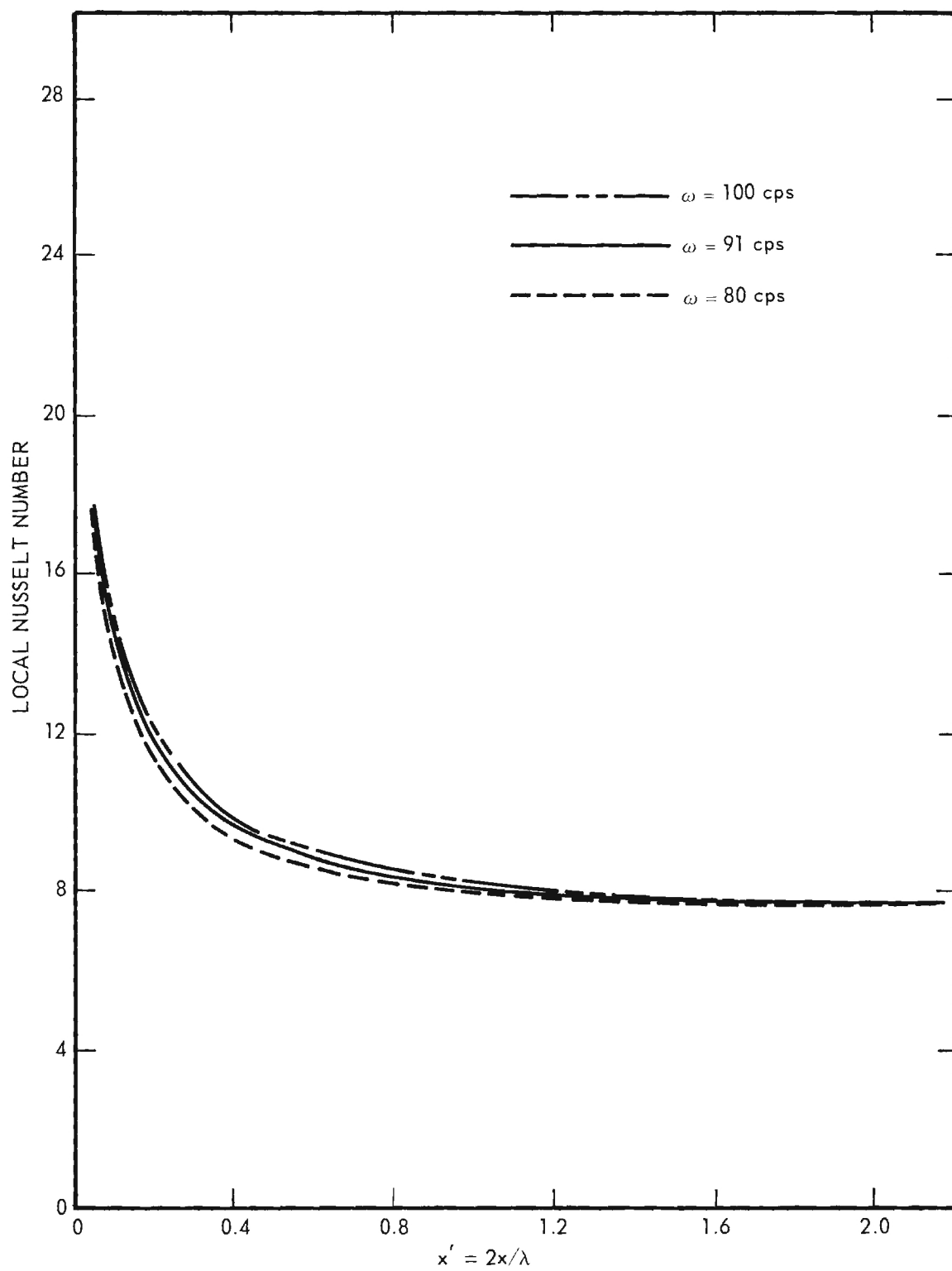Figure 33.   Correlation of Maximum Deviation from No Sound Nusselt Number.

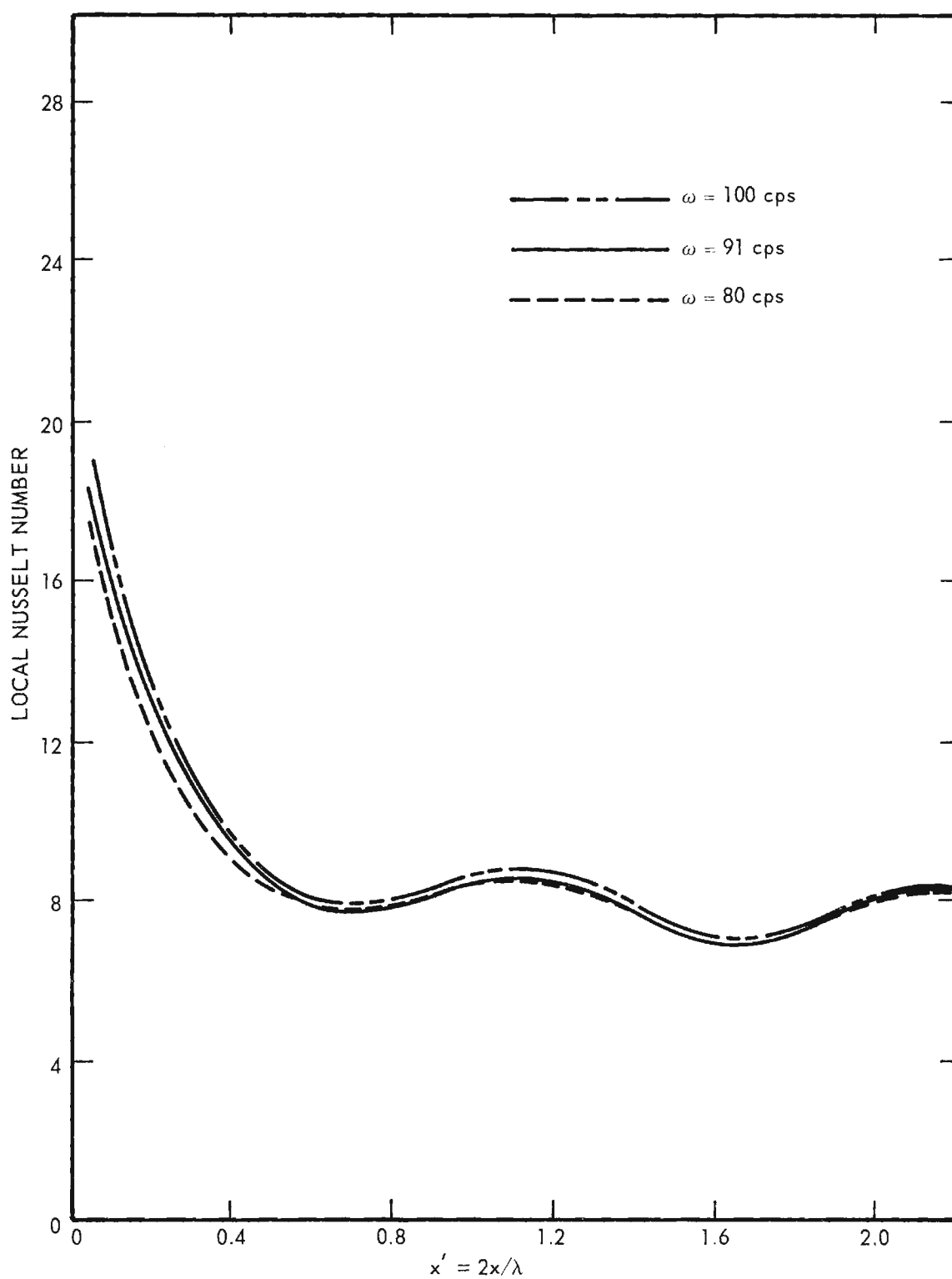Figure 34. Local Nusselt Number Versus x' With the Frequency, ω, as a Parameter. Channel Reynolds Number $\approx$ 2000. SPL = 0.

Figure 35. Local Nusselt Number Versus x' With the Frequency, ω, as a Parameter. Channel Reynolds Number $\approx$ 2000. SPL = 155.
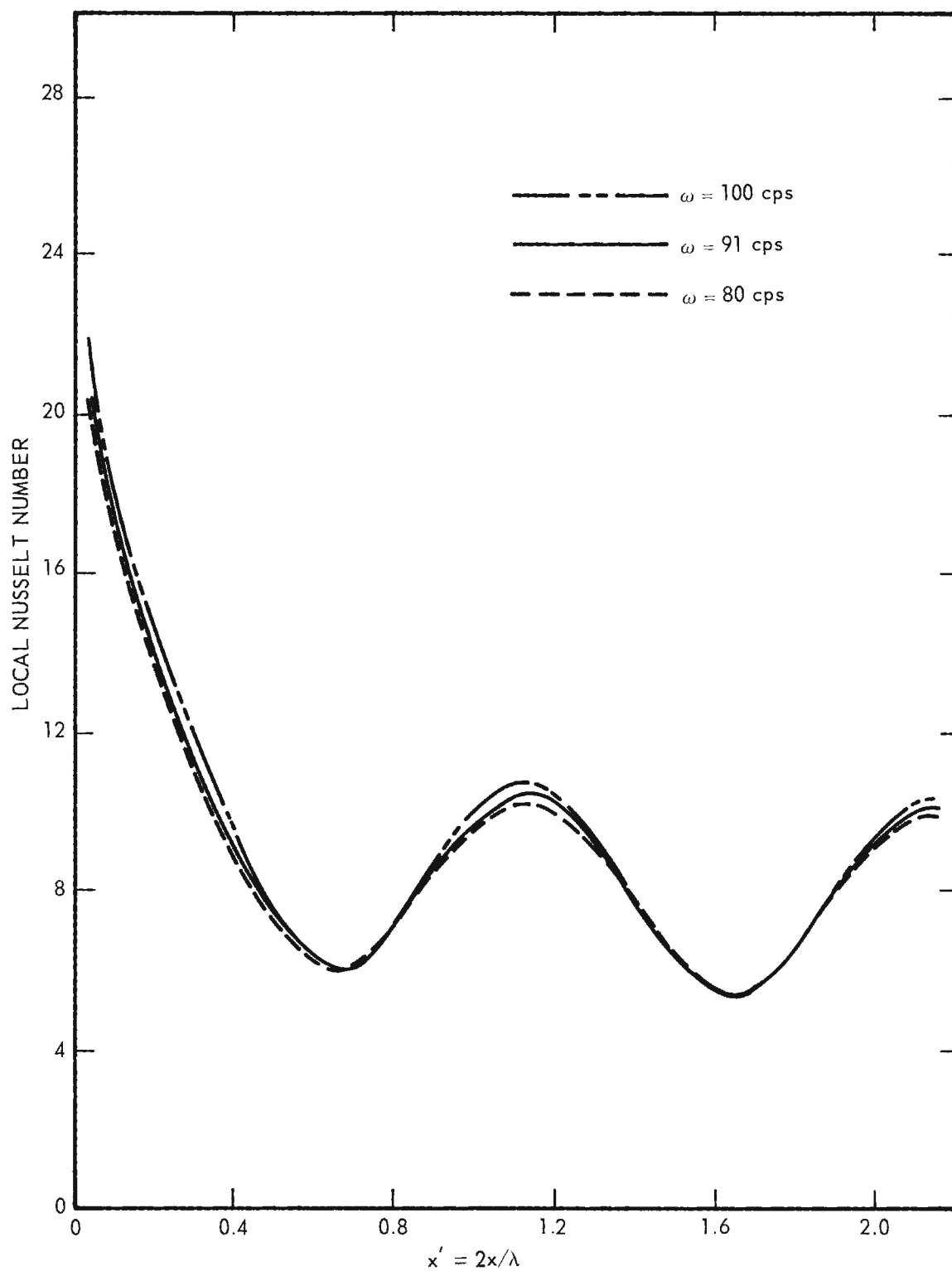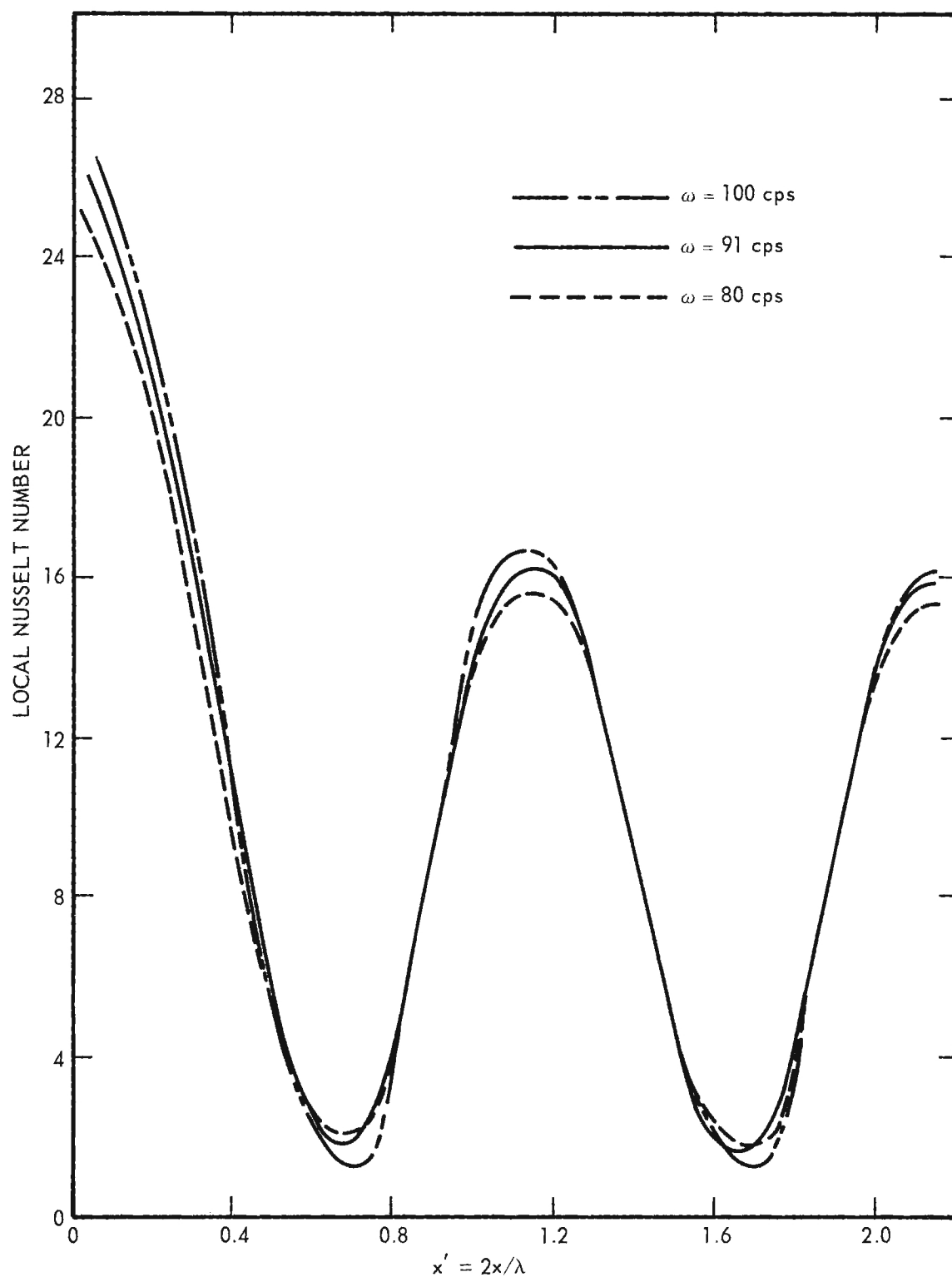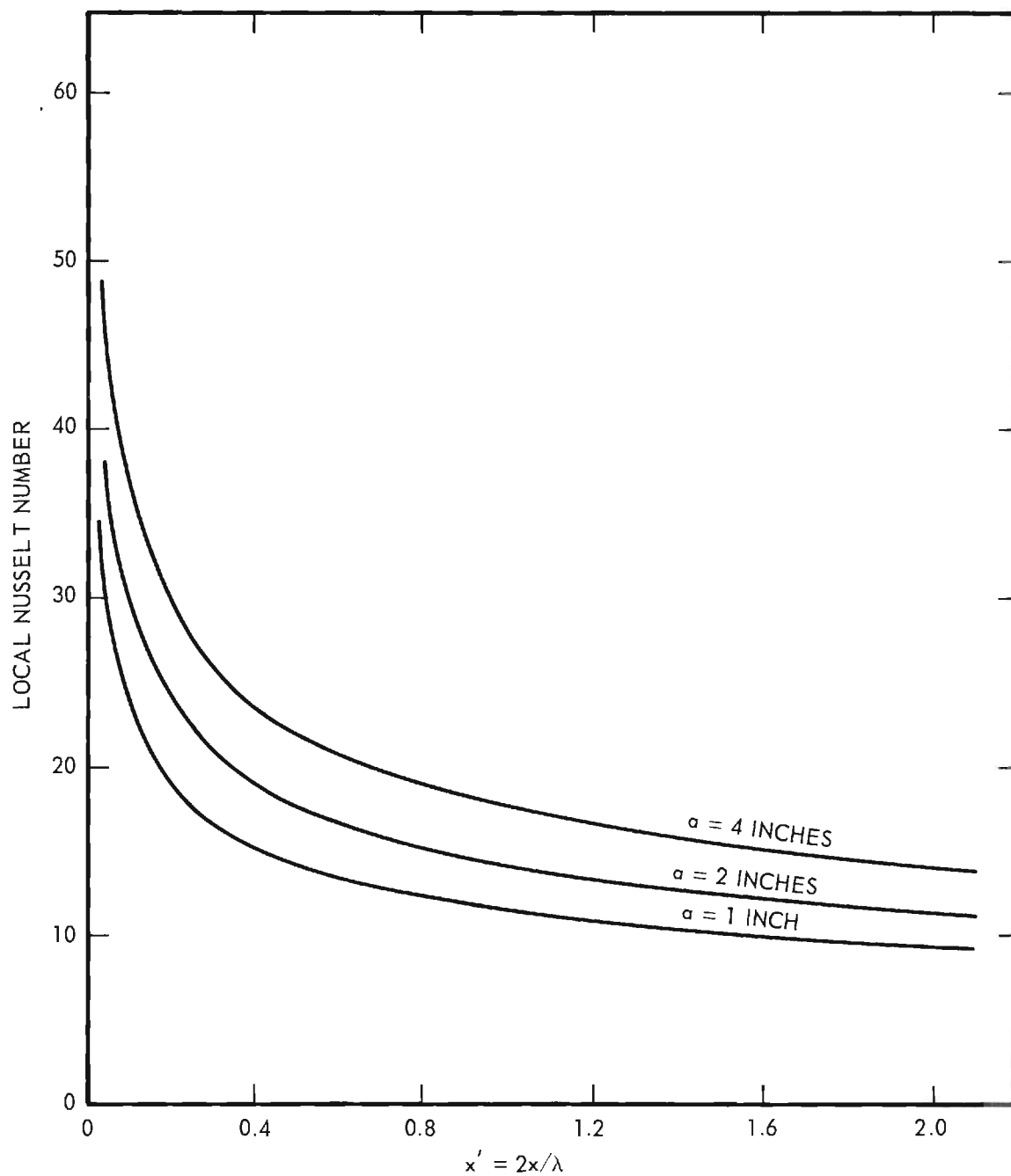
Figure 36. Local Nusselt Number Versus x' With the Frequency, ω, as a Parameter. Channel Reynolds Number $\approx$ 2000. SPL = 160 db.

Figure 37. Local Nusselt Number Versus x' With the Frequency, ω, as a Parameter. Channel Reynolds Number $\approx$ 2000. SPL = 165 db.

Figure 38. Local Nusselt Number Versus x' With the Channel Width, a, as a
            Parameter. Channel Reynolds Number $\approx$ 20000. SPL = 0 db.
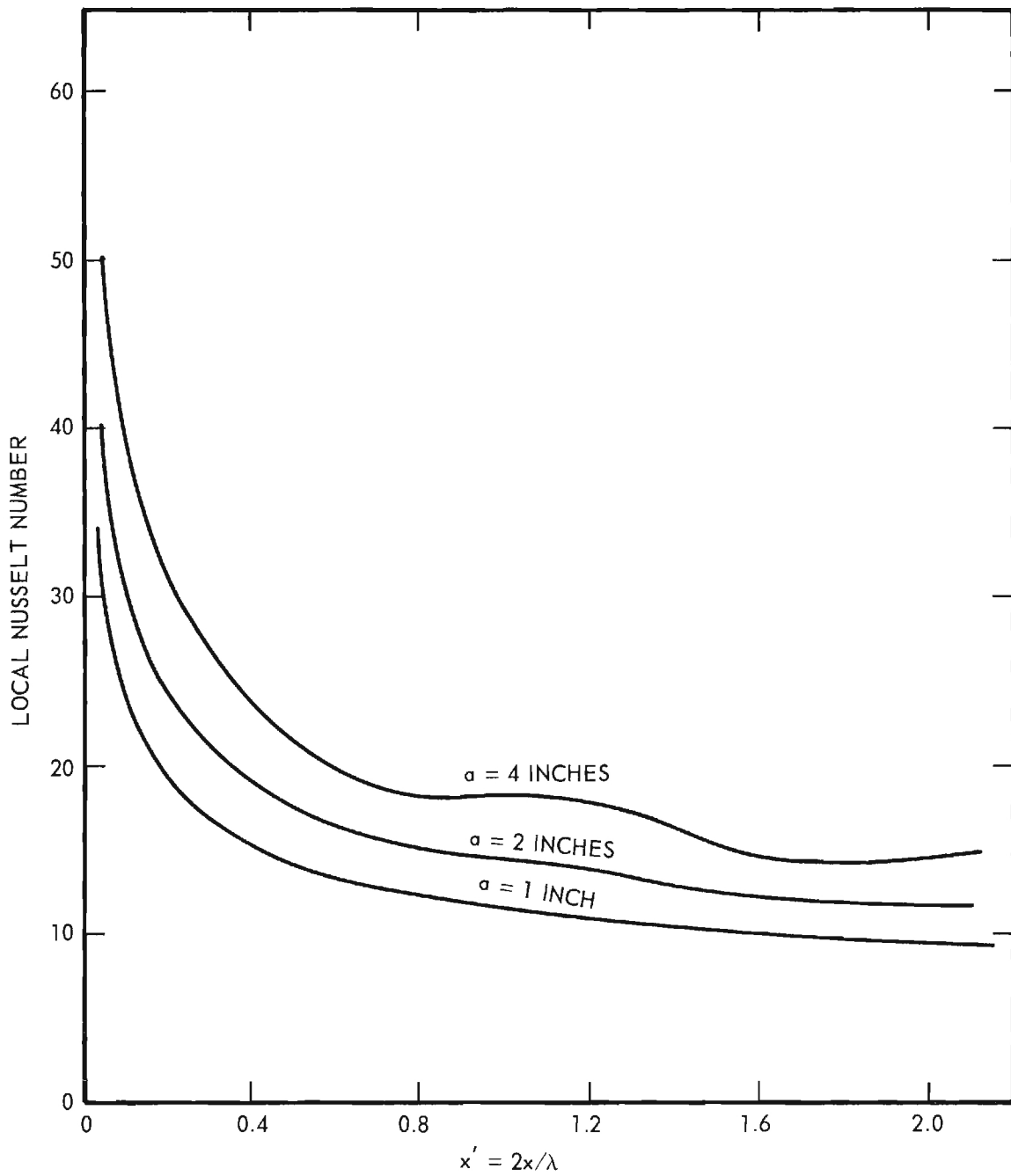
Figure 39.   Local Nusselt Number Versus x' With the Channel Width, a, as a Parameter.   Channel Reynolds Number ≈ 20000.   SPL = 155 db.

64
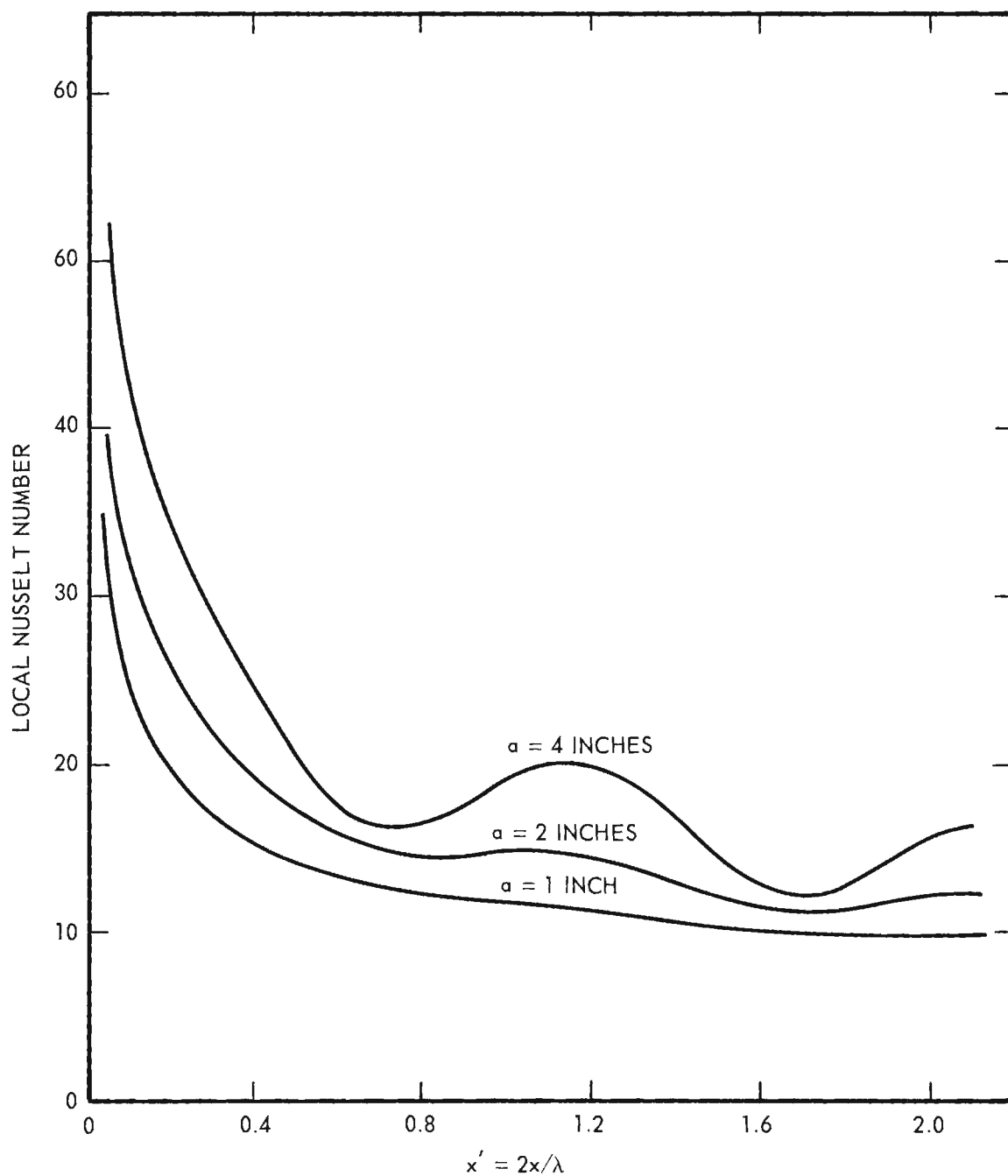
Figure 40. Local Nusselt Number Versus x' With the Channel Width, a, as a
Parameter. Channel Reynolds Number ≈ 20000. SPL = 160 db.
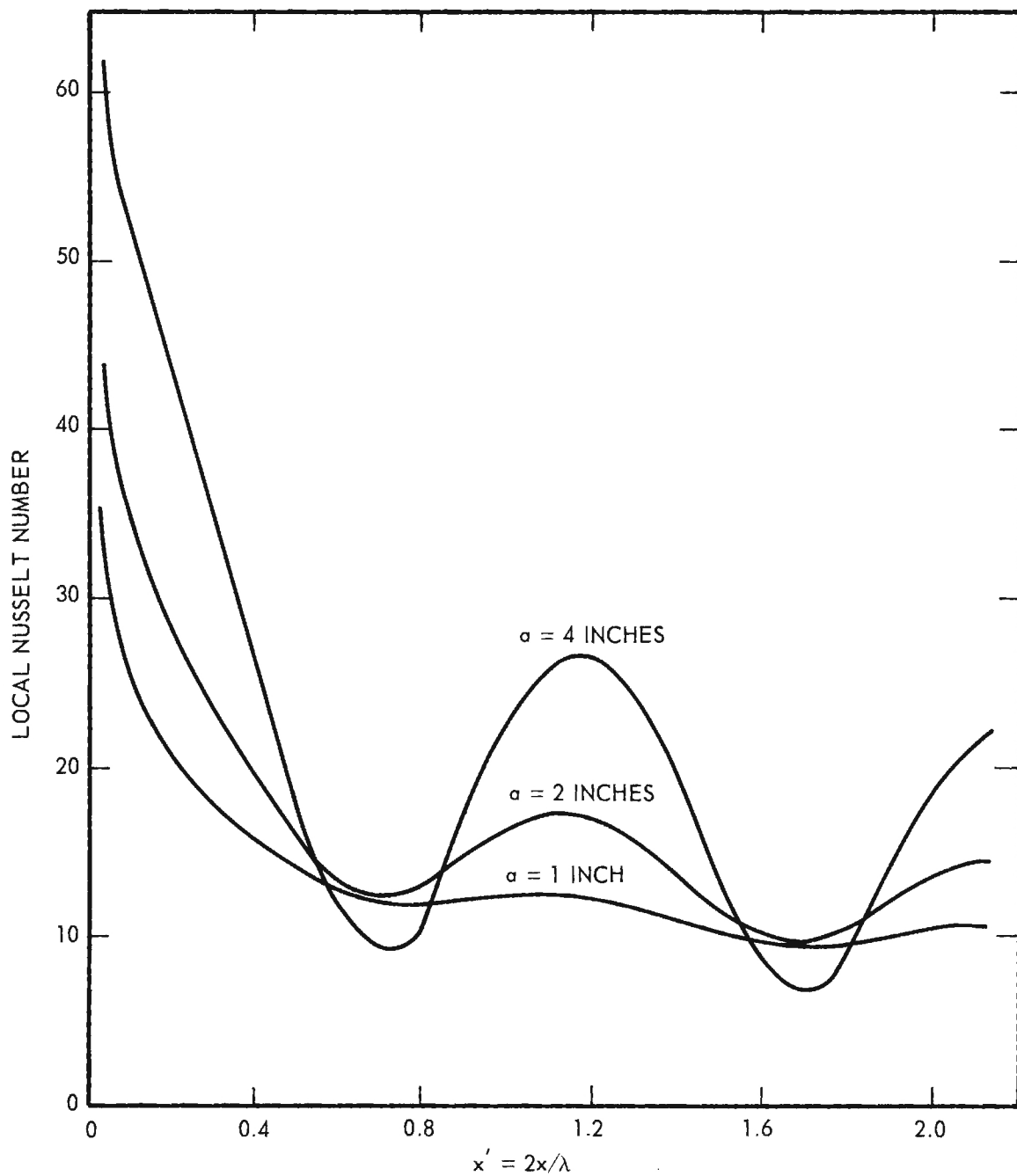
Figure 41.   Local Nusselt Number Versus x' With the Channel Width, a, as a
            Parameter.   Channel Reynolds Number ≈ 20000.   SPL = 165 db.

Experimental Heat Transfer Investigations. Experimental data are not available for comparison with the theoretical results given above. In reference (2) experimental data for entrance tube flow at a Reynolds number of 2100 and for various sound pressure levels are given which indicate in a qualitative way the validity of the theoretical results. Figure 1 of this reference indicates the effect of sound pressure level on the local heat transfer coefficient. Unfortunately, for the low Reynolds number (less than 2000) required for laminar flow, free convection effects are important and influence the experimental results.

Discussion of Results. The discussion which follows will be concerned with a qualitative comparison of the similarities of the results of the analytical solution for the parallel plate channel and the experimental results using a circular tube.

In each case the acoustical vibrations produced a local Nusselt number which was a slightly-damped periodic function which oscillated above and below the corresponding values of the no-sound Nusselt number. The amplitude of this periodic function appears to be dependent upon the intensity, or amplitude, of the acoustical vibration.

Both the analytical and experimental investigations show that the maxima of the heat transfer coefficient (Nusselt number) occur at, or near, the velocity antinodes and the minima occur at, or near, the velocity nodes. Actually, there is a phase lag and the maxima and minima occur slightly downstream of the positions at which they would be expected to occur. This phase lag, in some instances, was as high as 20 percent of the half-wave-length of the acoustic field. The phase lag seems to be dependent upon the flow rate and the intensity of the acoustic vibration.

The analytical investigation indicated that the heat transfer coefficient is primarily dependent upon the parameter M/M_o^2. Unfortunately, the experimental system made it impractical to study the effect of this parameter in detail, especially since the experimental system was concerned with tube flow and not channel flow. For the tube flow situation the variation of parameter M/M_o^2 was achieved by varying the through-flow Mach number M. Both the analytical and experimental studies show that an increase in the parameter M_o produces an increase in the maximum deviation of the local Nusselt number from the corresponding no-sound value. For high Reynolds numbers in the turbulent range the deviation is always to decrease the heat transfer coefficient as indicated in Chapter 2.

From the analytical work discussed in this chapter it can be concluded that:

1. A resonant acoustic field will produce variations in the local heat transfer coefficient from the corresponding values obtaind without the resonant acoustic field.

2. The amplitude of the variations which are produced by the reasonant acoustic field is, as far as can be ascertained from the governing differential equation, primarily a function of the parameter M/M_o^2.

67

3. The frequency of the acoustic disturbance has a negligible effect on the local heat transfer rate except in the regions near the maximum deviation from the corresponding no-sound values.

4. The solution to the analytical model for the parallel plate system predicts a phase-lag in the local heat transfer rate.

It is evident that further investigations involving experimental, as well as analytical, studies are necessary. The following are suggested.

1. Additional analytical development should be undertaken to determine if the results obtained here can be presented in a more universal form than has been established thus far.

2. Additional experimental as well as analytical studies should be conducted to study the effects of: (i) high intensity sound, (ii) off-resonance, and (iii) free convection effects on the flow field and on rates of heat transfer.

3. The solution for the circular tube geometry should also be obtained. Possibly then the experimental work could be correlated with the analytical results.

CHAPTER IV

HOT-WIRE ANEMOMETER STUDIES

The experimental work discussed in this chapter was concerned with the measurement of velocity profiles and turbulence levels in the heat transfer tube. Measurements were made for various Reynolds numbers, with and without the influence of resonant acoustic vibrations, and at various radial positions.

Flow Corporation's Model HWB2 Hot Wire Anemometer was used with a 0.00035 inch diameter Tungsten wire. In addition a Model 12A1 Random Signal True RMS Voltmeter, a Hewlett Packard 300A Wave Analyzer, and a Type 502 Techtronic Cathode Ray Dual Beam Oscilloscope were used in the turbulence measurements. The calibration of the hot wire was done on a Flow Corporation Model WT4 tunnel and a Model MM-3 micromanometer. The calibration curves verified the linear relationship predicted by theory for the hot-wire anemometer.

In order to move the hot-wire perpendicular to the direction of flow as well as along the direction of flow, a movable arm was built. This arm (see Figure 42) could be accurately positioned radially to within 0.001 of an inch. The probe was supported along most of its length for rigidity and the tip was bent toward the wall so that measurements could be made to within 0.023 inches of the wall. Using the average velocity technique and the above equipment, data were obtained for various Reynolds numbers between 10,000 and 60,000 (i.e., average velocity from 6 fps to 35 fps), at a position 19 feet 8 inches from the entrance of the tube, for normal turbulent flow as well as for flow under the influence of a 91 cps resonant acoustic wave at a SPL of approximately 165 db.

Figure 43 indicates typical no-sound velocity profiles for four through flow velocities. In Figure 44 are shown three so-called velocity profiles for resonant conditions. The velocity values indicated are influenced by the rms particle velocity due to the acoustic wave and, therefore, in reality are not true velocity indications. Each curve in the figure contains 60 experimental points, however, for convenience in plotting only a few of the points are indicated. It is interesting to note that the acoustic effect appears to flatten out the profile, assuming the sound effect is uniform across the tube. It is also interesting to note that for the no-sound condition the velocity at the midpoint of the tube is approximately 1.25 the mean velocity in the tube. This is characteristic of turbulent flow profiles.

After the velocity profiles had been obtained, a turbulent study was made for several Reynolds numbers and radial positions in the duct. Using the Flow Corporation's Handbook formula for turbulence intensity and data obtained from the hot wire equipment, the curves in Figure 45 were drawn.
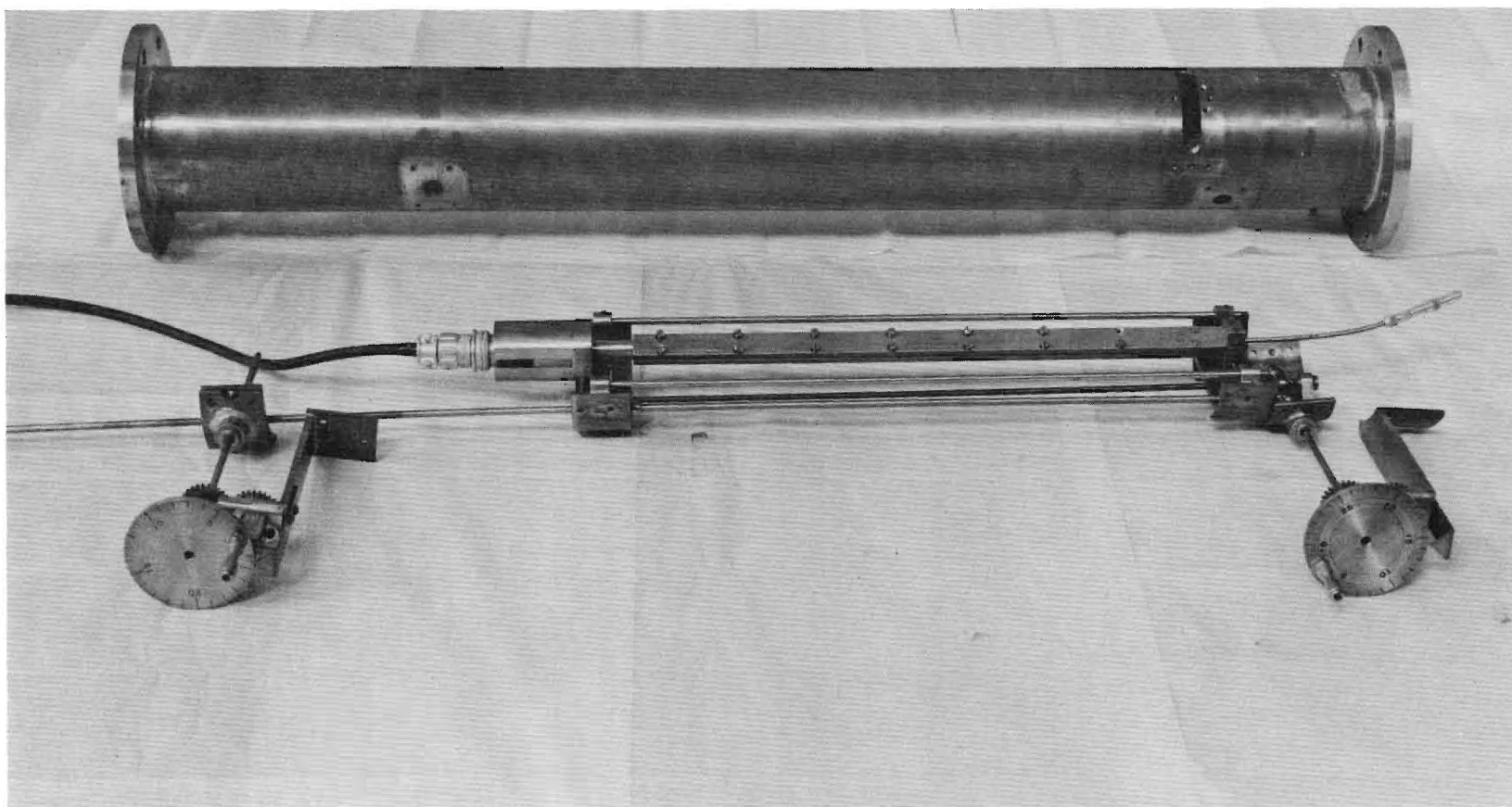
69

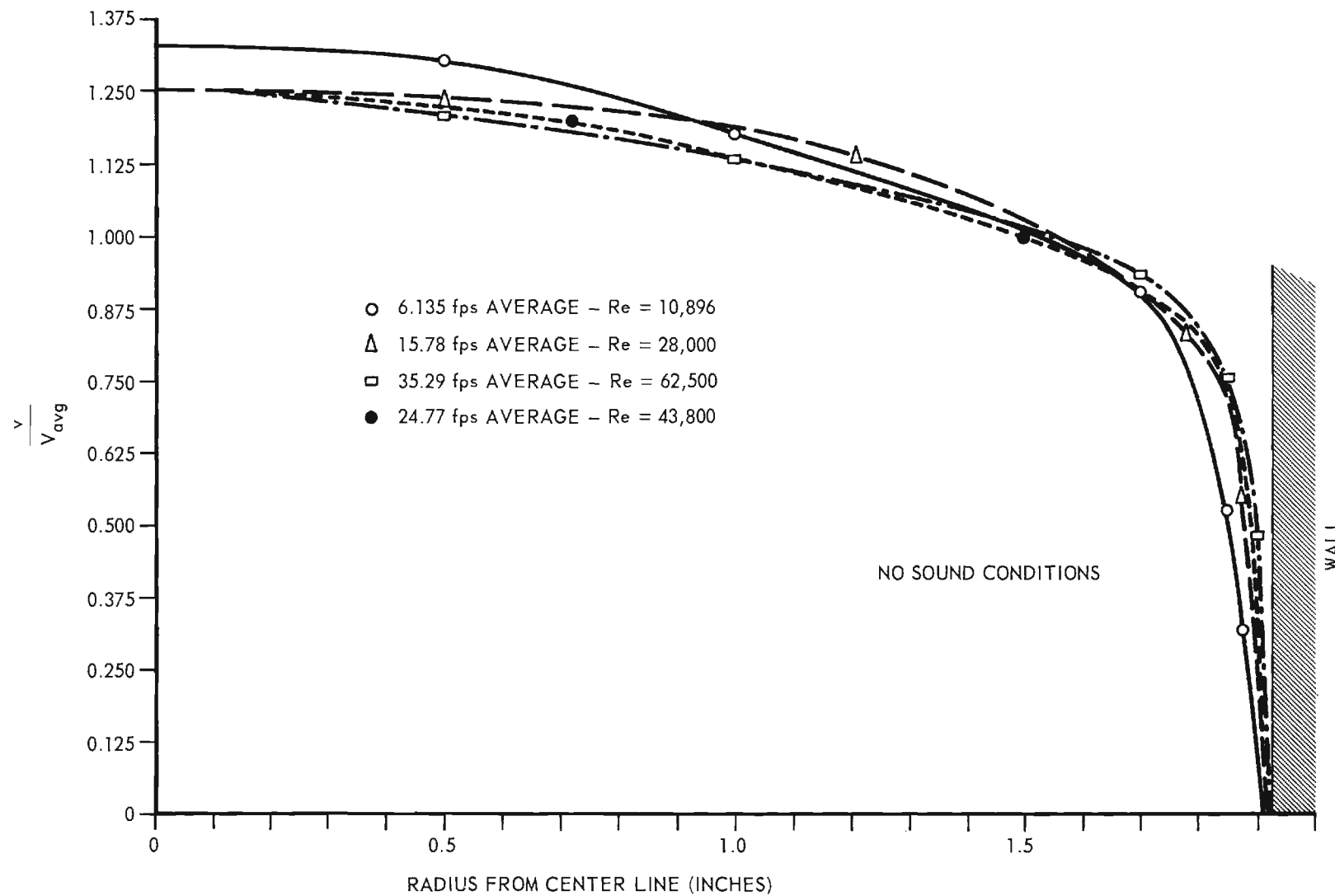Figure 42.   Photograph of Hot Wire Anemometer Probe.

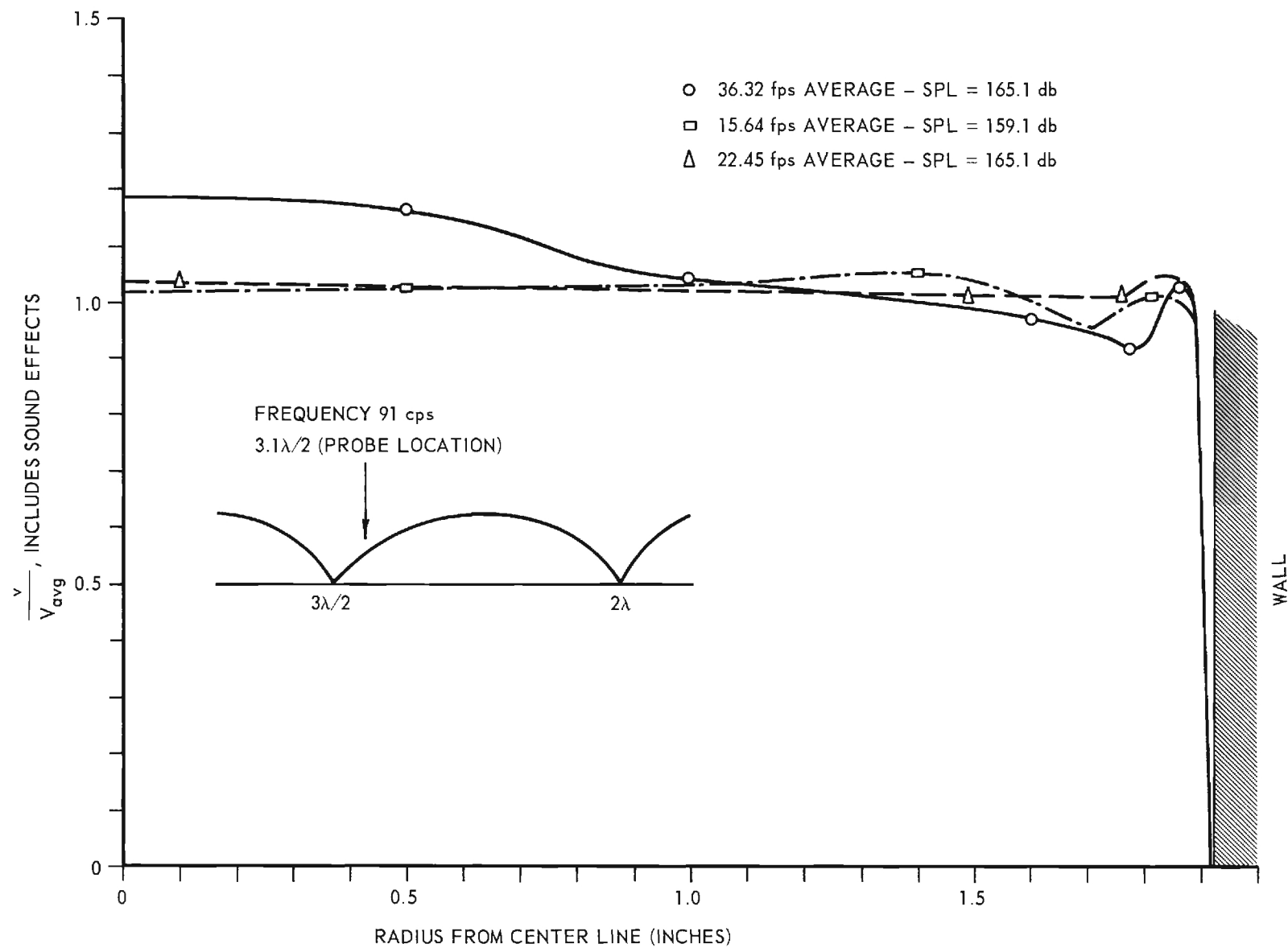Figure 43. Turbulent Non-dimensionalized Velocity Profiles — No Sound.

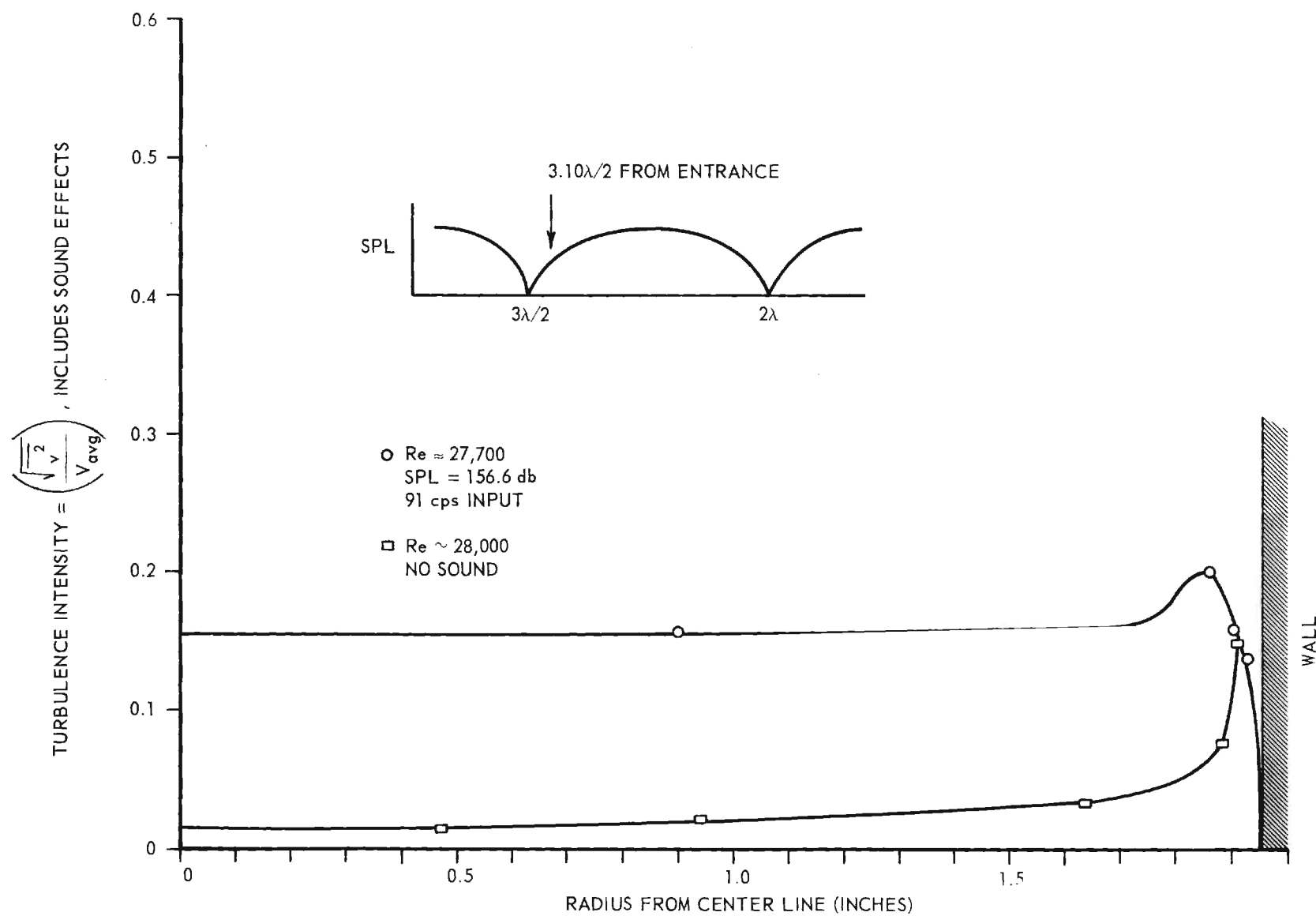Figure 44. Non-dimensionalized Velocity Profiles With Sound.

Figure 45.   Turbulent Intensity Versus Position.

The turbulence intensity across the entire duct appears to increase as the acoustic wave is impressed upon the system. The increase is probably due to the rms particle velocity for the resonant condition. For no-sound the turbulence is small in the center of the tube and slowly increases until near the wall it suddenly increases (essentially at the maximum gradient in the velocity profile) and then goes to zero at the wall itself. For sound conditions the turbulence level as indicated probably does not have much significance since it appears to be influenced by the rms particle velocity. The no-sound values of turbulence appear to be reasonable since it is logical to assume that the turbulence intensity should be greatest in regions of maximum shear.

In order to determine the effect of harmonics on a representative turbulence level, the Hewlett Packard wave analyzer was hooked to the system and the various frequencies examined. Unfortunately, when utilizing the wave analyzer it was impossible to determine a turbulent intensity since the calibration intensity signal could not be passed through the wave analyzer. Therefore, a turbulence number, which is the intensity multiplied by a constant, was used to give relative values of turbulence. This turbulence number represents the filtered voltage in millivolts from the hot-wire at the frequency under consideration. Consequently, the turbulence numbers in Figures 46 through 49 are only relative values, however, they indicate the important harmonics which are apparent in the experimental apparatus. It is interesting to note in Figures 46, 47, and 48 that the 364 cps harmonic has the largest turbulence number, however, in Figure 49 it is absent. The location of the probe in Figure 49 practically at the wall may have had some influence on removing this harmonic, but since the other harmonics are still present this does not seem to be a rational explanation. It is also interesting to note that the dashed lines, the turbulence numbers for sound conditions, are lower than the no-sound background. It may be that the sound field has decreased the turbulence level. This would be in accordance with the heat transfer results which show a decrease with sound conditions. The presence of such large turbulence numbers at the harmonics of the resonant frequency may indicate either a distorted sound wave or an amplification of the turbulence in these frequency bands.

Several interesting observations were made while performing the experiments. These are listed below:

1. Velocity profiles for no-sound were only slightly affected by changes in Reynolds number; however, the profile change that occurred when resonant sound waves were impressed on the system was appreciable and tended to make the profiles flatter.

2. The hot-wire anemometer was very sensitive to vibration and pressure changes and required repeated calibrations.

3. It appeared that 100,000 cps oscillations were being transmitted by the hot-wire at the resonant frequency of approximately 91 cps. It was assumed that this frequency was the characteristic frequency of vibration of the wire itself and that the acoustic vibrations were forcing this vibration. The effect of this situation could not be evaluated. Figure 50 shows a polaroid film of the no-sound condition and on a different scale Figure 51 shows the 100,000 cps noise wave. These pictures were made by hooking the hot-wire to an oscilloscope which had a polaroid camera mounting.
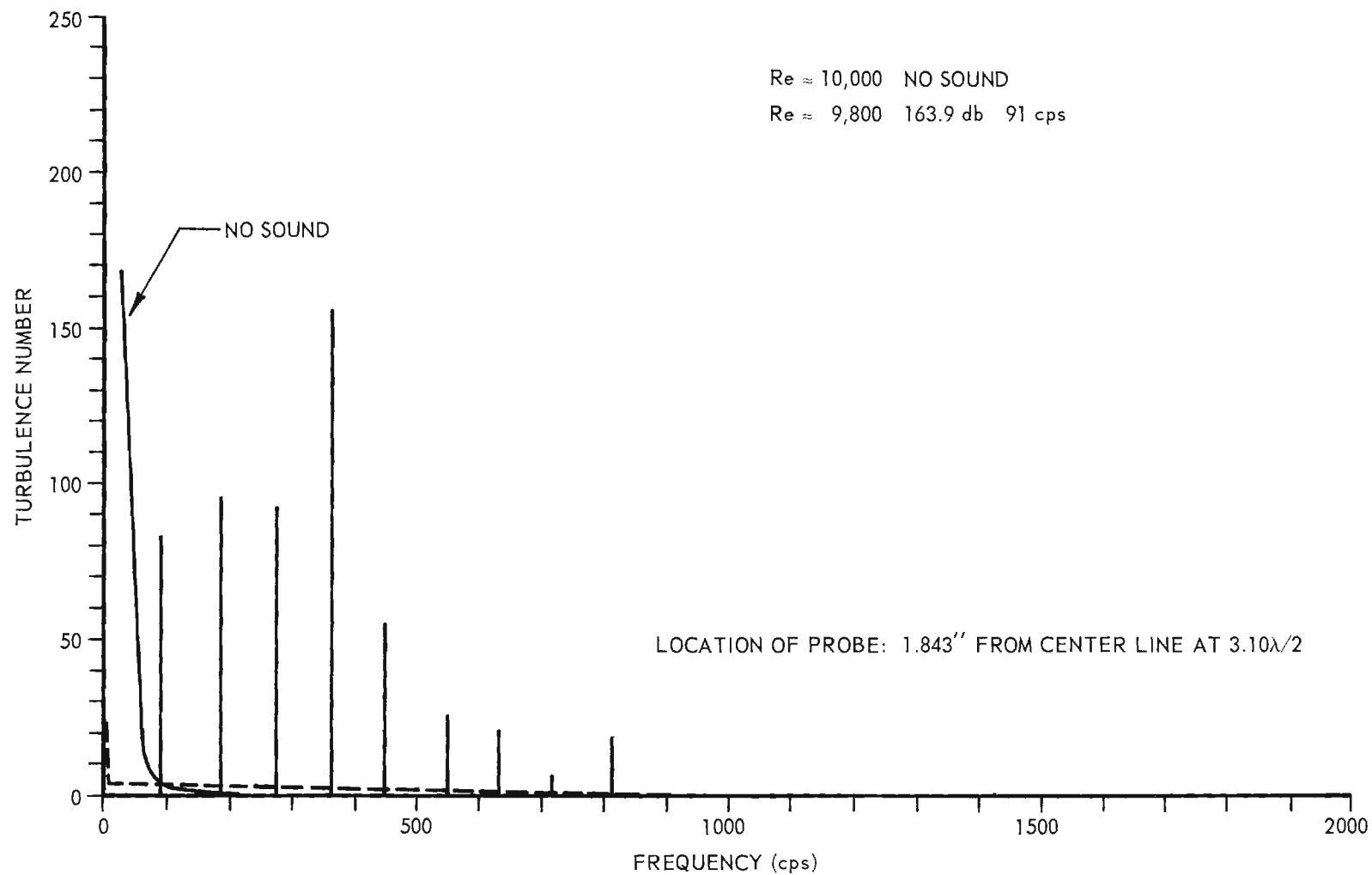
74

Figure 46.   Turbulence Number of Harmonics, Re ≈ 9,800.

75
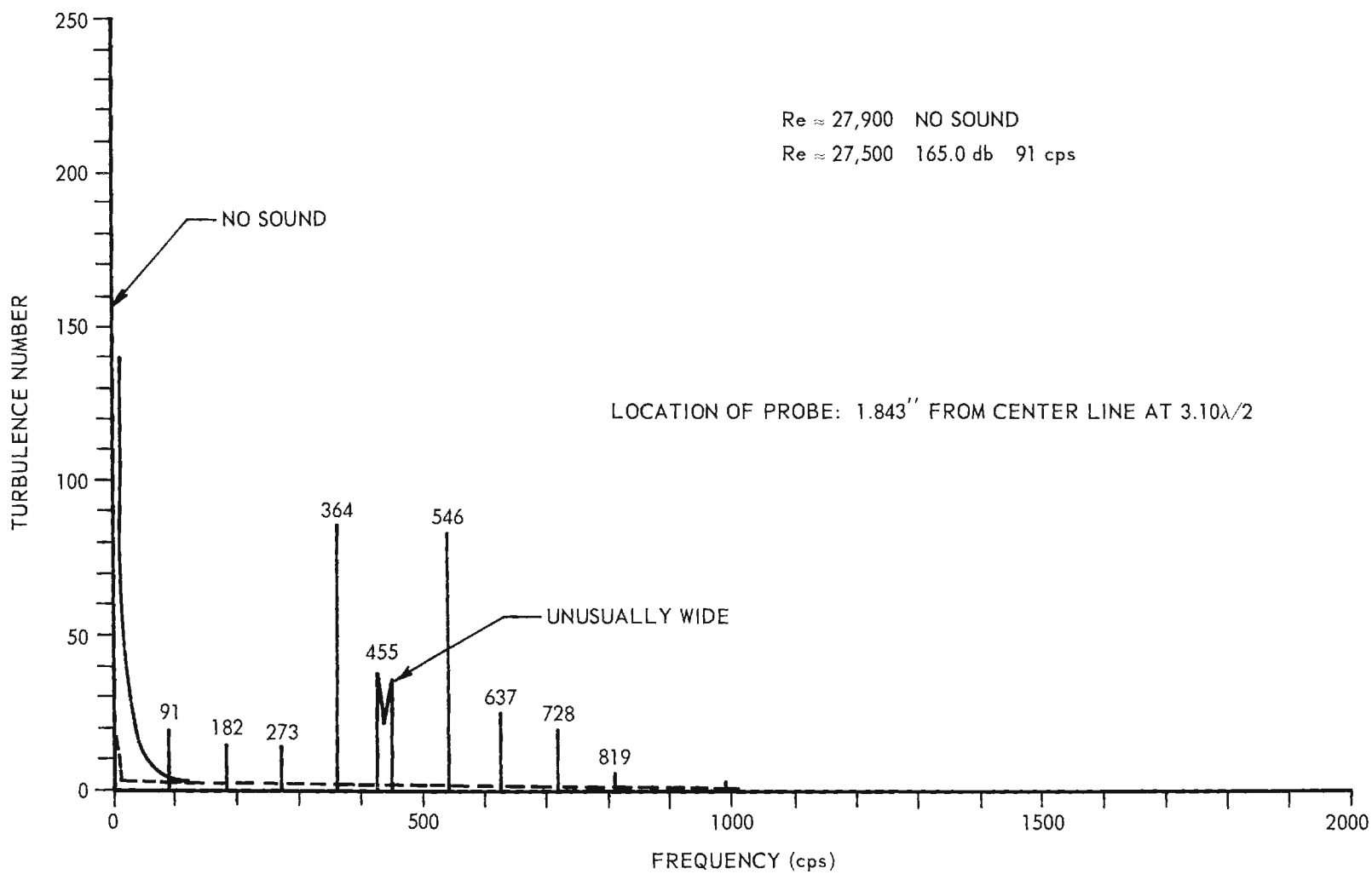
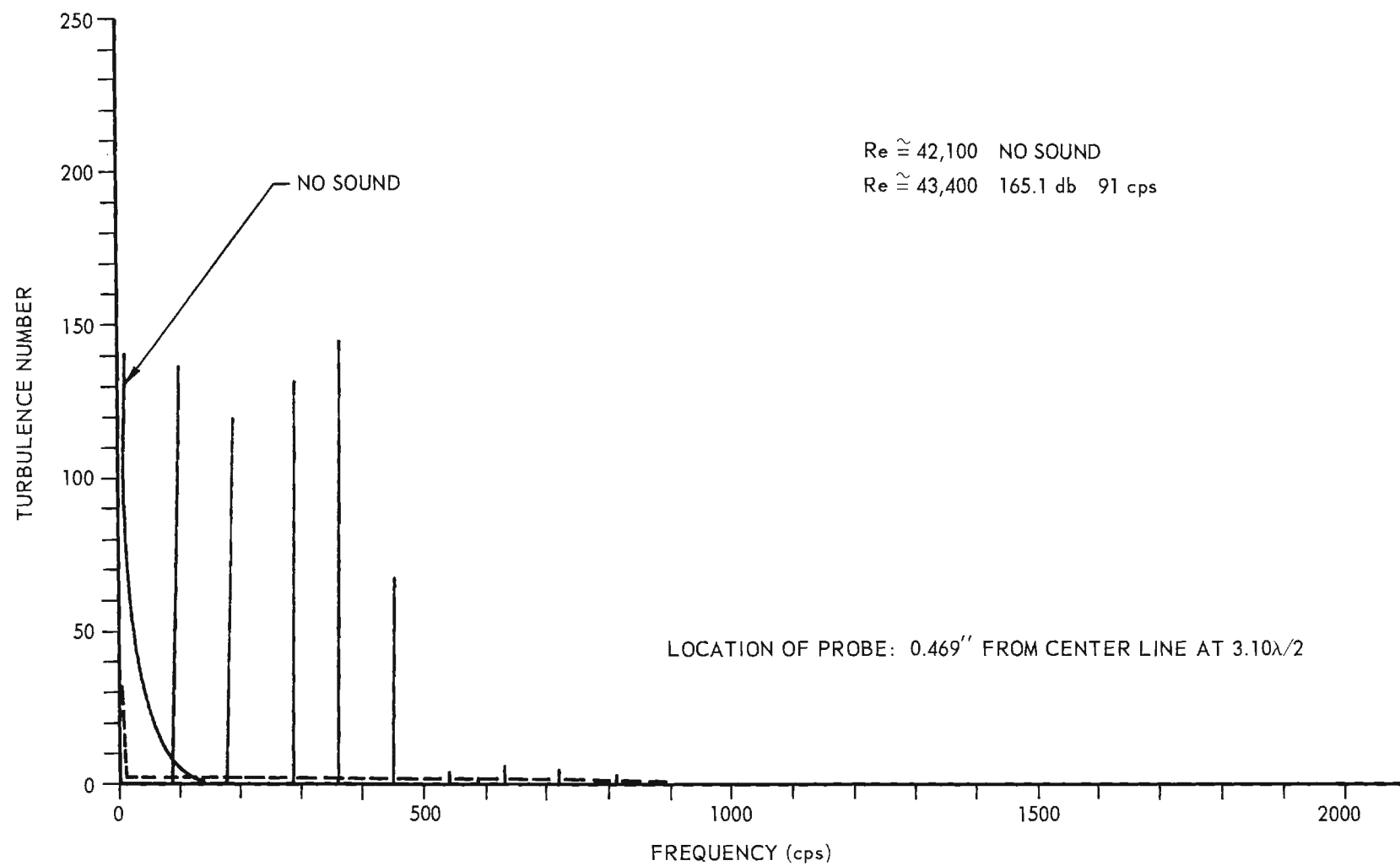Figure 47. Turbulence Number of Harmonics, Re ≈ 27,500.

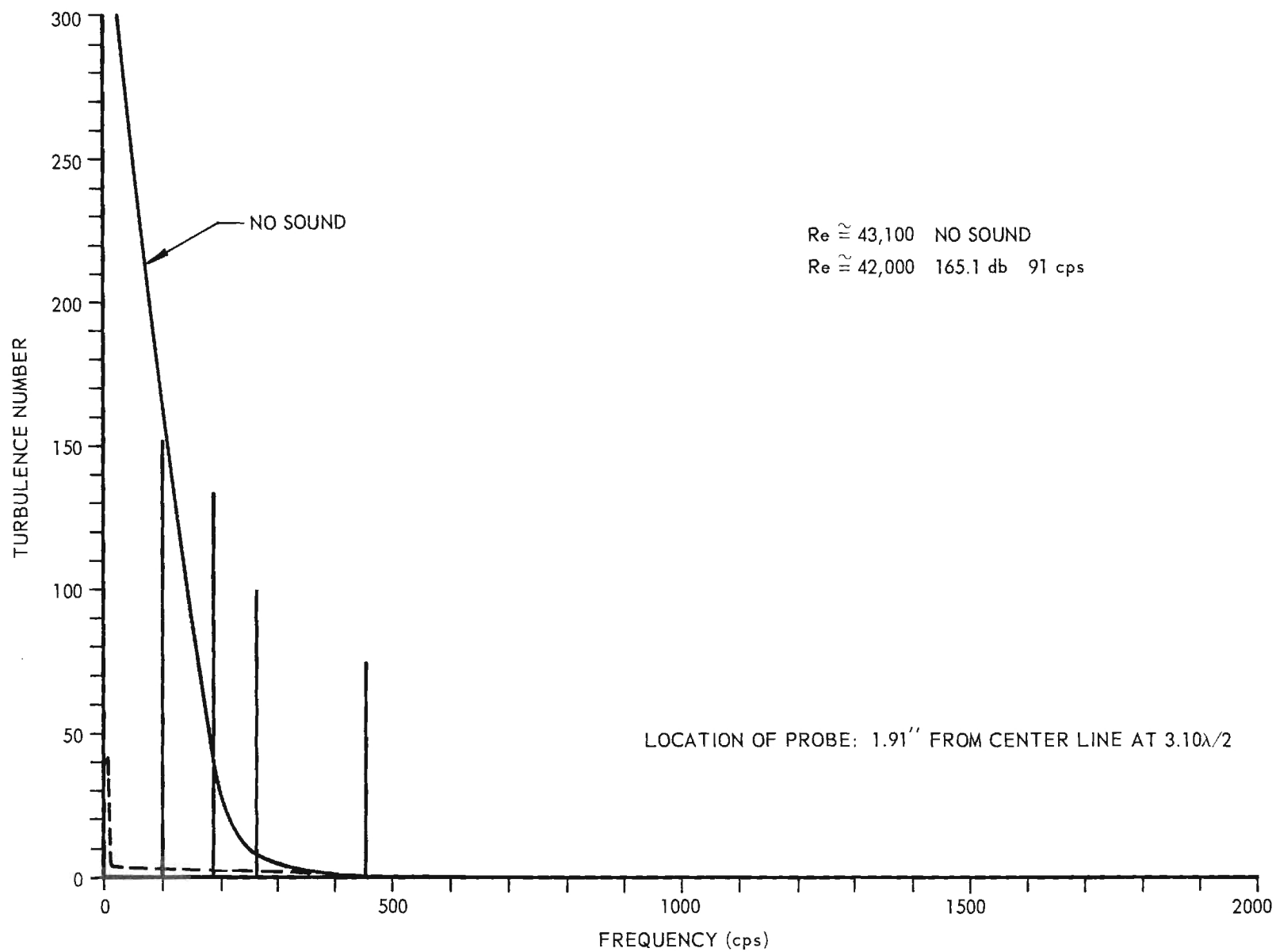Figure 48.   Turbulence Number of Harmonics, Re = 43,400.

Figure 49. Turbulence Number of Harmonics, Re ≈ 42,000.
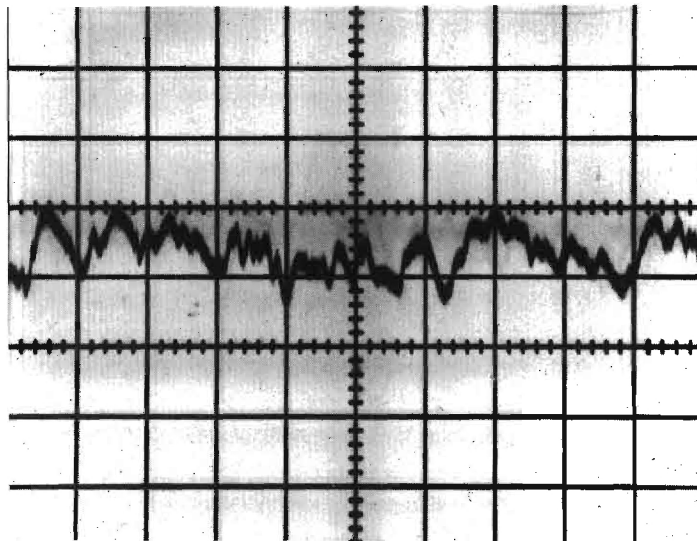
78

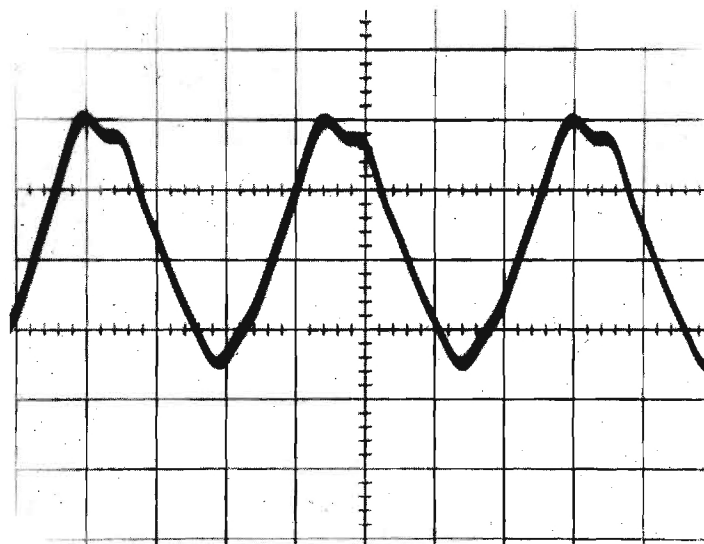Figure 50.   No Sound Background (Re $\approx$ 20,000).

Figure 51.   100,000 cps Frequency Imposed on System (Re $\approx$ 20,000, SPL = 163 db, 91 cps).

4.   It was evident from the oscilloscope display that the hot-wire was not picking up the acoustic wave as precisely as could be desired.   Figures 52 through 54 show photographs of the distortion of the wave; the rectified portions of the wave appear to be appreciably smaller than the unrectified portions.   It is not clear whether the velocity wave form is badly distorted or if the wire itself is producing the distortion.   A comparison of the pressure wave form at this section would probably answer, or help to answer, this question.

It is recommended that the hot-wire anemometer work be continued since it should be very rewarding in helping obtain an understanding of turbulence and its effect on flow and heat transfer.   Perhaps this may necessitate a development program to obtain better instrumentation set ups which will more rapidly and accurately represent the actual flow conditions.
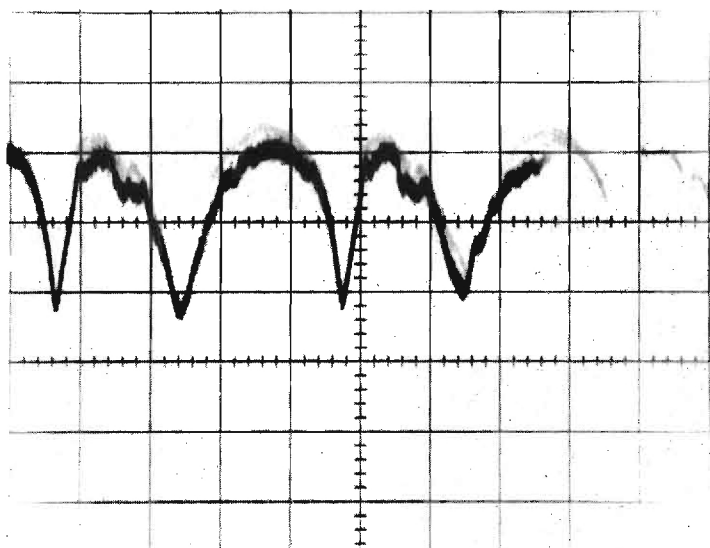
Figure 52. Acoustic Wave Form
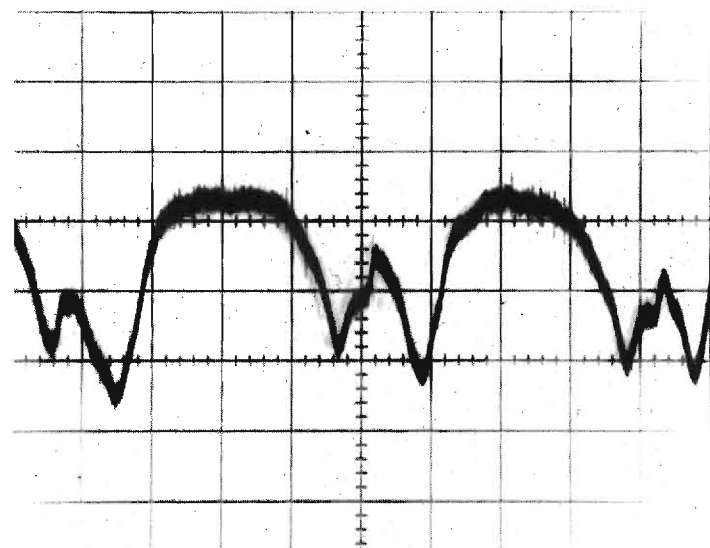(Re ≈ 11,300, SPL = 165
db, 91 cps, 1.85" from $\mathcal{C}_L$).

Figure 53. Acoustic Wave Form
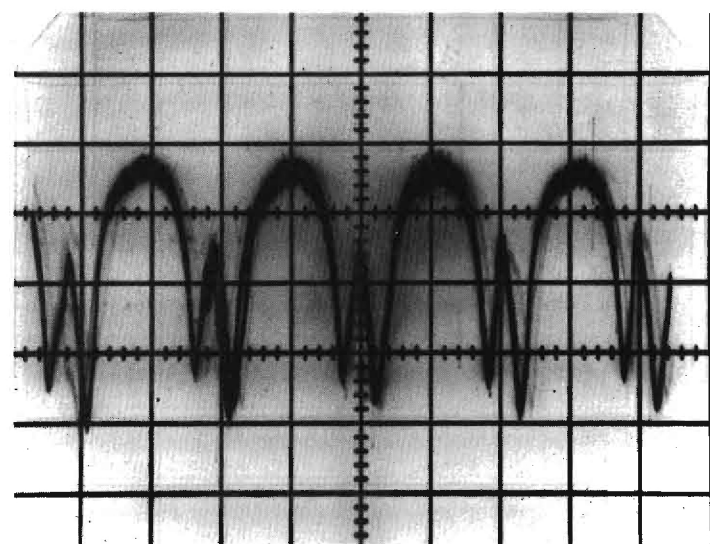(Re ≈ 65,000, SPL = 165
db, 91 cps, 1.85" from $\mathcal{C}_L$).

Figure 54. Acoustic Wave Form
(Re = 65,000, SPL = 165
db, 91 cps, 1.85" from $\mathcal{C}_L$).

CHAPTER V

OFF-RESONANT HEAT TRANSFER COEFFICIENTS

In order to determine the effect of "off" resonant sound waves on the convective heat transfer coefficient in a circular tube, the experimental apparatus described in Chapter I was operated at a Reynolds number of approximately 20,000 for several frequencies of the impressed acoustic wave. The data obtained are shown in Figure 55. It is interesting to note that at 0.5 cps above a resonant frequency of 91 cps, the data for the resonant situation were approximated within the experimental accuracy of the equipment. Such a small off-resonant condition seems to have the effect of slightly flattening out the typical resonant pressure and velocity waves. Also, at a frequency 1.1 cps below resonance, the effect of being off an exact resonant condition was negligible. However, when the frequency was 7.1 cps below resonance, difficulty was encountered in obtaining a sufficiently high sound pressure level to secure measurable effects on the local heat transfer coefficient. Although Figure 55 indicates that for the 7.1 cps below resonance situation the local heat transfer coefficient is lower than the no-sound condition, it should be noted that for this situation the Reynolds number was 1,400 less than that for the no-sound condition. Also the maximum sound pressure level was approximately 9 db below that for the resonant condition.

Because it was impossible, with the available equipment, to obtain appreciable sound pressure levels for off-resonant conditions, the data given herein are quite limited and should be interpreted with care. Tentatively, however, the following was noted:

1. For a slight increase (0.5 cps) in frequency above resonance the sound pressure level obtained with the equipment was practically the same as that for resonance. The increase, 0.1 db (see Figure 55), was within the accuracy of the meter and should not be considered an increase.

2. For the condition 1.1 cps below resonance the maximum sound pressure level obtained was approximately 3 db below that of resonant conditions and the local heat transfer coefficient curve had approximately the same shape as did that for a resonant condition.

3. For the condition 7.1 cps below resonance the maximum sound pressure level obtained was reduced about 9.0 db below that for resonance and this reduction made it impossible to determine whether or not the off-resonance condition was altering the no-sound heat transfer coefficient appreciably.

4. It appeared to be futile to attempt to obtain more data with the current apparatus since it was not accurate enough and could not maintain sufficiently high sound pressure levels for off-resonant conditions.

It is recommended that work be continued on off-resonant conditions and that means for increasing off-resonant sound pressure levels be developed.
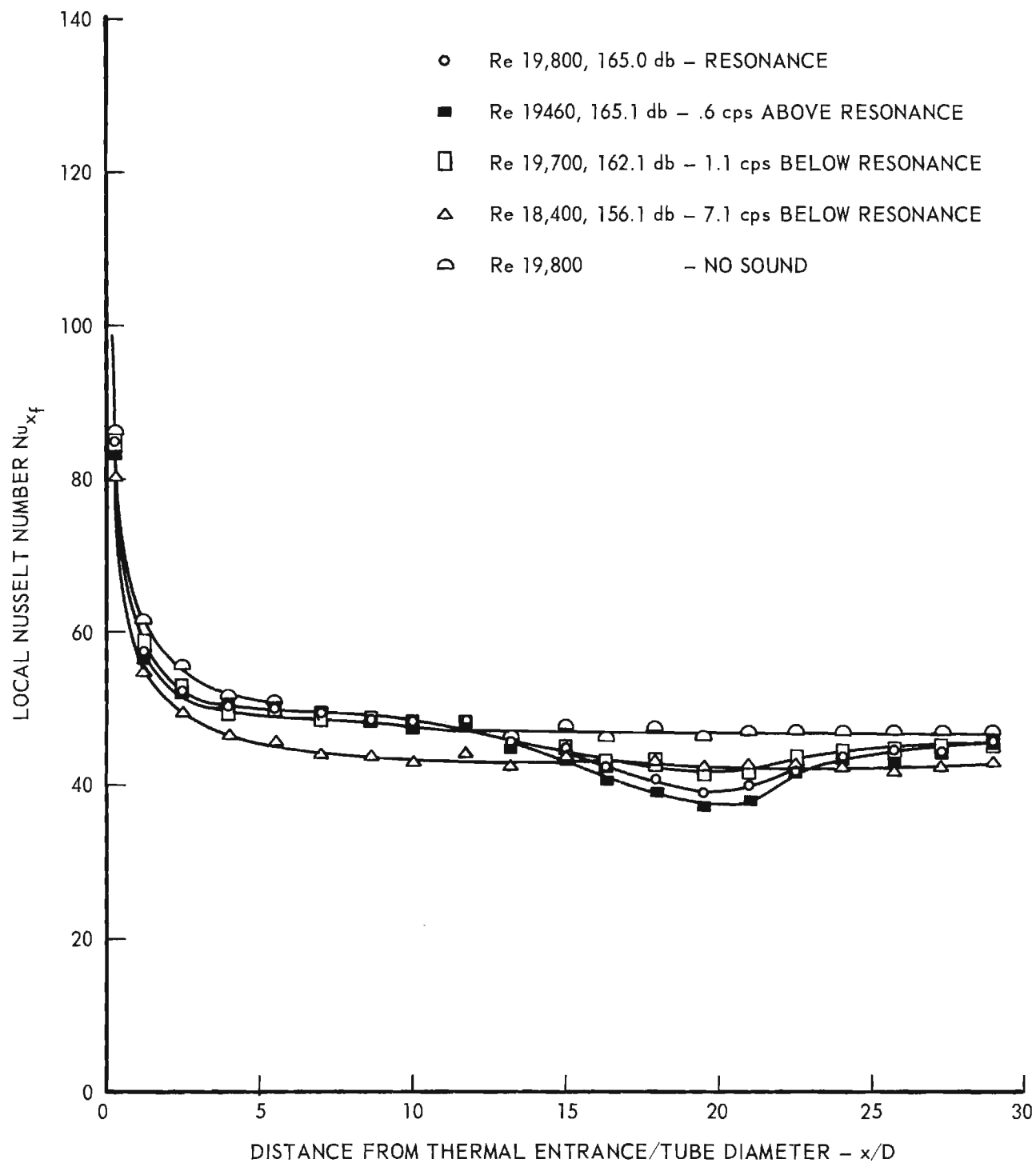
Figure 55.   Resonant and Off Resonant Nusselt Numbers Versus Distance in Duct - Re ≈ 19,700.

CHAPTER VI

EXPERIMENTAL STUDY OF PRESSURE GRADIENTS

WITH AND WITHOUT A RESONANT SOUND FIELD

In order to determine the effect of pressure gradients on the heat transfer coefficients for a circular tube, the experimental apparatus discussed in Chapter I was modified by inserting a tapered insert into the center of the heat transfer tube. By this means local experimental heat transfer data were obtained in a positive or negative pressure gradient. With the small end of the insert facing the direction of the through flow, the pressure gradient was a negative one, and with the large end of the insert facing the direction of through flow the pressure gradient was a positive one. Figures 56 and 57 show schematic drawings of the insert. It can be noted from the drawings that provisions were made to obtain two pressure readings along the face of the tapered insert. The horizontal distance between these pressure taps was 60.18-inches. The insert was centered in the tube by means of small streamlined struts on the entrance and exit cylindrical sections. A photograph of the insert is shown in Figure 58.

Figure 59 presents the data obtained for the pressure drop readings for both the adverse and favorable pressure gradient conditions. The pressure drop data are plotted versus tube Reynolds number. The data with and without sound are quite interesting. It appears that the level of increase of the pressure drop curve is approximately a fixed value for a given sound pressure level. This is logical since it is evident that a resonant sound pressure wave in the tube would have two different mean values at the two pressure taps. Therefore, although the data are interesting they do not have practical significance without a means of plotting the effect over a whole wave length. The data for the two pressure gradients are compared to the anticipated data for the ideal cases considering velocity changes and frictionless flow. The comparisons indicate that the favorable pressure drop case, acceleration of the fluid, appears to have the largest static pressure drop difference.

The adverse pressure gradient situation, decelerating flow, results in a small static pressure drop situation; however, for this case the drop with the resonant acoustic wave impressed on the system is appreciable. The amount of the increase due to sound appears to be large; this, however, is probably due to the relative locations of the pressure taps in respect to the impressed sound wave.

In regards to the heat transfer effects, it should be mentioned that the resonant acoustic wave was adjusted so that a velocity node was as close to the entrance of the thermal heat transfer section as possible. The precise location of this point could not be found with the center body in the tube since utilization of the sound pressure level probe to determine the pressure loop was impossible. The experimental data for Reynolds numbers from 19,000 to 58,000 for the favorable pressure gradient are shown in Figures 60 through 64. As could be expected the heat transfer coefficient increased over the anticipated no-sound value as the

1/4" COPPER TUBING

1-1/8" O.D. COPPER TUBING

A

A

48"

72"

48"

LOCATION OF THERMAL
ENTRANCE — ADVERSE
PRESSURE GRADIENT
SITUATION

LOCATION OF THERMAL
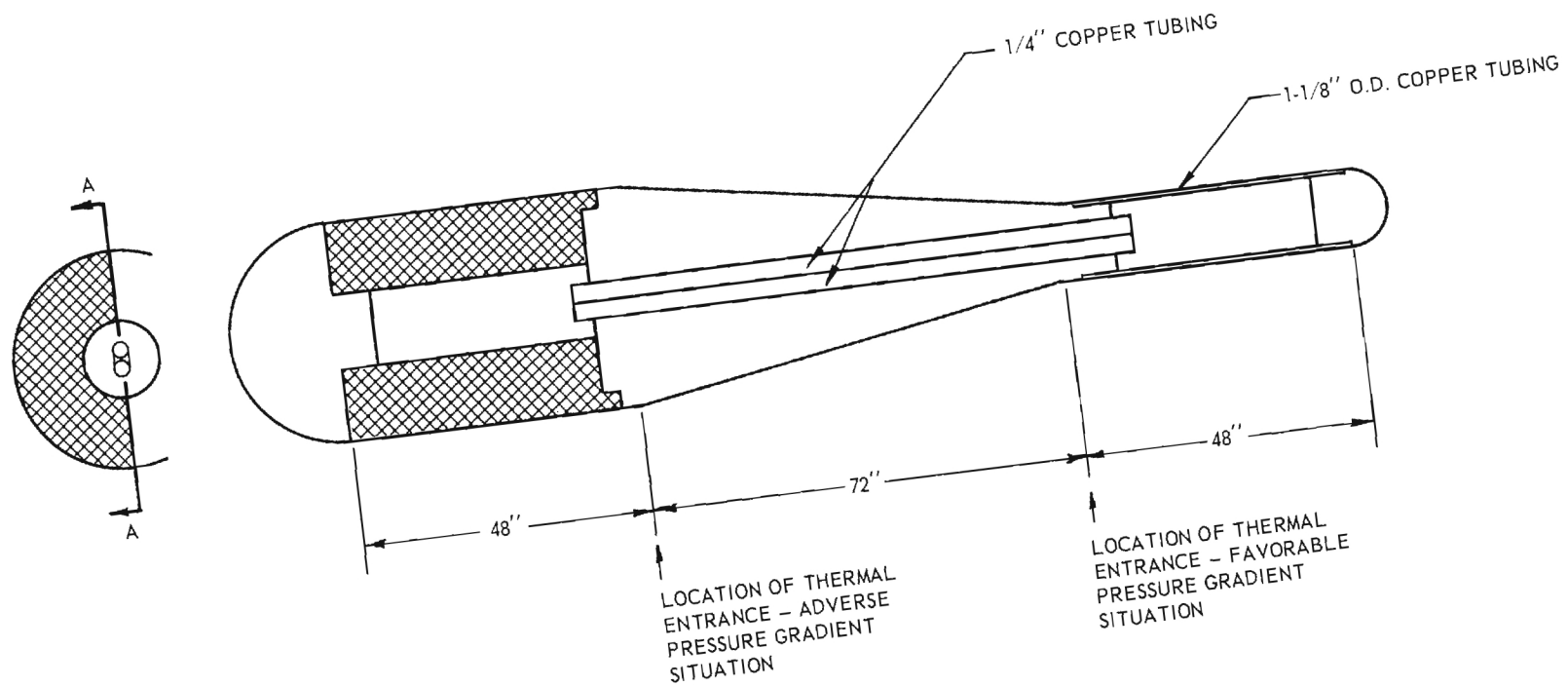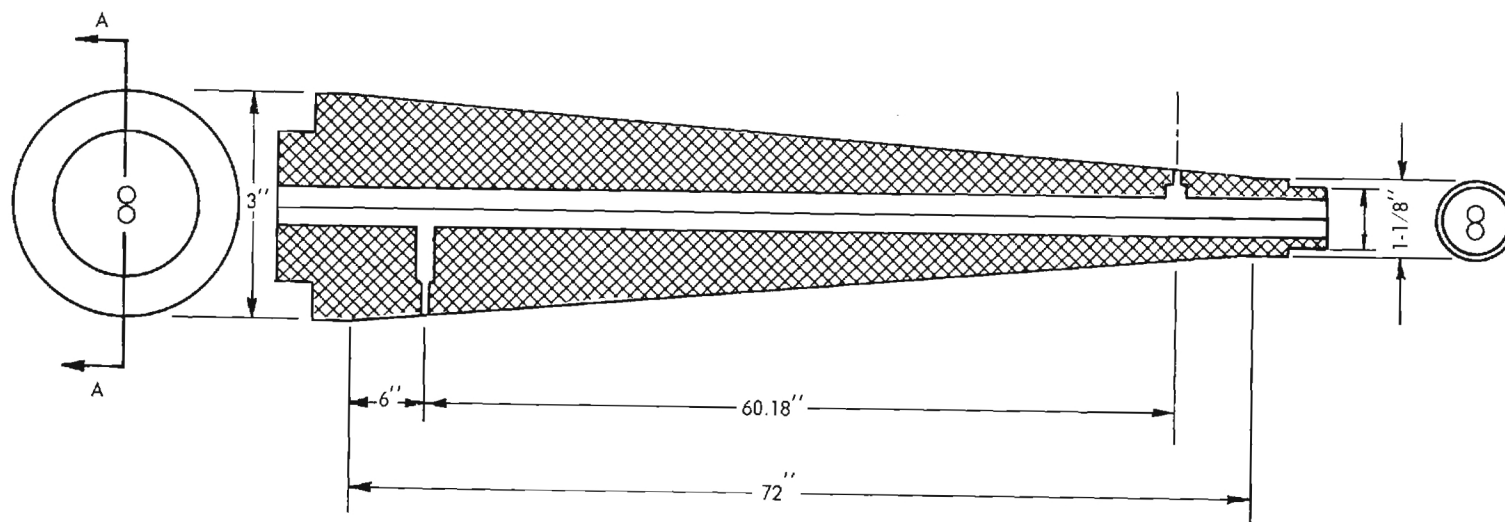ENTRANCE — FAVORABLE
PRESSURE GRADIENT
SITUATION

Figure 56. Schematic Drawing of Insert.

MATERIAL: SUGAR PINE

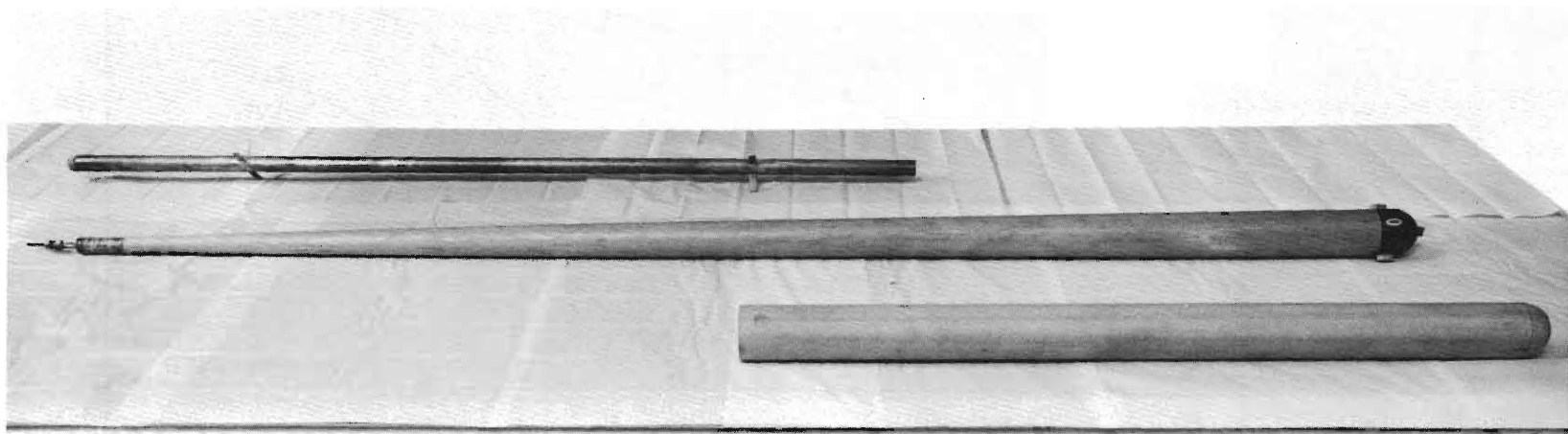Figure 57. Schematic Drawing of Insert Showing Location of Pressure Taps.
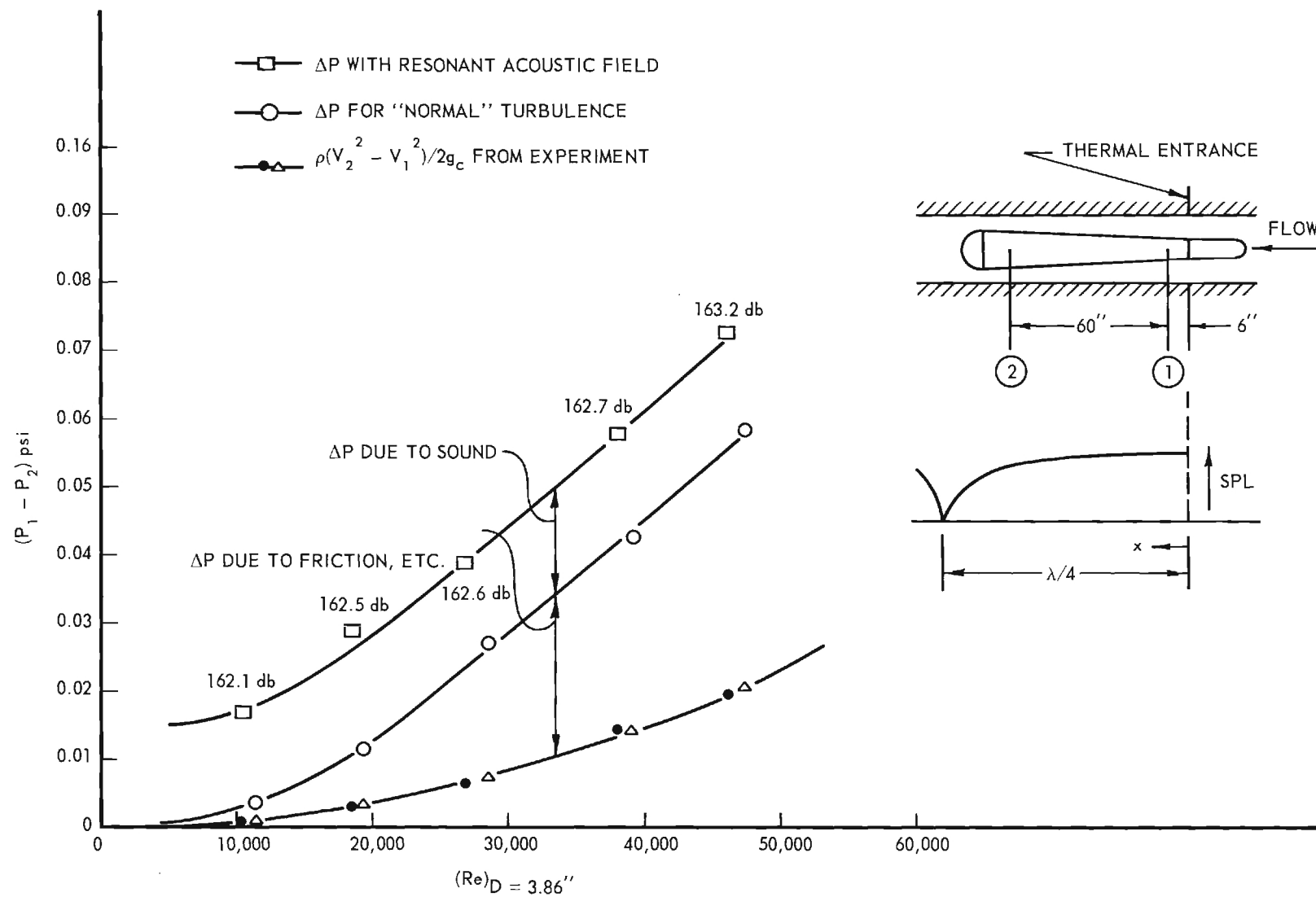
Figure 58.   Photograph of Insert.

Figure 59a. Pressure Drop Versus Reynolds Number - Favorable Pressure Gradient.
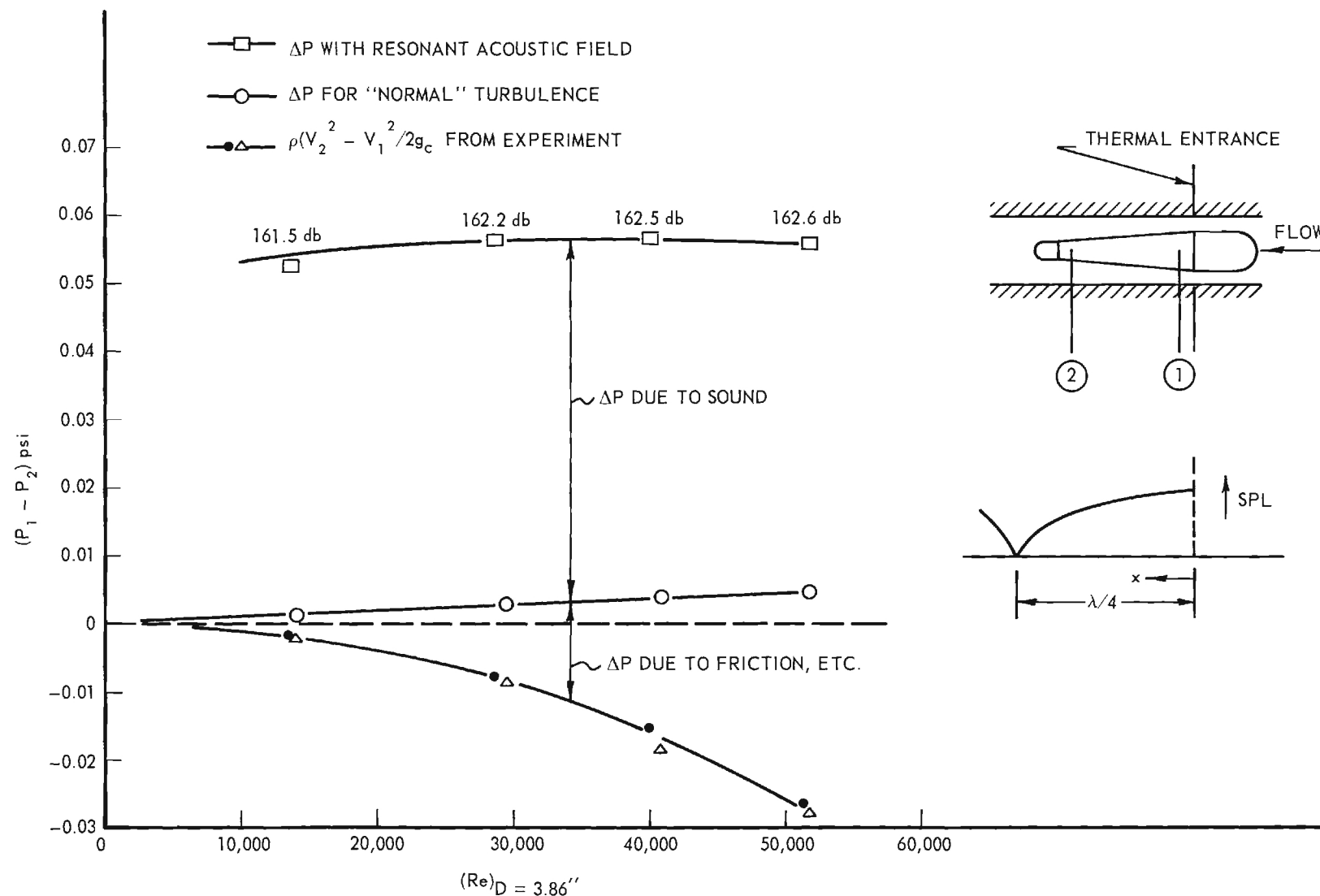
Figure 59b. Pressure Drop Versus Reynolds Number – Adverse Pressure Gradient.
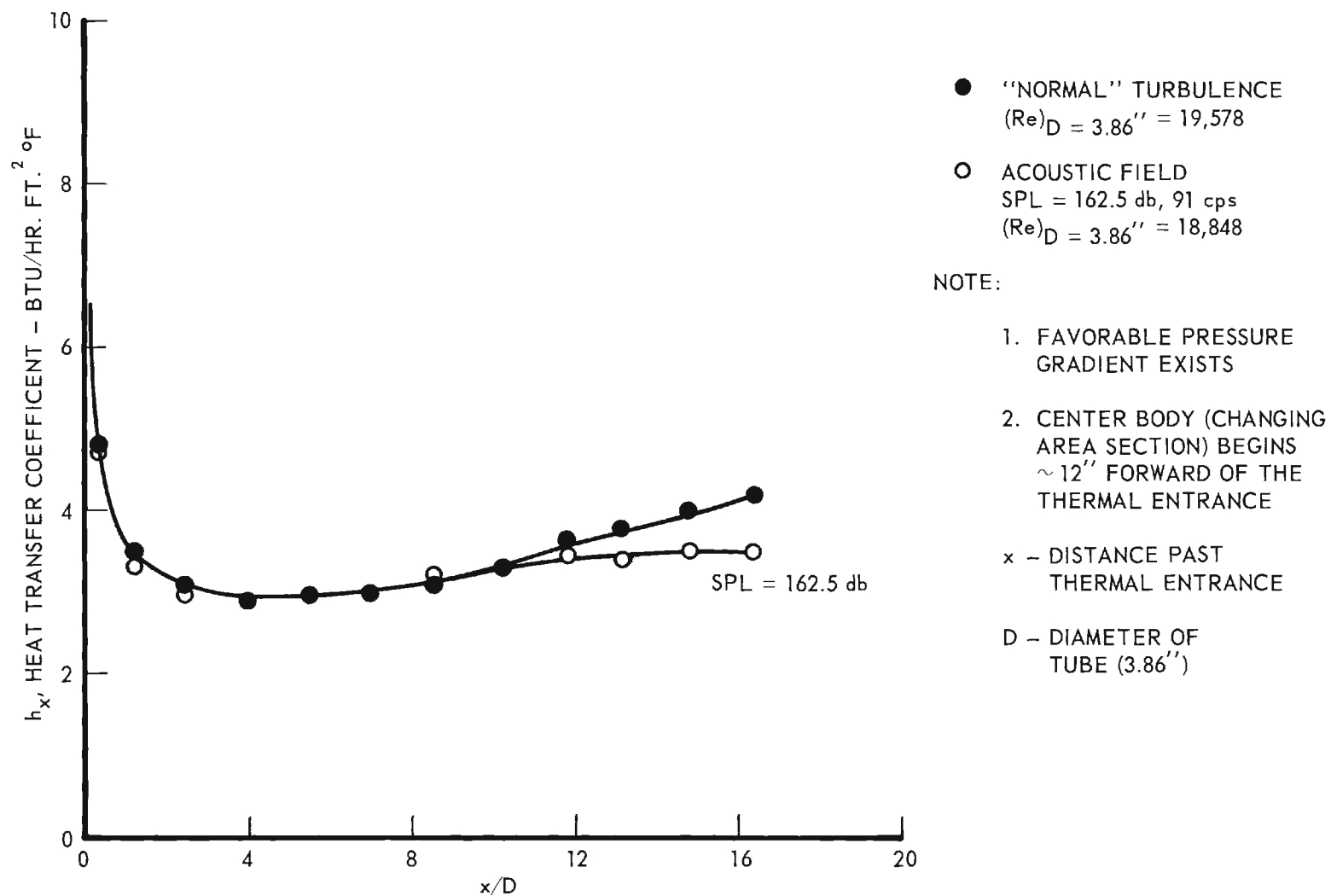
Figure 60.   Heat Transfer Coefficient Versus x/D – Favorable Pressure Gradient.
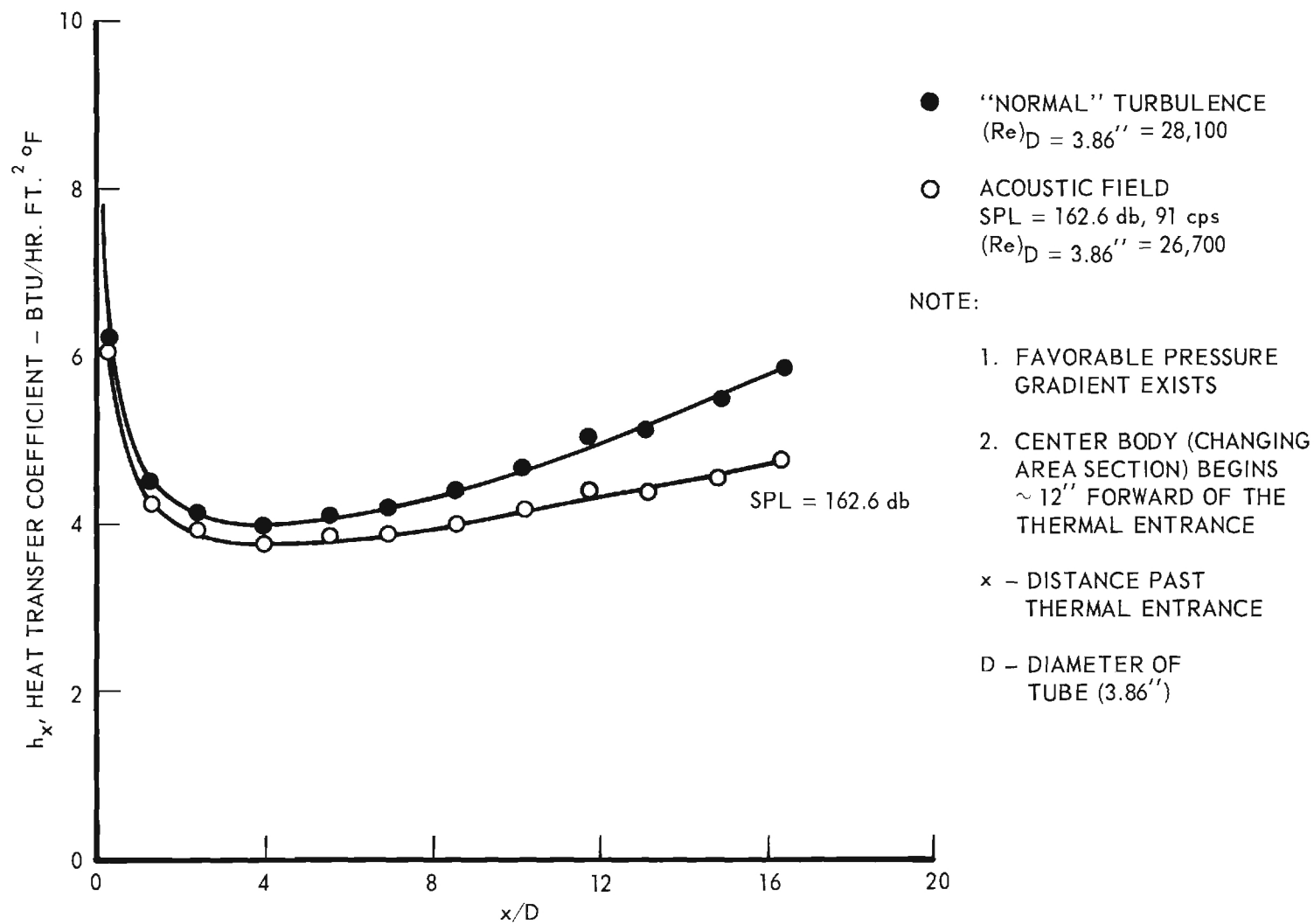
Figure 61.   Heat Transfer Coefficient Versus x/D - Favorable Pressure Gradient.
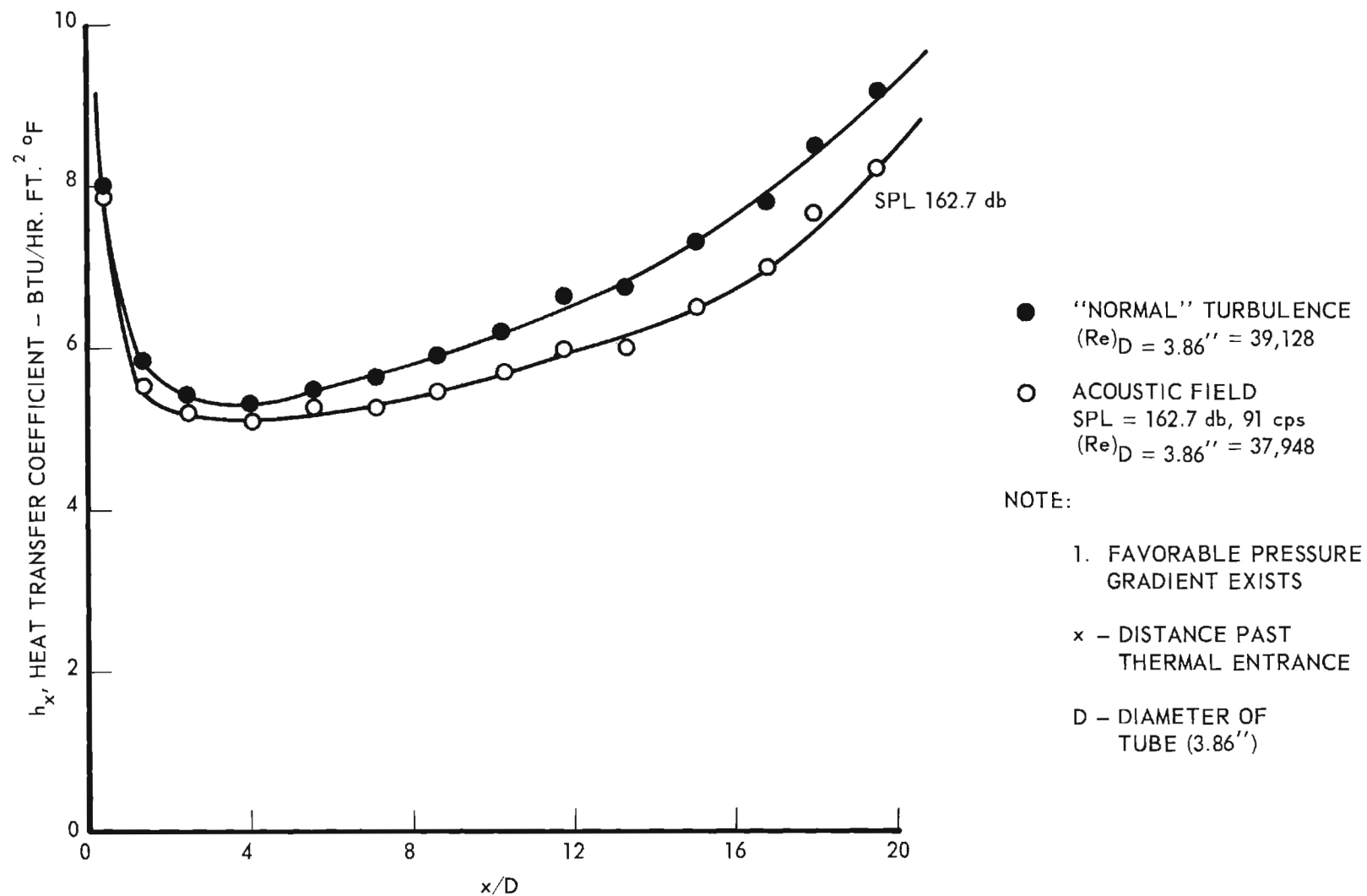
Figure 62. Heat Transfer Coefficient Versus x/D - Favorable Pressure Gradient.
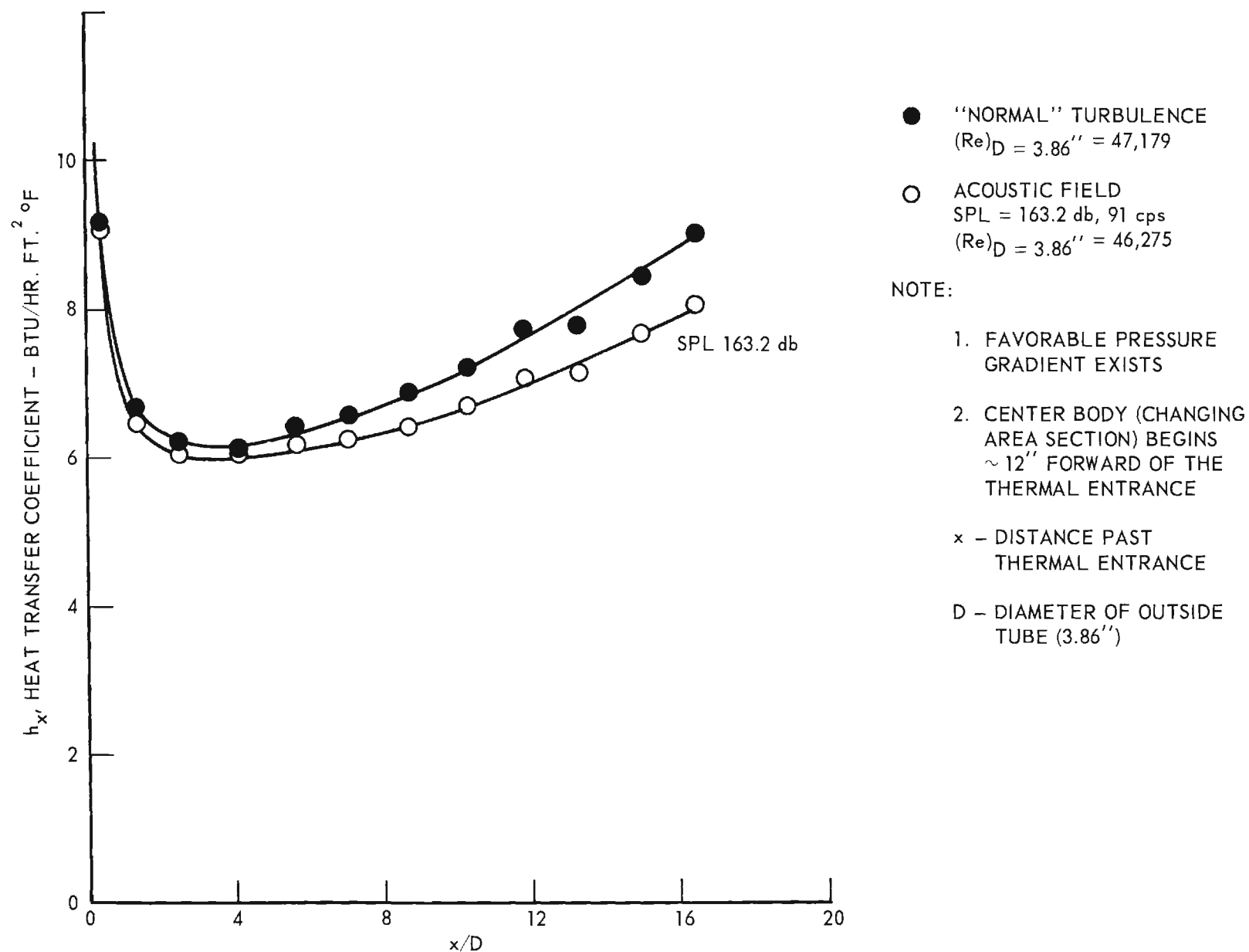
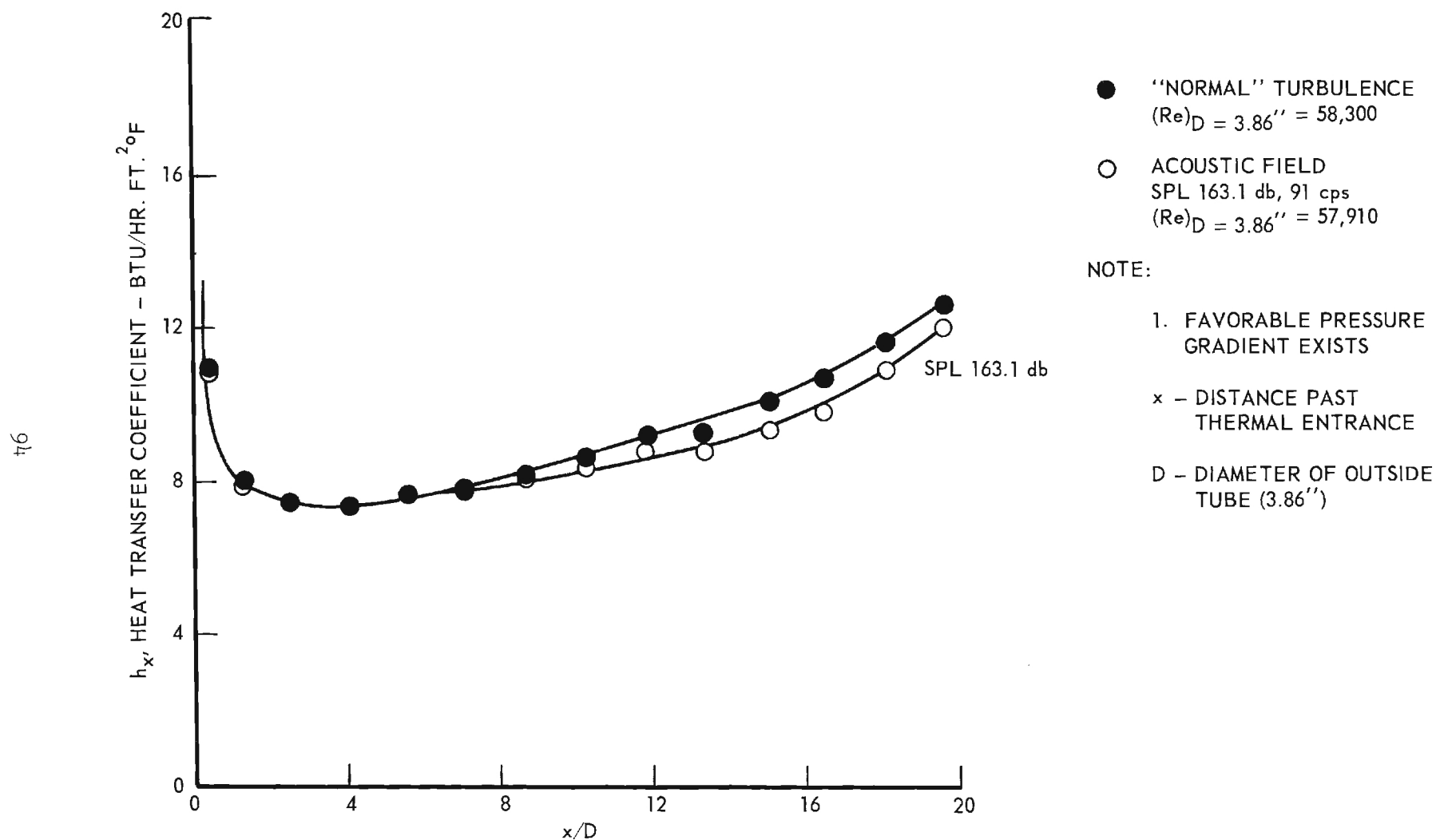Figure 63. Heat Transfer Coefficient Versus x/D - Favorable Pressure Gradient.

Figure 64. Heat Transfer Coefficient Versus x/D – Favorable Pressure Gradient.

fluid velocity increased in the downstream direction. This increase is shown in the figures by an increasing heat transfer coefficient with increasing distance into the heat transfer tube. The effect of sound on heat transfer, as in the case for turbulent tube flow, is to decrease the local heat transfer coefficient. (See Figure 16, Chapter II.) It should be kept in mind that the insert increases the fluid velocity in the tube so that the velocity for equivalent Reynolds numbers based upon the tube diameter is greater with the insert. Figures 60 through 64 are surprisingly similar to those of Chapter II if the increase in the fluid velocity due to the insert is considered.

For the adverse pressure gradient the data for the local heat transfer coefficient versus distance into the heat transfer tube are shown in Figures 65 through 68. These data do not show the increase in the heat transfer coefficient associated with the favorable pressure gradient since the velocity is decreasing with distance down the tube. The data actually decrease faster than the straight through flow data. This is to be expected since a decrease in velocity would naturally be expected to result in a decrease in the local heat transfer coefficient. The effect of sound for this situation is again to decrease the local heat transfer coefficient below that for no-sound.

For the turbulent flow situation with adverse and favorable pressure gradients the following comments can be made:

1. The local heat transfer coefficient is strongly dependent upon the local fluid velocity in the heat transfer tube. As the velocity is increased due to the pressure gradient the heat transfer coefficient increases; as the velocity is decreased the heat transfer coefficient decreases.

2. The effect of resonant acoustic vibration is to decrease the local heat transfer coefficient in a manner similar to that by which it was decreased for straight tube flow. This is for the turbulent flow regime.

3. The static pressure drops for the flow on which a resonant acoustic wave is impressed are altered by an amount which is determined by the locations of the pressure taps in relation to the standing wave. For the experimental apparatus used herein the adverse pressure gradient gave the biggest influence of the resonant wave on the static pressure difference. However, lack of precise measuring equipment made quantitative statements on this effect impossible.

Much work remains to be done before a complete understanding of the influence of pressure gradients on fluid flow and heat transfer in the presence of an acoustic field is available. Qualitatively, from the results of the experiments conducted here, it appears that if relative velocity situations are considered then the local heat transfer rates for tube flow and the pressure gradient situations may be comparable.

Figure 65. Heat Transfer Coefficient Versus x/D - Adverse Pressure Gradient.

Figure 66. Heat Transfer Coefficient Versus x/D - Adverse Pressure Gradient.
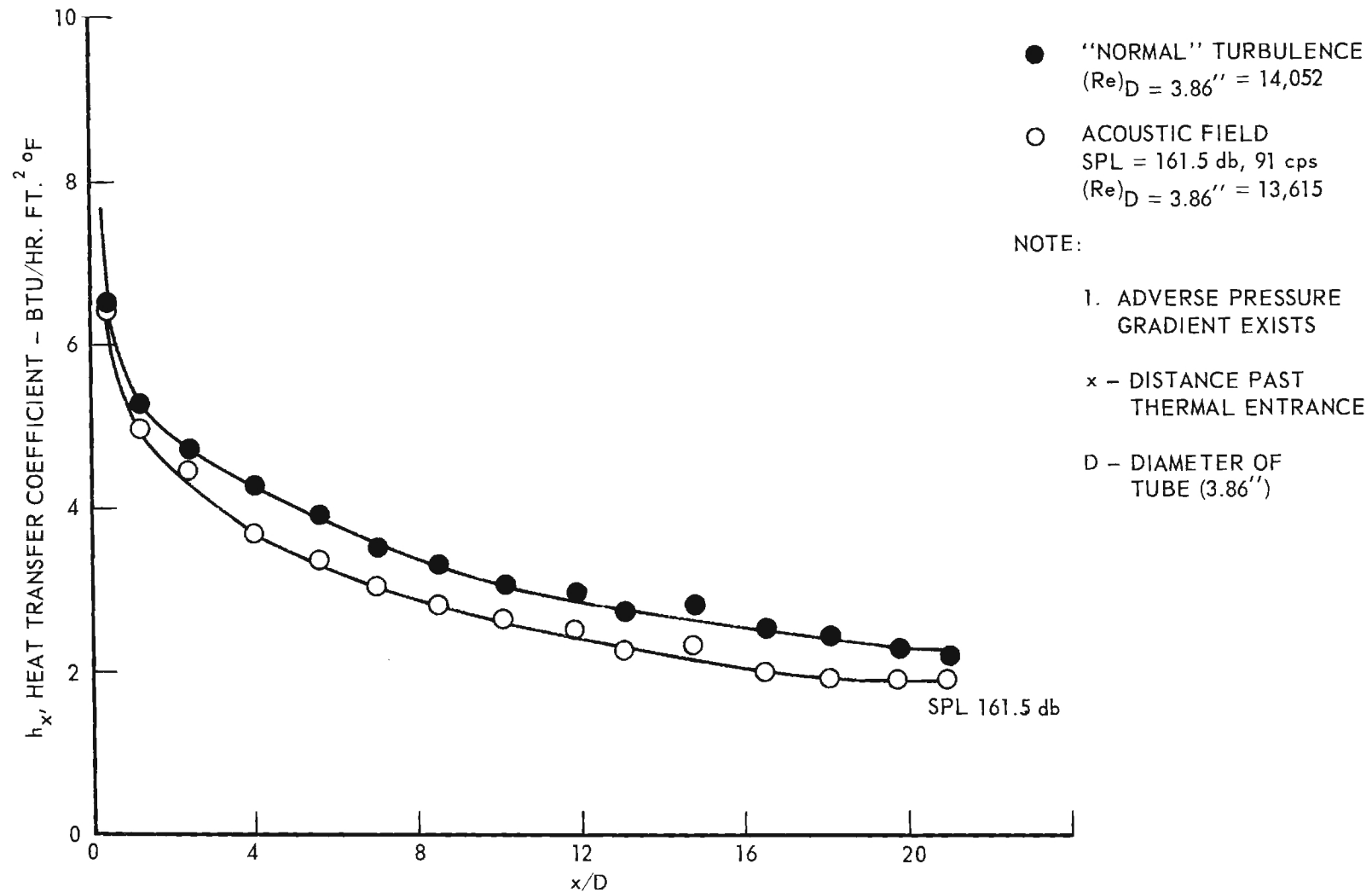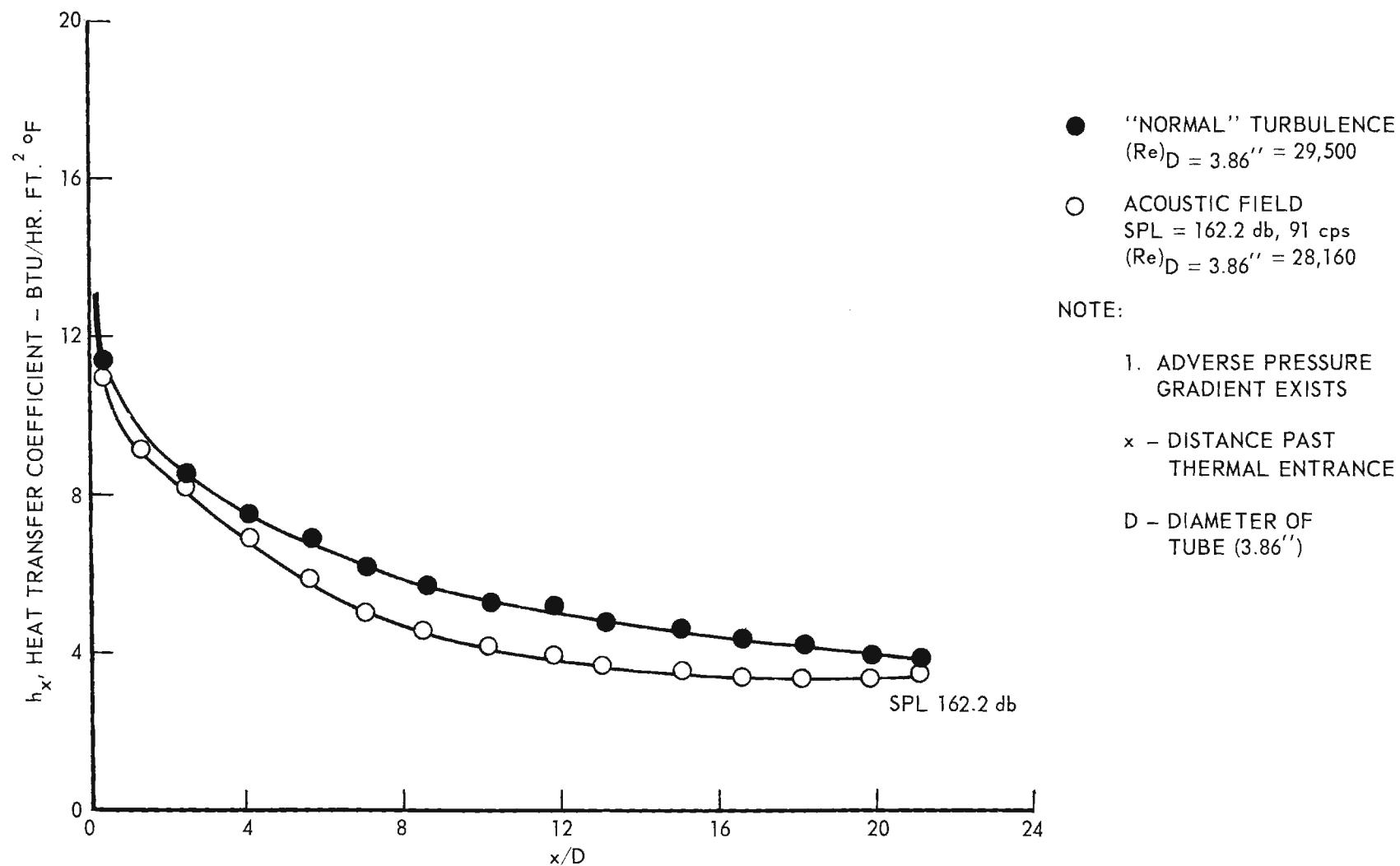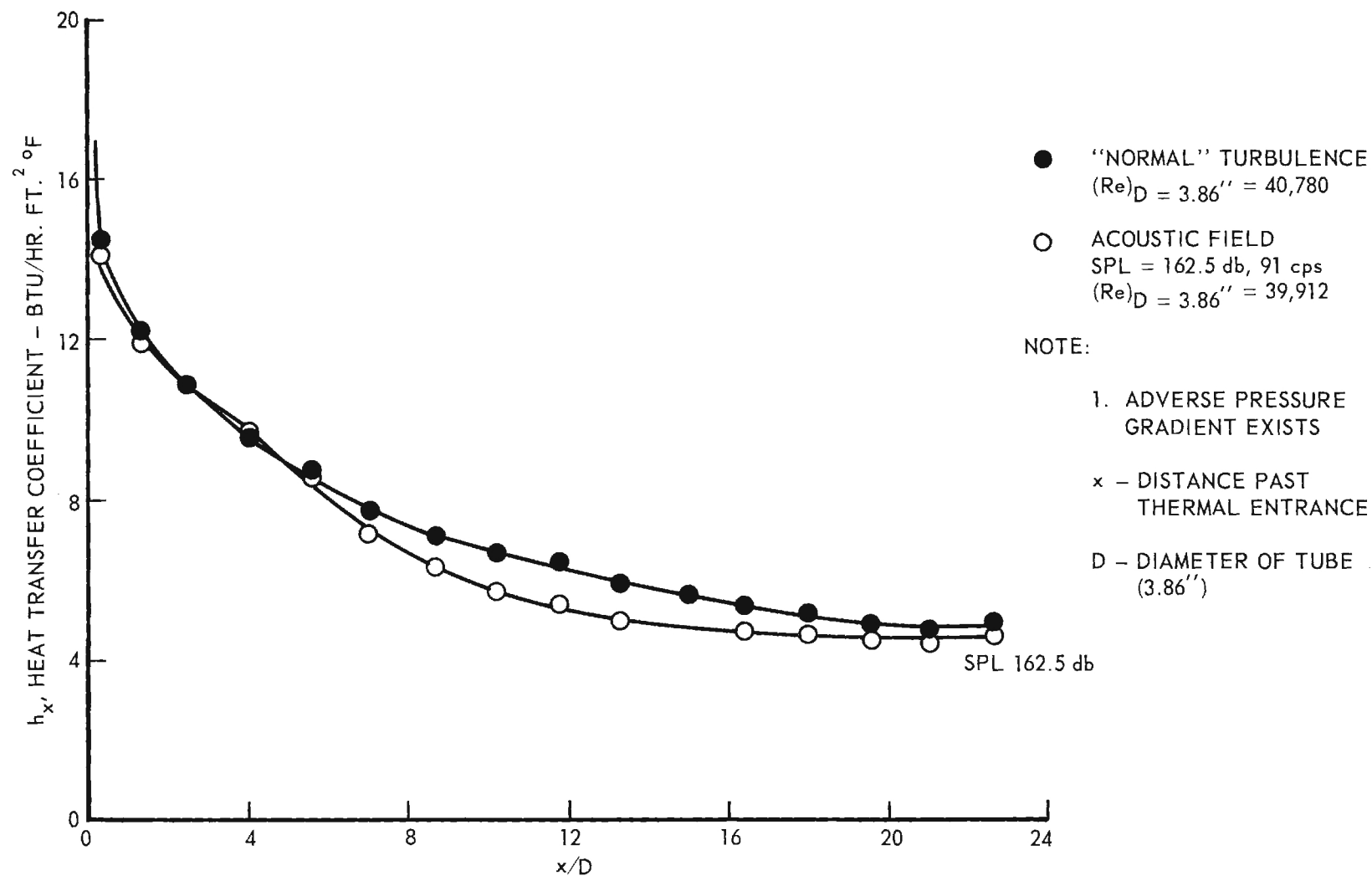
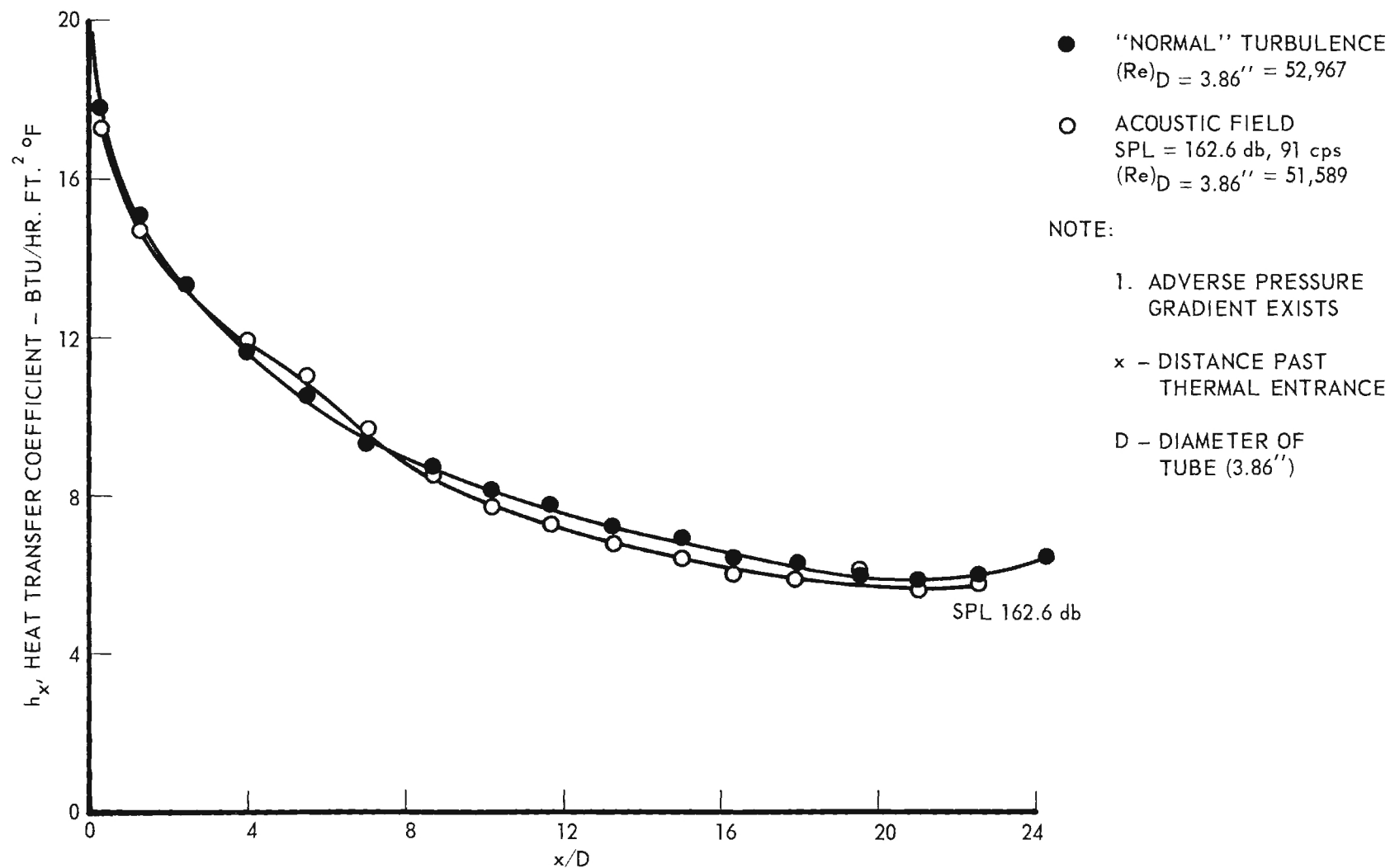Figure 67.   Heat Transfer Coefficient Versus x/D – Adverse Pressure Gradient.

Figure 68. Heat Transfer Coefficient Versus x/D — Adverse Pressure Gradient.

66

LITERATURE CITED

1. P. M. Morse, Vibration and Sound, second edition, New York; McGraw-Hill Book Company, Inc., (1948).

2. Kenneth R. Purdy and Thomas W. Jackson, "Viscous Compressible Fluid Flow Under the Influence of a Resonant Acoustic Field," ARL Technical Report 62-457, Aeronautical Research Laboratories, (1962).

3. J. Hilsenrath, et. al., Tables of Thermal Properties of Gases, National Bureau of Standards Circular 564, Washington, D. C., (1955).

4. W. H. McAdams, Heat Transmission, third edition, McGraw-Hill Book Company, Inc., New York, (1954).

5. H. Latzko, "Heat Transfer in a Turbulent Liquid or Gas Stream," NACA TM No. 1068, (1944).

6. L. M. K. Boelter, G. Young and H. W. Iversen, "An Investigation of Aircraft Heaters XXVII - Distribution of Heat-Transfer Rate in the Entrance Section of a Circular Tube," NACA TN No. 1451, (1948).

7. H. G. Keith, "Laminar Forced Convection Under the Influence of a Resonant Acoustic Field," Ph.D. Thesis, Georgia Institute of Technology, (1965).

8. M. Perlmutter and R. Siegel, "Unsteady Laminar Flow in a Duct with Unsteady Heat Addition," Trans. of ASME, Series C, 83, pp. 432-440, (1961).

9. S. L. Zeiberg and W. K. Mueller, "Transcient Laminar, Combined Free and Forced Convection in a Duct," Trans of ASME, Series C, 84, pp. 141-148, (1962).

10. R. Siegel and M. Perlmutter, "Heat Transfer for Pulsating Laminar Duct Flow," Trans. of ASME, Series C, 84, pp. 111-123, (1962).

11. R. Siegel and M. Perlmutter, "Two-Dimensional Pulsating Laminar Flow in a Duct with a Constant Wall Temperature," International Developments in Heat Transfer, Part II, pp. 517-525, (1961).

12. R. L. Ewen, "Laminar Heat Transfer with Oscillating Flow in a Parallel Plate Channel," Ph.D. Thesis, University of Pittsburgh, (1962).

13. K. R. Purdy, "Viscous Fluid Flow Under the Influence of a Resonant Acoustic Field," Ph.D. Thesis, Georgia Institute of Technology, (1963).

14. R. H. Norris and D. D. Stried, "Laminar Flow Heat Transfer Coefficients for Ducts," Trans. ASME, 62, pp. 525-533, (1940).

15. J. R. Sellars, M. Tribus, and J. S. Klein, "Heat Transfer to Laminar Flow in a Round Tube or Flat Conduit - The Graetz Problem Extended," Trans. of ASME, 78, pp. 441-448, (1956).

DOCUMENT CONTROL DATA - R&D

(Security classification of title, body of abstract and indexing annotation must be entered when the overall report is classified)

1. ORIGINATING ACTIVITY (Corporate author)	2a. REPORT SECURITY CLASSIFICATION
Georgia Tech Research Institute Georgia Institute of Technology Atlanta, Georgia 30332	Unclassified
	2b. GROUP

3. REPORT TITLE

INVESTIGATIONS OF THE EFFECT OF ACOUSTIC
VIBRATIONS ON CONVECTIVE HEAT TRANSFER

4. DESCRIPTIVE NOTES *(Type of report and inclusive dates)*

Final Report Oct. 1963 to Jan. 1965

5. AUTHOR(S) *(Last name, first name, initial)*

Jackson, Thomas W.   Rudland, Robert S.
Purdy, Kenneth R.
Keith, Henry G.

6. REPORT DATE	7a. TOTAL NO. OF PAGES	7b. NO. OF REFS
January 1965	101	15

8a. CONTRACT OR GRANT NO. AF-33(616)-8396 b. PROJECT NO. 7064 c. Task 706301 d.	9a. ORIGINATOR'S REPORT NUMBER(S) Final Report - Project A-567 9b. OTHER REPORT NO(S) (Any other numbers that may be assigned this report)

10. AVAILABILITY/LIMITATION NOTICES

Qualified requesters may obtain copies from DDC or
Aerospace Research Laboratories.

11. SUPPLEMENTARY NOTES	12. SPONSORING MILITARY ACTIVITY
	Aerospace Research Laboratories Wright-Patterson Air Force Base, Ohio

13. ABSTRACT

This report presents experimental and analytical results for heat transfer coefficients in an isothermal tube. Data on heat transfer coefficients for Reynolds numbers from 10,000 to 65,000 are presented for no-sound conditions as well as for conditions of a resonant frequency in the tube of 90 cps. For turbulent flow the sound reduces the heat transfer coefficient.

An analytical solution for the local heat transfer coefficient for laminar flow is given. A hot wire study indicated that sound tends to alter the velocity profile across the tube.

The effects of pressure gradients on the heat transfer coefficients was determined by placing an insert into the tube.

DD FORM 1 JAN 64 **1473**

14. KEY WORDS	LINK A		LINK B		LINK C	
	ROLE	WT	ROLE	WT	ROLE	WT
Heat transfer coefficients	8,6,7	3				
Experimental data	8,7	3				
Sound effects on heat transfer	8,6,7	3				
Local values of heat transfer coefficient	8,7	3				
Solution of energy equation			8	3		
Velocity profiles			8	2		
Turbulence			8	1		
Pressure gradient effects					8	3

INSTRUCTIONS

1. ORIGINATING ACTIVITY: Enter the name and address of the contractor, subcontractor, grantee, Department of Defense activity or other organization (corporate author) issuing the report.

2a. REPORT SECURITY CLASSIFICATION: Enter the overall security classification of the report. Indicate whether "Restricted Data" is included. Marking is to be in accordance with appropriate security regulations.

2b. GROUP: Automatic downgrading is specified in DoD Directive 5200.10 and Armed Forces Industrial Manual. Enter the group number. Also, when applicable, show that optional markings have been used for Group 3 and Group 4 as authorized.

3. REPORT TITLE: Enter the complete report title in all capital letters. Titles in all cases should be unclassified. If a meaningful title cannot be selected without classification, show title classification in all capitals in parenthesis immediately following the title.

4. DESCRIPTIVE NOTES: If appropriate, enter the type of report, e.g., interim, progress, summary, annual, or final. Give the inclusive dates when a specific reporting period is covered.

5. AUTHOR(S): Enter the name(s) of author(s) as shown on or in the report. Enter last name, first name, middle initial. If military, show rank and branch of service. The name of the principal author is an absolute minimum requirement.

6. REPORT DATE: Enter the date of the report as day, month, year; or month, year. If more than one date appears on the report, use date of publication.

7a. TOTAL NUMBER OF PAGES: The total page count should follow normal pagination procedures, i.e., enter the number of pages containing information.

7b. NUMBER OF REFERENCES: Enter the total number of references cited in the report.

8a. CONTRACT OR GRANT NUMBER: If appropriate, enter the applicable number of the contract or grant under which the report was written.

8b, 8c, & 8d. PROJECT NUMBER: Enter the appropriate military department identification, such as project number, subproject number, system numbers, task number, etc.

9a. ORIGINATOR'S REPORT NUMBER(S): Enter the official report number by which the document will be identified and controlled by the originating activity. This number must be unique to this report.

9b. OTHER REPORT NUMBER(S): If the report has been assigned any other report numbers (either by the originator or by the sponsor), also enter this number(s).

10. AVAILABILITY/LIMITATION NOTICES: Enter any limitations on further dissemination of the report, other than those imposed by security classification, using standard statements such as:

   (1) "Qualified requesters may obtain copies of this report from DDC."

   (2) "Foreign announcement and dissemination of this report by DDC is not authorized."

   (3) "U. S. Government agencies may obtain copies of this report directly from DDC. Other qualified DDC users shall request through
_____."

   (4) "U. S. military agencies may obtain copies of this report directly from DDC. Other qualified users shall request through
_____."

   (5) "All distribution of this report is controlled. Qualified DDC users shall request through
_____."

If the report has been furnished to the Office of Technical Services, Department of Commerce, for sale to the public, indicate this fact and enter the price, if known.

11. SUPPLEMENTARY NOTES: Use for additional explanatory notes.

12. SPONSORING MILITARY ACTIVITY: Enter the name of the departmental project office or laboratory sponsoring (paying for) the research and development. Include address.

13. ABSTRACT: Enter an abstract giving a brief and factual summary of the document indicative of the report, even though it may also appear elsewhere in the body of the technical report. If additional space is required, a continuation sheet shall be attached.

It is highly desirable that the abstract of classified reports be unclassified. Each paragraph of the abstract shall end with an indication of the military security classification of the information in the paragraph, represented as (TS), (S), (C), or (U).

There is no limitation on the length of the abstract. However, the suggested length is from 150 to 225 words.

14. KEY WORDS: Key words are technically meaningful terms or short phrases that characterize a report and may be used as index entries for cataloging the report. Key words must be selected so that no security classification is required. Identifiers, such as equipment model designation, trade name, military project code name, geographic location, may be used as key words but will be followed by an indication of technical context. The assignment of links, roles, and weights is optional.